PHYSIOLOGICAL BASIS FOR ENVIRONMENTALLY-DRIVEN CHANGES IN PHYTOPLANKTON COMMUNITIES

by

ZOE VANESSA FINKEL

A Dissertation submitted to the

Graduate School-New Brunswick

Rutgers, The State University of New Jersey

in partial fulfillment of the requirements

for the degree of

Doctor of Philosophy

Graduate Program in Oceanography

written under the direction of

Paul Falkowski and Oscar Schofield

and approved by

Paul Falkowski

Oscar Schofield

John Reinfelder

Peter Morin

Edward Laws

New Brunswick, New Jersey

May 2005

Abstract

PHYSIOLOGICAL BASIS FOR ENVIRONMENTALLY-DRIVEN CHANGES IN PHYTOPLANKTON COMMUNITIES

By ZOE VANESSA FINKEL

Dissertation Directors: Paul Falkowski and Oscar Schofield

The ocean is one of the main reservoirs of carbon, and its ability to act as a long-term sink is affected by phytoplankton through the flux of photosynthetically produced carbon from the surface into the deep ocean, termed the biological pump. Environmentally-driven changes in phytoplankton taxonomic composition, size structure, and elemental composition can alter the biological pump causing climatic feedbacks. I test the hypothesis that physiological responses to resource availability can alter the elemental composition and size scaling of metabolic rates of phytoplankton taxa. I examine the link between taxonomy and elemental composition in phytoplankton over a range of light levels. I then develop a physiological model to examine the consequences of light and nutrient availability for the size scaling of metabolic rates. The physiological model is used as the foundation of an ecological model used to predict the effect of resource availability on the size structure of phytoplankton communities. I develop a record of the frustule size of diatoms that indicates there has been a ~3-fold decrease in the average frustule size of the dominant fossilized marine planktonic diatoms over the

Cenozoic. This change in size is highly correlated with paleoenvironmental indicators of climatic change associated with changes in nutrient availability in the surface ocean, in agreement with the predictions provided by the physiological and ecological size-resolved models. Unique physiological responses of different phytoplankton taxa to resource availability results in significant changes in elemental composition, metabolic rate, and community structure, indicating that climatic change and evolutionary shifts in the taxonomic composition of phytoplankton communities over ecological and geological time will dramatically alter the magnitude and efficiency of the biological pump and the biogeochemical cycling of elements in the ocean.

Acknowlegements

I thank my supervisors Paul Falkowski and Oscar Schofield, it was a true adventure to work with them and their guidance pushed me to work on “big” problems but still provided me with the freedom to follow my own particular obsessions. I thank my committee members, Ed Laws, John Reinfelder and Peter Morin, for their thoughtful and insightful comments.

I have really enjoyed my time at IMCS at Rutgers University, I am grateful to have had the opportunity to interact with an extraordinary group of students, faculty and staff. In particular I have to thank Alicia, Alex, Antonietta, Daniel, Danny, Dave, Hoon, Grant, Ilana, Jessie, Judy, Kay, Kevin, Liti, Liz, Matt, Max, Rob, Sasha, Sybil, Tuo, and Yair for many, many helpful discussions.

I thank Mimi Katz, Jim Wright, Ken Miller for their kind introduction to paleoceanography, and Lloyd Burckle, David Harwood, Cinzia Spencer-Cervato, Andrea Ableman, and Rainer Gersonde for their introduction to the micropaleontology of diatoms, and Marie Pierre-Aubry for wonderful discussions on the morphological evolution of phytoplankton.

My work has been strongly influenced by conversations with John Raven, Andy Knoll, Jon Payne, Jeremy Young, Rob Armstrong, and Victor Smetacek – thank you.

Lastly, and most importantly, I thank my collaborator in life as well as science, Andrew Irwin.

Table of Contents

List of Figures

List of Tables

Chapter 1. Introduction

One of the main questions challenging environmental scientists is to understand how the anthropogenic increase in carbon dioxide concentrations will change climate (Sarmiento et al. 1998). The ocean is one of the most important reservoirs of inorganic carbon, and its ability to act as a long-term sink for CO_2 is affected by phytoplankton through the flux of photosynthetically fixed carbon from the surface into the deep ocean, termed the biological pump (Laws et al. 2000). Over the last decade a general consensus has emerged that the magnitude and efficiency of the biological pump are among the most important and least understood components in climate research (Sarmiento and Wofsy 1999; Watson and Liss 1998). Current models that attempt to predict the effect of increasing anthropogenic CO_2 on climate are extremely sensitive to the parameterization of the biological pump (Sarmiento et al. 1998). Yet due to the lack of information on how the biological pump responds to climate change, models generally treat it as temporally invariant, and contrast simulations with no biological pump (the Strangelove ocean) to a constant biological pump or "super-biotic" model where the phytoplankton community consumes all nutrient in the surface and exports it to the deep sea (Sarmiento et al. 1998; Watson and Liss 1998).

The taxonomic composition of phytoplankton communities can have a profound effect on the biological pump due to phylogenetic differences in elemental composition (Falkowski 2004; Ho et al. 2003; Quigg et al. 2003), cell size, and growth and photosynthetic responses to environmental conditions (Falkowski et al. 1985; Langdon 1987; Langdon 1988). As a result, ecological and geological changes in the size and

taxonomic diversity of phytoplankton communities can effect large changes in the way that the phytoplankton community and therefore the biological pump will respond to climatic change. We will greatly improve our understanding of the biological pump once we explicitly include the effect of phytoplankton community structure, specifically size and taxonomic composition (Laws et al. 2000), which is in turn affected by physiological responses to environmental conditions on ecological and evolutionary timescales. In this dissertation I consider the effect of resource limitation (light and macro-nutrient supply) on two potentially important aspects of phytoplankton physiology: the size scaling of metabolic rates (Chapter 2) and elemental composition (Chapter 3), and the resulting influence on phytoplankton community structure (Chapter 4) and the biological pump on ecological and evolutionary timescales (Chapter 5).

Phytoplankton cell size - from physiological rates to biogeochemistry

> *You can drop a mouse down a thousand-yard mine shaft and, on arriving at the bottom, it gets a slight shock and walks away. A rat would probably be killed, though it can fall safely from the eleventh story of a building, a man is broken, a horse splashes* (Haldane 1985).

The response of an organism to its environment is affected by its size. Numerous fundamental patterns in physiology, ecology and evolution are affected by organism size (Bonner 1988; Bonner 2004; Brown 1995; Gould 1966; Kerr 2001; Peters 1983a). For the phytoplankton, their size not only influences their physiology and community structure over different spatial and temporal scales but because they are the principal primary producers their community size structure has a profound impact on the structure and function of aquatic ecosystems and global climate. Smaller phytoplankton cells tend

to be associated with complex microbial food webs and efficient recycling in the surface ocean, while larger phytoplankton tend to be grazed by large zooplankton, resulting in shorter, simpler food webs and an increase in the magnitude and efficiency of the biological pump (Laws et al. 2000; Legendre 1981; Michaels and Silver 1988). If phytoplankton community size structure is altered by environmental conditions, and phytoplankton size structure has the potential to alter climate through changes in the biological pump, there is a potential biological climate feedback. An improved understanding of the mechanisms controlling the size structure of the phytoplankton community in response to environmental forcing is essential to understanding temporal and spatial fluctuations in food web structure, the regulation of the biological pump, and the ability of the ocean to act as a long-term sink for atmospheric carbon dioxide.

Size scaling of physiological rates

Size scaling laws are a remarkably general and widely observed phenomenon in biology (Kleiber 1961; Peters 1983a). From bacteria to large mammals, body size can be used to predict metabolic rate:

$$B = B_0\left(\frac{M}{M_0}\right)^b \qquad (1.1)$$

where b is the size scaling exponent of the relationship between the metabolic rate (B) and the organism's size (M). Organism size is often quantified by volume, carbon content, or dry weight and should be normalized to a reference size M_0. This scaling relationship appears to influence many fundamental macroecological and evolutionary patterns (Bonner 1988; Brown 1995; Gould 1966; Kerr 2001; Peters 1983a; Trammer 2002). Recently several new hypotheses have been proposed to explain the origins of the

¾ scaling of metabolic rates (Darveau et al. 2002; West et al. 1997; West et al. 1999), but they all remain controversial due to yet untested assumptions, and in some cases key logical inconsistencies (see Dodds et al. 2001).

Until the mid 20th century the predominant belief, based on empirical evidence of metabolic size-scaling, was that *b* was 2/3, not 3/4. The usual explanation depended on the relative scaling of the surface area and volume of an organism. Since resources must pass through a surface that separates an organism from its environment, as an organism increases in size, the rate at which resources can be collected (assuming a constant aspect ratio and that a change in size does not affect the rate per unit of surface) increases only as mass or volume to the 2/3 power. Through the mid-20th century this "surface rule" became so well established that contradictory data were often considered the result of measurement error (Kleiber 1961; Lee 1939). For example, one of the most common explanations for deviations from the surface rule focused on the difficulty in estimating the surface area of organisms (Lee 1939). In the second half of the century the dominant opinion switched to supporting a value of ¾ for the size-scaling exponent (Kleiber 1947) although a recent reanalysis of many studies argues that data do not support an exponent of ¾ over 2/3 (Dodds et al. 2001).

The apparent universality of the ¾ metabolic size-scaling across all taxa demands a universal explanation. Recently, several new theories have been advanced which claim to derive the ¾ rule. One hypothesis suggests that the ¾ exponent emerges as a consequence of the sum of many different metabolic rates with different scaling exponents (Darveau et al. 2002). A number of alternative hypotheses claim the ¾ scaling of metabolic rates is a consequence of geometric scaling, specifically the scaling of

resource transportation networks inside an organism such as a closed circulatory system in animals and the vascular network in plants (Banavar et al. 2002; West et al. 1997). The hypotheses that depend on the geometric scaling of specific transportation networks are not general, as they do not appear applicable to organisms such as protists that lack vascular networks (Beuchat 1997). An alternative view is that there is no universal and static size-scaling exponent, but that the ¾ rule of metabolic rates is an emergent property that is shaped by natural selection. As organisms change in size, mechanical and hydrodynamic features of available strategies change (Gordon 1991), so there is no obvious *a priori* reason to expect that optimizing metabolic rate necessarily implies an optimization of the *size scaling* of metabolic rates, especially across taxa. Incorporating a reasonable definition of fitness is challenging but will make any new theory testable. Certainly changes in size, and the adaptations associated with these changes, often define the differences between higher taxonomic groupings (Gould 1966).

Deviations in the size-scaling exponent of metabolic rates have been associated with sub-optimal environmental conditions, such as extremes in temperature and irradiance (Finkel 2001; Gillooly et al. 2001b; Peters 1983a; Schlesinger et al. 1981; Sommer 1989). The theoretical models that derive the ¾ rule for the size scaling of metabolic rates based on geometric scaling properties of transport networks are based on an assumption of equilibrium between resource supply and demand (Banavar et al. 2002). In Chapter 2 I develop a theoretical model that demonstrates that the 3/4 rule of metabolic scaling does not apply to resource limited organisms. I show that resource limitation can alter the size scaling of metabolic rates if resource acquisition depends on organism size. The degree of deviation from the ¾ size scaling exponent depends on the

size-dependence of physiological acclimation in response to resource limitation. The quantitative understanding of how resource limitation will alter the size scaling of metabolic rates increases the general applicability of the ¾ rule by reconciling some of the discrepancies between measured data and theoretical models and can be used to understand changes in community size structure.

Biogeochemical consequences of environmentally-driven changes in taxonomic and elemental composition of phytoplankton communities

The elemental composition of phytoplankton biomass, especially the ratio of carbon assimilated into phytoplankton biomass relative to the limiting nutrient can affect the biological pump through a change in the ratio of carbon exported to the deep sea relative to the limiting nutrient (Sigman and Boyle 2000). Recent experimental evidence indicates there are significant phylogenetic differences in macronutrient (C:N:P) and trace metal composition (Mn, Fe, Zn, Cu, Co, Cd) in marine phytoplankton (Geider and LaRoche 2002; Ho et al. 2003; Quigg et al. 2003), indicating that shifts in the relative abundance of diatoms, dinoflagellates and coccolithophorid species over ecological and geological timescales could correspond to large changes in the elemental composition of phytoplankton standing stock and the composition of the export flux. Improving our understanding of the physiological differences between different taxonomic groups is critical for understanding how shifts in the taxonomic composition of marine phytoplankton communities would have altered the biological pump in response to changing climate over time. Surprisingly, measurements of the macro- and micro-elemental composition of phytoplankton are only available under a small set of relevant

environmental conditions, and there is no information on whether the phylogenic differences hold under different environmental conditions.

In Chapter 3 I summarize the analysis of the elemental composition, C, N, P, S, K, Mg, Ca, Sr, Fe, Mn, Zn, Cu, Co, Mo and Ni of 5 marine phytoplankton species representing the 4 major marine phyla over a light gradient. Substantial variability in the elemental composition of different taxa was observed between taxa, consistent with previously reported differences associated with evolutionary history (Falkowski 2004; Ho et al. 2003; Quigg et al. 2003). Large changes in Fe:P and Mn:P have been previously reported as a function of irradiance (Sunda and Huntsman 1997; Sunda and Huntsman 1998a). I show that many elements were enriched relative to phosphorus under irradiances that are limiting for growth including: Fe, Mn, Zn, Cu, Co, Mo, Sr, and Mg. For some species a select number of elements became enriched relative to phosphorus at saturating irradiances including Fe, Mn and Zn in the coastal diatom *Thalassiosira weissfloggi*, and Co in the diazotroph, *Cyanothece* sp. and the Prasinophyte, *Pycnococcus provasolii*, indicating an increased requirement for these elements under saturating irradiance and high growth rates. The interaction between genetic differences and the phenotypic response to irradiance acts to amplify the differences in elemental composition. The significant changes in elemental composition as a function of irradiance suggest that changes in the proportion of biomass and primary production that is light-limited could alter the biogeochemical cycles of many of the bio-limiting elements in the oceans.

Ecological consequences of the size scaling of metabolic rate under different environmental conditions

Phytoplankton cells span over ten orders of magnitude in cell volume and phytoplankton communities and often exhibit a characteristic size structure. The majority of field data suggests that small phytoplankton cells dominate in stable, oligotrophic environments such as the open ocean while larger cells can dominate biomass in variable, eutrophic environments such as coastal areas (Ahrens and Peters 1991; Chisholm 1992; Sprules and Munawar 1986). A complementary rule, also generated from field observations, is that cell abundance (A) per unit volume is inversely related to organism size:

$$A = c_2 V^{\xi}, \qquad (1.2)$$

where the size scaling exponent (ξ) is often –1 (Sheldon and Kerr 1972; Sheldon and Parsons 1967; Sheldon et al. 1972). Subsequent studies have found considerable variability in ξ which often ranges between -2/3 to -5/3 (Boss et al. 2001; Peters 1983a; Sprules and Munawar 1986). The size scaling abundance in biological communities is often used as a basis for interpreting body-size diversity relationships (Allen et al. 2002; May 1978).

Hypotheses for the abundance-body size relationship, such as size-dependent differences in energy use (Damuth 1981), competitive interactions (Grover 1989; Nee 1991), or the scale-free self-organization of complex adaptive systems (Rinaldo et al. 2002) do not explain why nutrient limitation alters the size structure of phytoplankton communities, although Sprules and Munawar have hypothesized that variations in ξ indicate a deviation from steady state (Sprules and Munawar 1986). Food web models

that include several trophic levels (often autotrophs, heterotrophs and detritivores) and many size-dependent processes (uptake, respiration, sinking rate, grazing rate etc.) have successfully simulated a large number of population and community level patterns, but due to a large number of parameters it can be difficult to attribute any particular pattern to any specific mechanism (Kerr 2001; Moloney and Field 1991; Moloney et al. 1991). The physical constraints body size places on metabolic rate and resource acquisition ability has been largely neglected and has not been fully analyzed in the attempt to understand this general relationship between abundance and body size.

In Chapter 4, a modeling framework is developed to predict the taxonomic and size structure of phytoplankton communities based on the size and taxonomically determined physiological responses to environmental conditions. This model demonstrates that a steady-state physiological null model with size scaling of cellular nutrient requirements and growth, and no competitive interactions, can reproduce the power-law relationship between cell size and abundance and the dominance of small phytoplankton cells under oligotrophic conditions, and relative increase in abundance of larger phytoplankton cells under eutrophic conditions. If physiological differences associated with the taxonomic composition of different community size fractions is considered, then the null model can replicate more detailed field observations such as the absence of small, slow growing *Prochlorococcus* spp. and the relative dominance of large diatom species in nutrient-rich, upwelling regions of the ocean. Deviations from the patterns predicted by the physiological null model can be used to identify if extrinsic processes such as competition or loss rates through grazing or aggregation and sinking become the dominant forces shaping phytoplankton community size distributions.

Macroevolutionary consequences of the size scaling of metabolic rate under different environmental conditions

Generally, it appears that organisms have been getting larger over geological time. The oldest known fossil cells, ~3.2 billion years old, were small rods <0.7 μm in length (Tappan 1980). By the early Proterozoic, a range of cell sizes and shapes had developed with an average cell diameter of 5 μm, with a range of 1-35 μm. Average cell diameter increased again to an average of 13 μm with a range from 1 to 80 μm, 850±100 million years ago, with the transition from procaryotic to eucaryotic cells (Schopf and Oehler 1976). Often the origination of new taxonomic groups is associated with an increase in the maximal body size. For example, the transition to the Ediacaran fauna (575-543 Ma), introduced a number of organisms that ranged from centimeters to ~1 meter in the case of *Dickinsonia* (Carroll 2001). The largest organisms to date are the flowering plants, with their origins in the Cretaceous. There is some suggestion that this trend does not extend indefinitely but saturates once the disadvantages of getting larger can no longer be overcome by an increase in complexity.

Macroevolutionary change in body size has been documented in unicellular foraminifera (Schmidt et al. 2004), as well as a variety of aquatic and terrestrial metazoans (Alroy 1998; Hallam 1975). A combination of size bias in origination or extinction, physiologically imposed boundaries on minimum and maximum size, and active selection pressures can result in complex temporal patterns in the evolution of body size. In conjunction with species radiation, passive evolutionary mechanisms tend to result in increases in both the maximum and minimum size with no change in the mean

body size of the group (Gould 1997; Stanley 1973). Bias towards the survival of small species after mass extinction events, and a physiological boundary on minimum body size often results in increases in both the maximum and mean size within a taxonomic group, referred to as Cope's rule (Kitchell 1986; McShea 1994a; Stanley 1973). Active selection pressures, such as trended changes in resource availability or predation pressure, can result in shifts in the size of taxonomic groups towards a particular size with a contraction in the size range (McShea 1994a). Different selection pressures may act on individuals of different size, resulting in a large variety of size distributions.

Evolutionary shifts in the size of phytoplankton cells would have had a profound influence on oceanic food web dynamics (Laws et al. 2000), carbon cycling, and the interpretation of $\delta^{13}C$ of organic carbon over the Cenozoic (Hayes et al. 1999). Several studies on a few single, morphologically defined species of marine diatoms have documented size shifts in response to temperature and upwelling zones over hundreds of thousands to several millions of years (Burckle 1977; Fenster et al. 1989; Sorhannus et al. 1988; Sorhannus et al. 1991; Wimpenny 1936). The size structure of fossil phytoplankton communities has not been previously investigated.

In Chapter 5, I develop a macroevolutionary record of the size of the dominant fossilized marine planktonic diatoms over the Cenozoic and apply conclusions from Chapter 2 and 4 to interpret the record of marine diatom community size structure in response to climate change and the effect on the biological pump. The minimum and maximum size of the diatom frustule of the marine planktonic community has expanded in concert with species diversity. In contrast, the mean area of the diatom frustule is highly correlated with vertical temperature gradients inferred from the $\delta^{18}O$ of

foraminiferal calcite. This is consistent with the hypothesis that climatically induced changes in oceanic mixing have altered nutrient availability in the euphotic zone and driven macroevolutionary shifts in the size of marine pelagic diatoms through the Cenozoic. Thus, climate-induced environmental changes in nutrient availability have the potential to result in climatic feedbacks through ecological and evolutionary shifts in phytoplankton community size structure and the efficiency of the biological pump.

Chapter 2. A theoretical framework for the size scaling of growth under resource limitation

Abstract

Under optimal growth conditions, many metabolic rates scale to the ¾ power of mass. We show that resource limitation can alter this size scaling of metabolic rates if resource acquisition depends on organism size. A prime example of size dependent resource acquisition is light harvesting by phytoplankton. The size-dependence of light acquisition causes a deviation in the ¾ size-scaling of growth and photosynthetic rates under growth limiting irradiance. The degree of deviation from the ¾ size scaling exponent depends on the size-dependence of physiological acclimation in response to resource limitation. Phytoplankton acclimate to light limitation by changes in pigment concentration. We calculate the pigment concentration required to maximize photosynthetic rate, and predict that light-limited photosynthetic rate must scale to the 2/3 power of cell volume. These theoretical results are consistent with the size scaling of pigment concentration and photosynthetic rate of phytoplankton cultures. Our results suggest that deviation from the ¾ size scaling exponent for metabolic rate under resource limiting conditions is the consequence of the size-dependence of both resource acquisition and physiological acclimation to resource availability.

Introduction

Macroecology is the study of the emergent statistical properties of complex ecological systems (Brown 1995). Many fundamental macroecological patterns, such as

abundance and diversity, have been related to organism size (Bonner 1988; Brown 1995; Gould 1966; Kerr 2001; Peters 1983a; Trammer 2002). These patterns, in part, reflect the relationship between an organism's size and its metabolic rate (Brown 1995; Peters 1983a). From bacteria to large mammals, body size can be used to predict metabolic rate:

$$M = k\left(\frac{V}{V_0}\right)^b, \qquad (2.1)$$

where b is the size scaling exponent of the relationship between the metabolic rate (M) and the organism's size (V). Metabolic rate most commonly refers to growth or respiratory rate but can include any anabolic or catabolic rate. Organism size can be quantified as total body mass as estimated by total carbon or dry weight, or for microbes, cell volume (Montagnes et al. 1994). Regardless of the proxy used for body size, normalizing organism size to a reference size, V_0, is necessary to keep the dimensions consistent with metabolic rate as defined in Eq. 2.1. Related organisms often have similar values of k but it can be quite variable between taxonomically distinct groups (Chisholm 1992). In contrast, under optimal growth conditions, b for the organism's metabolic rate is so frequently ¾ that it is referred to as the ¾ rule (Kleiber 1947; Peters 1983a; West et al. 1997).

Recent work suggests that this ¾ rule for metabolic rates is a consequence of the geometric scaling properties of transport networks (Banavar et al. 2002; West et al. 1997). (West et al. 1997) have argued that fractal transport networks regulate metabolic rates with a maximum possible size-scaling exponent of ¾. They observe that many biological surfaces are effectively fractal and thus have non-Euclidean scaling. They modify a surface-rule argument to obtain a scaling exponent of ¾ instead of 2/3.

(Banavar et al. 2002) show that an efficient Euclidean resource delivery network which allows metabolic rate to be independent of organism size, must itself scale as $V^{4/3}$. In many organisms the transport network is an approximately constant proportion of body mass, and thus the metabolic rate scales to the ¾ power of body volume or mass (Banavar et al. 2002) .

Every rule has exceptions. Deviations in the size-scaling exponent have been associated with sub-optimal environmental conditions, such as extremes in temperature and irradiance (Finkel 2001; Gillooly et al. 2001b; Peters 1983a; Schlesinger et al. 1981; Sommer 1989). Theoretical models based on geometric scaling properties of transport networks suggest that imbalances in supply and demand could cause deviations from the ¾ rule (Banavar et al. 2002). Under resource limitation the supply of energy and nutrients does not match the demand of the growth rate. There is at present no theoretical description of how resource limitation will alter the size scaling of metabolic rates. Under optimal environmental conditions, the energy required to acquire resources is at a minimum and organisms can maximize the conversion of resources into growth and reproduction. Under these optimal growth conditions, the maximum intrinsic growth rate is obtained, and the ¾ size scaling of metabolism is achieved (Kleiber 1961; Peters 1983a). As the environmental conditions depart from optimal conditions, resources become more difficult to obtain, resulting in a decreased growth rate. In order to maximize the efficiency of resource acquisition in a variable environment, cellular physiology adjusts through a suite of acclimation processes (Berry and Bjorkman 1980; Evans and Poorter 2001; Falkowski and LaRoche 1991; Jones 1978; Morris and Glover 1974). The cost of acclimation combined with the degree to which resources are limiting

is dependent on body size (Agusti 1991; Hudson and Morel 1993; Raven 1984). This, in turn, alters the size-scaling exponent associated with metabolic rate. A quantitative understanding of how resource limitation will alter the size scaling of metabolic rates increases the general applicability of the ¾ rule by reconciling some of the discrepancies between measured data and theoretical models. Furthermore we suggest that this approach could be used to diagnose resource limitation in natural systems.

We use light-limited phytoplankton as a model system to assess resource driven deviations from the ¾ rule. Phytoplankton are ideal experimental organisms for allometric studies due to their extremely large size range: ~1μm to several millimeters in diameter (Raven and Kubler 2002; Round et al. 1990). Phytoplankton metabolic rates are central to the global biogeochemical cycles of carbon, nitrogen, oxygen, silicon, phosphorus and iron, and account for 40% of global primary production (Falkowski 1994). We focus on light limitation as the limiting resource for 3 reasons: (1) there is a mature physical theory that describes light acquisition in cells (Kirk 1976; Morel and Bricaud 1981), (2) there are well tested, mechanistic, quantitative models of light harvesting and growth as a function of irradiance, and (3) the growth rate of a majority of the phytoplankton cells in the oceans are limited by light (Cullen 1982). Nutrients such as nitrate, phosphate and iron are also known to limit primary production in the ocean. We chose to not explicitly model the effect of nutrient limitation on the size scaling of metabolic rate because there is much less data on how the different nutrient uptake systems respond to changes in nutrient concentration and how this influences the size-dependence of nutrient uptake.

Here, we develop a physiologically-based mechanistic model to explain how disequilibria between supply and demand for light can alter the ¾ size scaling of metabolic rates. Our objectives are to calculate how physiological acclimation to light-limitation leads to altered cellular composition and the anomalous size scaling of photosynthesis in unicellular phytoplankton. We use a biophysical model of light absorption to determine the cellular chlorophyll concentration that maximizes photosynthesis for cells of different sizes. This permits us to calculate the size-dependence of photosynthesis as a function of irradiance. Model results are compared with experimental data, testing our hypothesis that resource limitation can alter the ¾ size scaling of metabolic rates.

Modeling framework

We assume that natural selection acts to maximize the cell division rate of the individual cell. Over large size ranges and within taxonomically similar groups, under optimal experimental growth conditions, evidence suggests that growth rate is a function of the internal transport network and is described by the ¾ rule, Eq. 2.1 (Banavar et al. 2002; Hemmingsen 1960; Kleiber 1961; Peters 1983a; West et al. 1997). Under light limitation, growth rate is limited by the acquisition of photons. Below, we describe the photosynthetic response to varying irradiance as a function of cell size and show how an optimal light harvesting strategy can be used to predict the change in size scaling of photosynthetic rate with resource supply.

Steady-state photosynthesis as a function of irradiance

The relationship between irradiance and photosynthetic rate (P) is commonly expressed as an exponential or hyperbolic tangent function of irradiance:

$$P(I) = P_{max} \cdot \tanh (a \, \phi \, I / P_{max}) , \qquad (2.2)$$

where I is irradiance, a is the cellular absorption cross-section weighted to the spectral irradiance, ϕ, the quantum yield of photosynthesis is a saturating function of the maximum quantum yield (ϕ_m) and irradiance (Welschmeyer and Lorenzen 1981), and P_{max} is the maximum photosynthetic rate (see Table 2.1 for a list of symbols, their units, and typical values). As I increases from zero, P increases approximately linearly with irradiance. The slope of P versus I, as $I \rightarrow 0$, is referred to as α or photosynthetic efficiency. When irradiances become saturating (at $I_k = P_{max}/\alpha$), photosynthesis is close to its maximum rate (P_{max}), and there is very little increase in photosynthetic rate with irradiance. Although size-dependence has been reported for P_{max} and α (Finkel 2001; Taguchi 1976), the size scaling of photosynthesis has generally not been explicitly considered in models of photosynthesis (Cullen et al. 1993).

Steady-state size scaling of photosynthesis under light limiting conditions

Under light-limiting conditions photosynthetic rate is proportional to $\alpha\phi I$. For cells grown at irradiances below I_k, quantum yield is at its maximum, and here is assumed to be 0.1 mol carbon (mol photons)$^{-1}$ (Kirk 1994). For simplicity, we assign ϕ a value of 0.1 mol carbon (mol photons)$^{-1}$ for all I. Light absorption is much more variable. It is a function of pigment composition, pigment concentration and cell size.

Table 2-1. List of symbols

Symbol	Definition & examples	Typical range	Units
A	Cell opt. abs. cross-section	10^{-13} to $10^{-9a,b}$	m^2 $cell^{-1}$
a^*	Chl-*a*- opt. abs. cross-section	$5 \cdot 10^{-14}$ to $5 \cdot 10^{-10}$ [a,b]	m^2 mg chl-a^{-1}
a^*_s	In vitro a^* (unpackaged)	0.06 to 0.11[c]	m^2 mg chl-a^{-1}
B	Benefit of the LHC		mg carbon $cell^{-1}$ h^{-1}
B	Size scaling exponent		Dimensionless
C	Cost of the LHC		mg carbon $cell^{-1}$ h^{-1}
c_i	Intracellular chlorophyll-*a* concentration	10^5 to 10^{8b}	mg chl-*a* m^{-3}
D	Cell diameter	10^{-6} to 10^{-3}	m
I	Growth irradiance	10^{-6} to $2 \cdot 10^{-3}$	mol photons m^{-2} s^{-1}
K	Metabolic rate at reference size		h^{-1}
k_{Pmax}	Maximum photosynthetic rate per cell at reference size	$10^{-9.95a}$	mg C $cell^{-1}$ h^{-1}
M	Metabolic rate; net photosynthetic rate, etc.		h^{-1}
N	Net benefit, photons harvested resulting in carbon fixed		mg carbon $cell^{-1}$ s^{-1}
τ	Average lifetime of the LHC over which the cost is amortized	~24[f]	hours
ϕ	Quantum yield of photosynthesis	0.1[d]	mol C/ mol photons
V	Organism size, normalized to a reference volume.		Dimensionless
ξ	Cost of the LHC (upper estimate for chlorophyll-*a*)	$7 \cdot 10^{-4g}$	mol photons mg chl-a^{-1}

a) Finkel (2001); b) Agustí (1991); c) Morel and Bricaud (1981); d) Kirk (1994);f) Riper et al. (1979); g) Raven (1984).

Following Morel and Bricaud (1981), light absorption for a spherical cell can be approximated as:

$$a = a^{*} c_i V, \quad (2.3)$$

where c_i is the intracellular chlorophyll-*a* concentration (mg chl-*a* m^{-3}), and a^{*} is the chlorophyll-*a* specific absorption cross-section (m^2 (mg chl-*a*)$^{-1}$), which is equal to,

$$a^{*} = \frac{3}{2} a_s^{*} \frac{Q(\rho)}{\rho} , \quad (2.4)$$

where a^{*}_s is the absorption coefficient of the cell's pigments in solution (m^{-2} mg chl-*a*) normalized to chl-*a*, and

$$Q(\rho) = 1 + 2\, e^{-\rho} / \rho + 2(e^{-\rho} - 1) / \rho^2 \quad (2.5)$$

where

$$\rho = a^{*}_s c_i d, \quad (2.6)$$

and d is cell diameter (m). For modeling purposes we use an intermediate estimate of 0.08 m^2 (mg chl-a)$^{-1}$ for the spectrally-averaged in vitro absorption coefficient of cellular pigment from Morel and Bricaud (1981).

The ratio a^{*}/a^{*}_s is known as the package effect because as the cell (or package) gets bigger, the specific optical absorption cross-section decreases. This has been established both theoretically and empirically. Internal geometry such as the packaging of pigments into chloroplasts (Berner et al. 1989) and the optical properties of vacuoles (Raven 1997) can also alter the light absorptive properties of photosynthetic cells, but for simplicity these details will not be included in this analysis.

Steady-state size scaling of photosynthesis under light saturating conditions

We integrate allometry into our resource-based model by defining P_{max}, the maximum cellular metabolic rate by a function similar to M in Eq. 2.1, with a size-scaling exponent of ¾,

$$P_{max} = k_{p_{\max}} \left(\frac{V}{V_0} \right)^{3/4}. \qquad (2.7)$$

The intercept, k_{Pmax}, is specific to the taxonomic group and steady-state growth irradiance (Finkel 2001). Under light-saturating conditions, photosynthesis (P) will scale with cell volume with an exponent of ¾, while under light-limitation the size scaling of photosynthesis is dictated by the size scaling associated with light absorption. This formulation is consistent with the two potential rate limiting processes: (1) the metabolic rate based on the acquisition of resources under light limiting conditions (M_R), and (2) the transport and metabolic consumption of those internal resources under light saturating conditions (M_T) (Figure 2.1).

Under steady-state conditions, the overall photosynthetic rate will be determined by the slower of these two processes: M = minimum (M_R, M_T) (Figure 2.1). Resource acquisition depends on external resource supply (for example, irradiance or nutrient flux), the fraction of internal resources allocated to the resource acquisition system (for example, light harvesting complexes, or enzymes and nutrient transporters), and the organism's size. In the case of light acquisition in unicellular phytoplankton, the rate of photon capture depends on total intracellular pigment concentration and cell size. The photons captured by photosynthetic pigments are used to generate reductant and, via an electrochemical H^+ gradient, ATP (Falkowski and Raven 1997). If the supply of photons

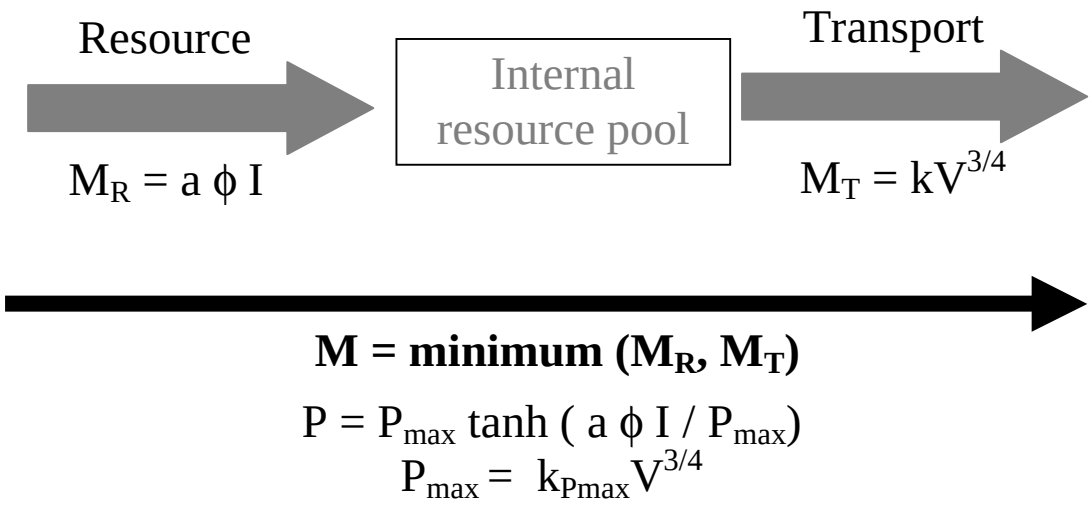

Figure 2-1. Metabolic rate (*M*) is determined by the minimum of the rate of supply of resources (M_R) and the transport of the supply of resources (M_T) within the cell. When phytoplankton are limited by light, their photosynthetic rate is determined by light acquisition (M_R). Light absorption by unicellular organisms is size-dependent due to the package effect, which affects steady state pigment concentrations and the effectiveness of the pigment at intercepting photons. When resources are not limiting and the internal resource pools are full, photosynthetic rate is determined by the transport of internal resources throughout the cell (M_T).

is insufficient to sustain the maximum photosynthetic rate, then photosynthesis is proportional to the rate of light acquisition. If the ATP and reductant pools are large enough to sustain the maximum photosynthetic rate, then the transport network that distributes the internal resources will ultimately limit the photosynthetic rate. We determine the consequences of this scheme on the size scaling of photosynthesis under light limiting versus light saturating conditions, and compare our theoretical predictions with experimental data.

How much pigment is required to maximize photosynthetic rate?

Phytoplankton cells regulate their pigment concentration in response to a change in incident irradiance (Falkowski and LaRoche 1991; MacIntyre et al. 2002; Richardson et al. 1983). To determine the size scaling of the resource driven photosynthetic rate we need to know how photosynthetic rate and resource acquisition depend on cell size and how the cell acclimates to the resource concentration in order to maximize its growth rate. It is therefore necessary to calculate the intracellular pigment concentration required to maximize photosynthesis for a given cell size at a given irradiance. This provides the basis for determining the size scaling exponent for light-limited photosynthetic rates. The intracellular pigment concentration required to maximize photosynthesis for a given cell size can be determined from a cost-benefit analysis of pigment. The benefit (B) of the pigment is the fixed carbon generated from the photons captured by the pigments that make up the light harvesting complex (LHC). For any single cell, Eqns. 2.2-2.6 describe the collection of metabolically useful energy by the LHCs. For simplicity, we are operationally assigning all pigment within the cell to the LHCs and assume that

chlorophyll-*a* is a dependable proxy for the total amount of pigment. This is a deliberately general description of the allocation of pigment; we are not distinguishing between changes in the ratio of photosystem II to photosystem I, the size or number of photosynthetic units, or the presence of non-photosynthetic pigments (Raven and Kubler 2002).

The cost (*C*) of the LHCs is the product of the quantum yield of photosynthesis ϕ, the total pigment per cell ($c_i V$, mg chl-*a* cell^{-1}), the inverse of the lifetime of the pigment within the cell (τ in hours) and its biosynthetic cost (ξ, mg carbon mg chl-a^{-1}). This cost function represents the synthesis and maintenance costs of the LHC, and is intended to account for the energetic cost of light acquisition. The LHCs of phytoplankton are genetically and phenotypically variable. Changes in the composition of the LHC alter the biosynthetic cost and lifetime of the LHC. Using the data available (Goericke and Welschmeyer 1992; Raven 1984; Riper et al. 1979), we assume a constant τ of one day, and use an average biosynthetic cost for chlorophyll-*a* as calculated by Raven (1984).

Steady-state size scaling of photosynthesis over a light gradient with explicit photoacclimation

The optimal intracellular pigment concentrations were determined by maximizing the net benefit (*N*), which can be expressed as the difference between the carbon equivalents harvested (*B*) and the cost (*C*) of producing and maintaining the photosynthetic machinery necessary for harvesting light,

$$N = B - C = P(I) - \frac{c_i V \xi \phi}{\tau}. \qquad (2.8)$$

Numerical optimization and other computations were performed using the statistical package R (Ihaka and Gentleman 1996). We first computed optimal values of c_i as a function of d. These optimal intracellular pigment concentrations were then used to predict photosynthetic rates as a function of cell volume and irradiance.

Growth and photosynthetic rates are commonly reported normalized to carbon, chlorophyll content or cell number, P^C, P^* and P^{cell}, respectively. This has the potential to cause considerable confusion, especially when comparing different size-scaling exponents. Under ideal conditions, P^{cell} should have a size-scaling exponent of ¾, while P^C and P^* are normalized by a measure of cell size and thus will have smaller size-scaling exponents. We expect that this exponent will be 1 less than the exponent of P^{cell}, because C cell$^{-1} \propto V$ and $P^C \propto P^{cell} \cdot C$ cell^{-1}, but this is not always the case (Montagnes et al. 1994; Montagnes and Franklin 2001; Strathmann 1967). Cellular carbon content in phytoplankton is species-specific and varies with growth irradiance (Thompson et al. 1991). In the present study, we assume carbon increases linearly with volume.

In accordance with previous experimental data (Agustí 1991, Finkel & Irwin 2000, Finkel 2001), we view c_i and P^{cell} as power-law functions of cell volume. The size-scaling exponents were estimated from linear regression. Over the size-ranges considered, model outputs are not always straight lines, thus the range of cell volumes considered influences the estimate of the size-scaling exponent. We used the numerical model to produce data, which might have been obtained from experiments if our models were perfectly correct, and then determine the size-scaling exponent from this simulated data in the same way we estimate exponents from laboratory data.

Results

Steady-state size scaling of photosynthesis over a light gradient

The size dependence of the cellular photosynthetic rate depends on the steady state irradiance and I_k (the irradiance where saturation occurs). At irradiances below I_k, the size-dependence of light absorption and intracellular pigment concentration. At irradiances above I_k, the size-dependence of photosynthesis is dictated by the size-dependence of the maximum photosynthetic rate and is proportional to $V^{3/4}$ (Eq. 2.7). When we assume c_i does not change with cell size the model predicts that cellular light-limited photosynthetic rates scales from $V^{2/3}$ to V^{1} as a function of c_i (Figure 2.2). Experimental evidence shows c_i does change with cell size, suggesting we must determine how c_i changes as function of cell size and irradiance to have a realistic prediction of the size scaling of light-limited photosynthetic rate.

How much pigment is needed to reap the largest photosynthetic rate?

Under sub-saturating irradiance we can approximate the benefit of pigment as $B_L = a\phi I$. We then determine the intracellular pigment concentration required to optimize the net benefit ($N=B_L - C$) per cell by differentiating with respect to c_i and setting the derivative equal to 0,

$$\frac{dN}{dc_i} = \frac{\pi}{6} d^3 \left(a^* I - \xi/\tau\right) - \frac{\pi I a_s^* d^3}{4\rho^3}\left(2\left(3+3\rho+\rho^2\right)e^{-\rho} - 6 + \rho^2\right) = 0, \quad (2.9)$$

and after some straightforward algebra we obtain

$$6 - 3\left(2+2\rho+\rho^2\right)e^{-\rho} - \frac{\xi}{a_s^* I \tau}\rho^3 = 0. \quad (2.10)$$

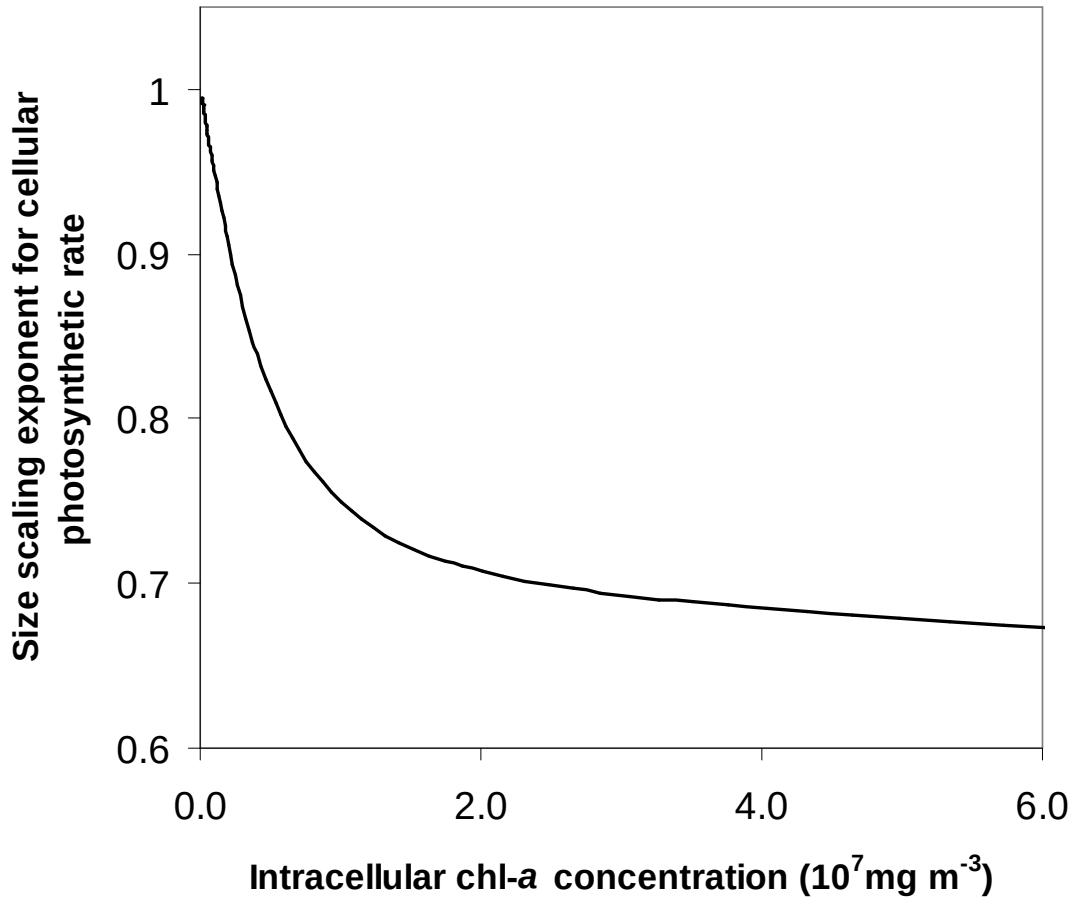

Figure 2-2. The volume scaling exponent (*b*) associated with cellular photosynthetic rate (*P*, mg C cell^{-1} h^{-1}) under low irradiance as a function of intracellular chlorophyll-*a* concentrations ($c_{i,}$ mg chl-*a* m^{-3}). Intracellular chlorophyll-*a* concentrations are treated as independent of cell volume.

Solving for c_i we find,

$$c_i = \frac{f(z)}{a_s^* d} \propto \frac{1}{d}, \tag{2.11}$$

where

$$z = \frac{a_s^* I \tau}{\xi}. \tag{2.12}$$

The magnitude of c_i depends on z, but the size-scaling exponent is independent of z. Our result, $c_i \propto \frac{1}{d}$, (Eqns. 2.11-2.12) is in excellent agreement with laboratory measurements of light-limited phytoplankton cultures (Figure 2.3).

The size-dependence of the optimal intracellular chlorophyll concentrations at all irradiances can be determined using numerical optimizations to maximize photosynthetic rate based on Eqns. 2.2-2.8. Our computations, in close agreement with measured data, show that intracellular pigment concentration increases with I under very low I, and above I_k decreases with I (Figure 2.4). Different species have different intracellular pigment concentrations based on species and class-specific differences in cell size, a^*_s, and the cost and turnover time of the different types of LHC. The increase in c_i with increasing irradiance at low I, despite corresponding increases in the package effect, is due to an increase in the marginal benefit with irradiance. As irradiances become saturating, harvesting more photons provides no additional net benefit, therefore intracellular pigment concentration decreases with irradiance and the package effect decreases. Given that the maximum cellular photosynthetic rate is proportional to $V^{3/4}$, our model predicts that the optimal c_i is proportional to $V^{-1/4}$ for $I \geq I_k$, and is proportional to $V^{-1/3}$ for $I < I_k$.

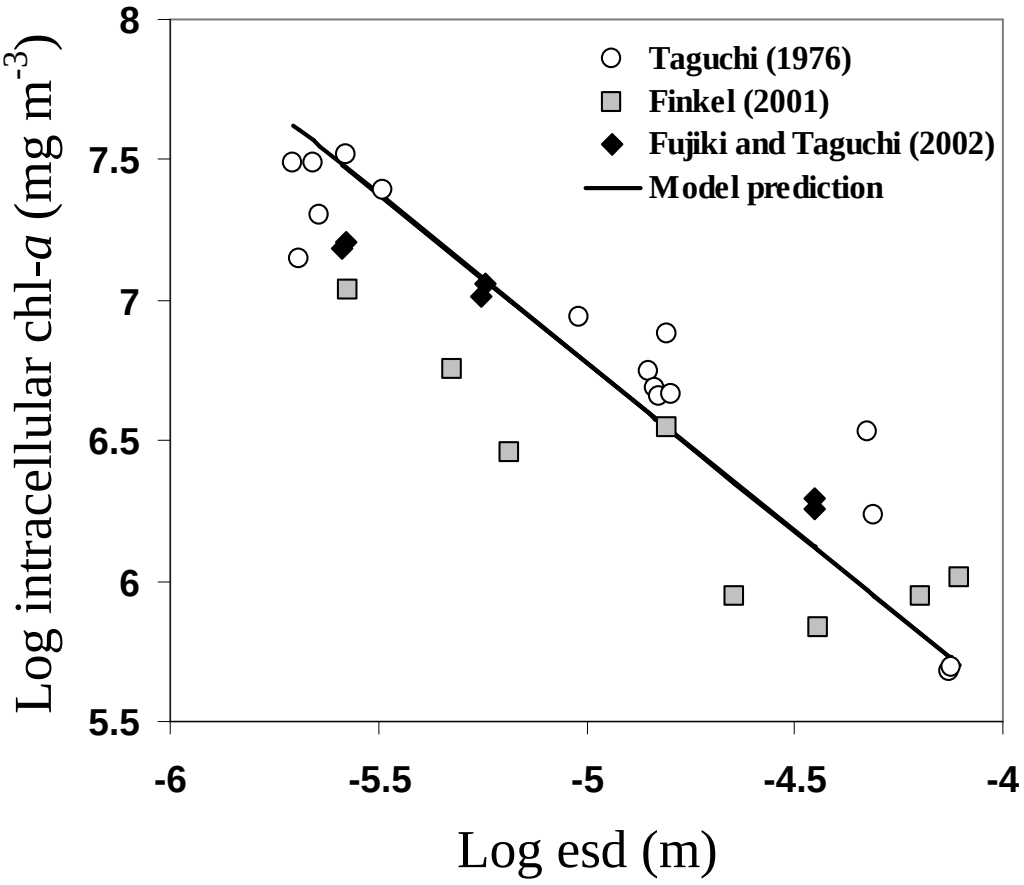

Figure 2-3. Intracellular chlorophyll-a concentration (c_i, mg chl-a m^{-3}) as a function of equivalent spherical diameter (μm) in 30 different species of light-limited, nutrient-saturated diatom cultures. The open circles are from (Taguchi 1976), the closed diamonds are from (Fujiki and Taguchi 2002), and the shaded squares are from (Finkel 2001). The volume scaling exponent calculated from reduced major axis regression on the experimental data is -1.01 ± 0.15, in agreement with our theoretical prediction (-1)

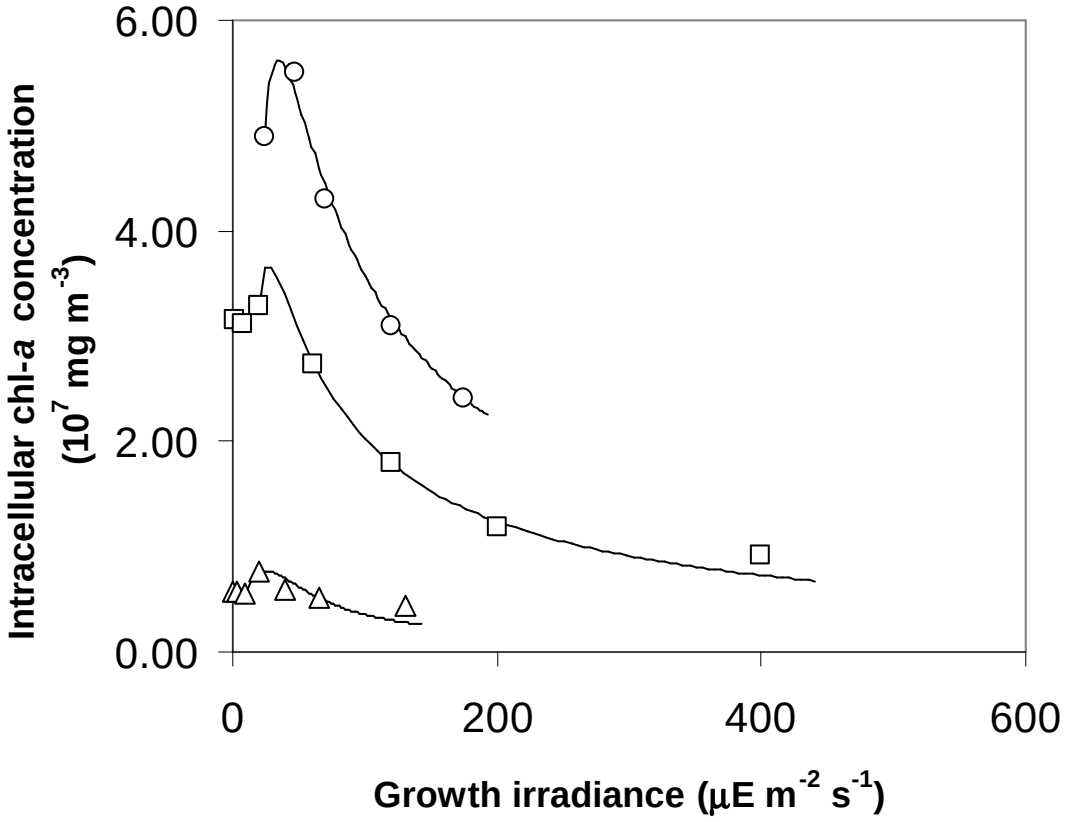

Figure 2-4. Comparison of experimentally derived and modeled intracellular chlorophyll-a concentration (c_i, mg chl-*a* m^{-3}) as a function of growth irradiance (I, μE m^{-2} s^{-1}). The theoretical model (solid lines) is the optimal c_i for each species, *Skeletonema costatum* (triangles) and *Dunaliella tertiolecta* (squares) from (Falkowski and Owens 1980), and *Emiliania huxleyi* (circles) from (Muggli and Harrison 1996). The models for different species differ from one another only by having different values of a^*_s, k_{Pmax}, τ and ξ. The values of these constants were selected by minimizing the sum of squared deviations between the data points and the predictions of c_i at the corresponding irradiance.

The theoretical predictions for the size scaling of intracellular pigment concentration compare well with Fujiti and Taguchi's (2002) experimental results on phytoplankton cultures. In this study, six different species, representing three different taxonomic groups, were grown over a range of irradiances. We calculated the size scaling of chlorophyll-*a* content per cell, Chl-*a* cell^{-1} = k_{Chl} V^{b}, for each irradiance by multiplying c_i by cell volume. The results show that under saturating irradiance the size-scaling exponent of cellular chlorophyll-*a* content with cell volume is ¾, in agreement with our theoretical prediction ($V^{-1/4} \cdot V = V^{3/4}$). As the growth irradiance decreases, the size scaling of chlorophyll content decreases towards 0.71±0.05 (95% confidence interval), in agreement with our theoretically predicted value under light-limitation (Figure 2.5).

The parameters in *z* (Eq. 2.12) can change the intercept, but not the slope of log c_i versus log *d*. This is important as different taxonomic groups, under different growth conditions, can have different values of a^{*}_{s}, ξ, and τ, which will alter the value of *z*. Changes in *z* that are correlated with cell size will appear to alter the slope of log c_i versus log *d*. For example, many of the largest cells are not spherical, but instead resemble very long and narrow, or, flat and squat, cylinders. A systematic shift in shape, from spherical cells to cylinders, with increasing cell size, will reduce the effect of self-shading on the size-scaling of photosynthesis and growth (Kirk 1976; Kirk 1994). Thus a change in shape can reduce the package effect and mitigate the potential reduction in size-scaling exponent of cellular pigment concentration and growth rates. This means that it is important to compare organisms with similar pigment composition and under similar growth conditions when calculating and comparing the slope of log c_i versus log

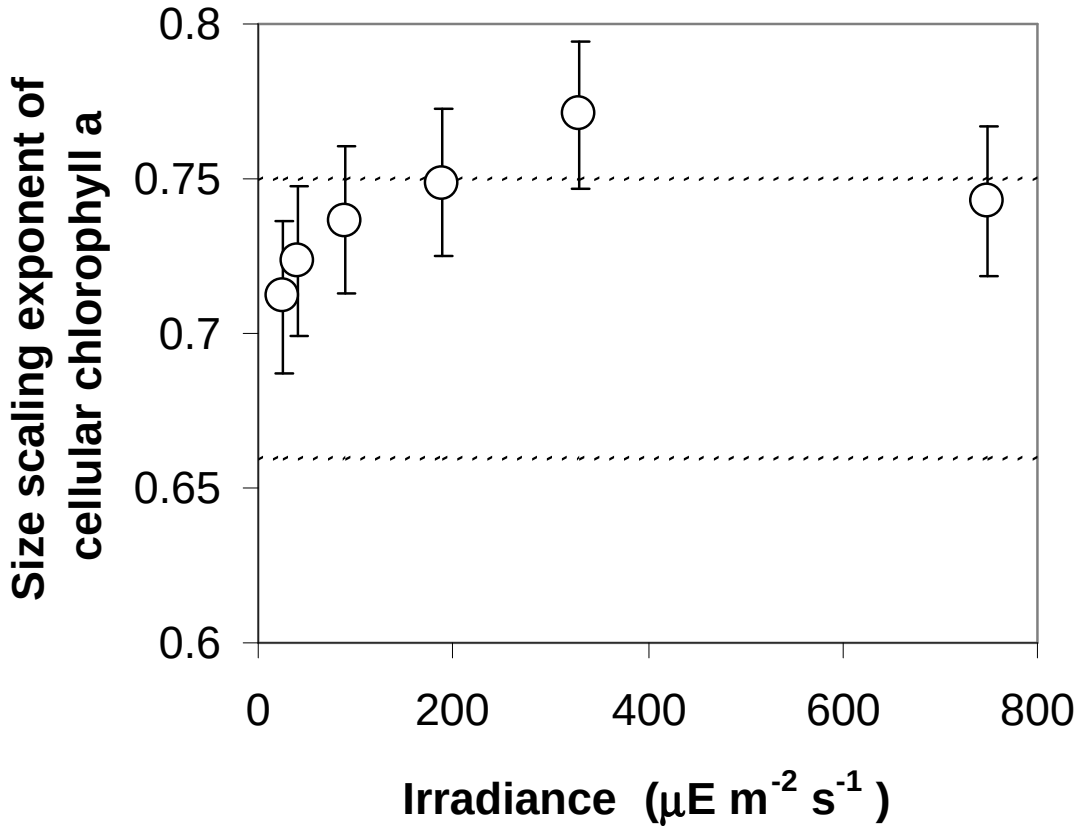

Figure 2-5. Comparison between the size scaling exponent (*b*) associated with chlorophyll-*a* per cell (mg chl-*a* cell^{-1}) as a function of steady-state irradiance (*I*, μE m^{-2} s^{-1}) as predicted by theory (dotted lines) and observed in experimental cultures (symbols, 1 s.e.). The size-scaling exponent of intracellular pigment content decreases with increasing light limitation. Open circles from (Fujiki and Taguchi 2002). As light becomes limiting, the size-scaling exponent decreases from a theoretical maximum of 0.75 to a theoretical minimum of 0.67.

d. Species-specific changes in the parameters in *z*, and changes in cell shape (aspect ratio), and subtle changes in growth conditions, are likely responsible for much of the variability in the experimental data presented in Figures 2.3-2.5.

Steady-state size scaling of photosynthesis over a light gradient with explicit photoacclimation

The relationship between the optimal c_i and cell size can be used to determine photosynthetic rate as a function of cell size, and the resultant size-scaling exponent. Under sub-saturating irradiance, photosynthetic rate is a function of the rate of light acquisition, and therefore scales with cell volume with a 2/3 exponent. Under saturating irradiance, growth is a function of the size-dependent transport network and therefore scales with cell volume with a ¾ exponent. These results are in good agreement with experimental work on phytoplankton (Table 2.2). These results should not be applied to organisms that are < 1 μm in diameter because non-scalable components such as a minimum DNA content can result in radical changes in cellular composition (Raven 1994). At intermediate irradiances between extreme light-limitation and saturation, photosynthetic rates will scale with cell volume with an exponent somewhere between 2/3 and ¾. This is because I_k, the irradiance that characterizes the transition from light limitation to light saturation is size-dependent. Commonly I_k is defined as $P_{max}/(a\ \phi)$ at low I. This means that I_k is affected by both the size-dependence of the transport network ($P_{\max} = kV^{3/4}$) and the size-dependence of light acquisition ($a = a^*\ c_i\ V$). Numerical calculations show that the volume size scaling of $I_k \propto V^{1/12}$. This means that there are

light intensities where photoacclimated small cells will be saturated for light, while larger cells are limited for light.

Table 2-2: The size scaling exponent as a function of cell volume of cellular photosynthetic rate (P^{cell}, mg C cell^{-1} h^{-1}) and cellular chl-*a* content (mg chl-*a* cell^{-1}) under light-limiting (25 μE m^{-2} s^{-1}) and saturating conditions. Numbers in parentheses are 2 s.e.

	P^{cell}		Chl-*a* cell^{-1}	
	Theory	Experiment	Theory	Experiment
Light-limiting	0.67	0.60 (0.08)[a,b*]	0.67	0.70 (0.03)[a,b,c]
Light-saturating	0.75	0.79 (0.04)[c]	0.75	0.75 (0.02)[c]

a) Finkel (2001), b)Taguchi (1976), c) Fujiki and Taguchi (2002)

* P^{cell} was calculated using the photosynthesis-irradiance parameters reported in (b), using an I of 25 μE m^{-2} s^{-1} to match (a), and an RMA regression was performed on the merged dataset.

Discussion

As organisms increase in size, their mass specific metabolic rates decrease due to geometric constraints (Banavar et al. 2002; West et al. 1997). Specifically, larger organisms must allocate a larger proportion of their mass to their resource transportation systems or suffer a reduction in their mass-specific metabolic rates. Generally, the

proportion of biomass allocated to transport systems is not strongly correlated with body size. As a consequence, under optimal growth conditions when resource supply matches demand, metabolic rate scales to the ¾ power of biomass (Banavar et al. 2002).

Under resource limiting conditions organisms must allocate an increasing proportion of their internal resources and total biomass towards resource acquisition. A size-dependence in resource gathering abilities can counter, or augment, the geometric constraints that cause the ¾ size scaling of metabolic rates. An increase in the ability to harvest resources with body size might lead to an increase in the size-scaling exponent of individual based metabolic rate, although constraints imposed by the demands of transportation networks will limit this effect. A decrease in the ability to harvest resources with body size will cause a decrease in the size-scaling exponent of individual based metabolic rate because there is no way for a transportation network to compensate for unavailable resources. Light acquisition by unicellular phytoplankton is just one example of the size-dependence of the ability to harvest resources due to geometric constraints.

Under light-limiting conditions, the rate of photon absorption determines the photosynthetic rate (Falkowski et al. 1985; Kiefer and Mitchell 1983). Light absorption in unicellular photoautotrophs depends on the incident irradiance, cell volume and shape, pigment concentration, composition, and distribution within the cell (Kirk 1994). Assuming optimal pigment composition and distribution, a cell can gather more photons only by increasing its pigment concentration. Under light saturating conditions, in the absence of any package effect, pigment scales with body mass with a ¾ exponent (Figure 2.5), not only for phytoplankton but also for higher plants (Niklas and Enquist 2001). As

Niklas and Enquist (2001) point out, this is precisely what is expected if natural selection adjusts pigment concentration to maximize metabolic rate. In other words, an organism should not harvest more energy than it can effectively use.

Photoautotrophs generally increase their pigment concentration in response to decreasing growth irradiance. Phytoplankton cellular pigment concentrations can increase as much as 5 to 9-fold in response to decreases in irradiance, in a matter of hours to days (Cullen and Lewis 1988; Falkowski and Owens 1980; Falkowski and LaRoche 1991; Ley and Mauzerall 1982; Post et al. 1984; Prezelin et al. 1986). Pigment responses to changes in growth irradiance are less dramatic in higher plants, although increases of 2 to 3-fold are not uncommon (Evans and Poorter 2001). This is not surprising given land plants generally experience higher photon flux densities, and spend their whole lives in one location. Phytoplankton cells are continually mixed throughout the water column, and have the ability to acclimate to a wide range of light intensities. Due to the cost of the LHC there is both a size and irradiance-dependent limit to pigment acclimation in response to irradiance.

The maximum pigment concentration or cell size that can be maintained at a given irradiance is governed by the cost of the LHC and the diminishing returns associated with the increasing internal self-shading of pigment that leads to the decrease in the pigment-specific light absorption coefficient. The package effect depends on the product of the intracellular pigment concentration and cell diameter ($c_i d$, Eqns 2.3-2.6). If c_i is constant, the package effect increases with diameter, and light-limited pigment-specific light acquisition drops rapidly with cell volume. As a result, larger phytoplankton cannot afford to maintain the same intracellular pigment concentrations as

smaller cells. This accounts for the inverse relationship between c_i and d reported for phytoplankton (Agustí 1991, Finkel 2001). Consequently, the decrease in cellular photosynthesis with decreasing irradiance is size-dependent with an exponent other than ¾.

Other forms of resource limitation may also alter the ¾ size scaling of metabolic rates if the acquisition of the resource is size-dependent. For example, nutrient limitation may also cause anomalous size scaling of metabolic rates in a variety of organisms, including phytoplankton (Eppley et al. 1969; Gavis 1976; Hein et al. 1995; Hudson and Morel 1993). Consider, nutrient uptake (U, Nutrient · (cell · h)$^{-1}$) by a phytoplankton cell, which depends on nutrient diffusion (Pasciak and Gavis 1974):

$$U \propto 4 \pi d D \Delta C, \qquad (2.13)$$

where d is the equivalent spherical diameter, D is the diffusion coefficient of the nutrient in question, and ΔC is the concentration gradient of the nutrient from the cell surface to the concentration in the bulk media. In a Droop-type model, uptake (U) is a function of the growth rate (μ, h^{-1}) and the cellular quota for that nutrient (q, Nutrient · cell^{-1}):

$$U = \mu q, \qquad (2.14)$$

where $q \propto V^{3/4}$ (Stolte and Riegman 1995). At equilibrium, we can assume that these two expressions for uptake are equal. Rearranging Eqns 2.13 & 2.14 we can solve for the size dependence of the growth rate; $\mu \propto V^{-5/12}$. Future models should also consider the dependence of uptake and cell quota on nutrient concentrations in the bulk media (nutrient acclimation). More research is needed to determine if size dependent resource acquisition for other limiting resources, and in other organisms, causes similar changes to the size scaling of metabolic rates.

Conclusions

The ¾ rule of metabolic rates is a key concept in macroecology (Brown 1995). It has been suggested that the ¾ rule is the key to understanding not only metabolic rates but also fundamental ecological and evolutionary patterns in abundance and diversity (Rosenweig 1995; Whitfield 2001). Yet there are many reported examples where ¾ rule does not apply. We present a model that demonstrates that resource limitation causes quantifiable, predictable deviations from the ¾ rule.

Specifically, we demonstrate that when irradiance limits photosynthetic rates in phytoplankton, light acquisition alters the size scaling of photosynthesis. In the absence of photoacclimation, the size scaling of cellular photosynthetic rate is proportional to V^b where b ranges from 2/3 to 1 depending on the intracellular pigment concentration, irradiance and size range considered. In actuality, phytoplankton acclimate to their incident irradiance via changes in intracellular pigment concentration in order to maximize their cellular photosynthetic rate as a function of irradiance. There is a size-dependence associated with the ability of phytoplankton cells to acclimate to decreases in irradiance via their intracellular pigment concentrations due to the package effect. As a consequence, larger phytoplankton cells support lower maximum intracellular pigment concentrations, and require higher irradiances to reach their maximum cellular photosynthetic rate. This suggests that smaller phytoplankton cells are at an advantage over larger cells under steady-state light-limiting conditions.

Incorporating pigment acclimation into our model allows us to predict the irradiance and size-dependence of intracellular pigment concentration, and the resultant

change in the size scaling of exponent associated with cellular photosynthetic rate. We predict that the size scaling of cellular photosynthesis is proportional to $V^{¾}$ under light saturating conditions and decreases towards $V^{2/3}$ as light becomes limiting, in good agreement with experimental data. This example suggests that other forms of resource limitation in other types of organisms may also alter the size scaling of metabolic rates.

Chapter 3. Irradiance-induced changes in the elemental composition of marine phytoplankton

Abstract

The elemental composition, C, N, P, S, K, Mg, Ca, Sr, Fe, Mn, Zn, Cu, Co, Mo and Ni of 5 marine phytoplankton species representing the 4 major marine phyla was analyzed over a light gradient. There is substantial variability in the elemental composition between different taxa consistent with previously reported differences associated with evolutionary history. Large changes in Fe:P and Mn:P have been previously reported as a function of irradiance. Many elements were enriched relative to phosphorus by up to 2-3 orders of magnitude under irradiances that are limiting for growth including: Fe, Mn, Zn, Cu, Co, Mo, Sr, and Mg. For some species a select number of elements became enriched relative to phosphorus at saturating irradiances including Fe, Mn and Zn in the coastal diatom *Thalassiosira weissfloggi*, and Co in the diazotroph, *Cyanothece* sp. and the Prasinophyte, *Pycnococcus provasolii*, indicating an increased requirement for these elements under saturating irradiance and high growth rates. For most elements the variability in element:P due to irradiance is comparable to the variability due to phylogenetic differences at any irradiance, but often the interaction between genetic differences and the phenotypic response to irradiance acts to amplify the differences between taxa in elemental composition. The fractionation of Cu and Mn relative to phosphorus into phytoplankton biomass under low light is consistent with depleted levels of Cu^{+2} and Mn^{+2} in deep chlorophyll maxima suggesting that the export of low light

acclimated phytoplankton may be a major source of trace element flux to the deep ocean and an important factor in the biogeochemical cycles of many of the biologically limiting elements in the oceans.

Introduction

The availability of light, macro- and micronutrients in the surface ocean plays a significant role in the regulation of phytoplankton community structure and rates of primary production. Many current models of primary production assume light and biomass are the principal determinant of rates of primary production (Behrenfeld and Falkowski 1997; Campbell et al. 2002), and nitrogen and then phosphorus are the most common limiting nutrients (Falkowski 1997a), although iron is proximately limiting in large regions of the ocean (Martin et al. 1994). There is little evidence to suggest that the other biologically required elements limit marine primary productivity, but several elements (eg. Si) have been hypothesized to affect phytoplankton community structure through genetic differences in elemental composition and rates of nutrient uptake.

A recent analysis of major nutrients and trace elements in 29 algal species from the major phylogenetic groups under uniform culture conditions indicated that there are systematic phylogenetic differences in the elemental composition of phytoplankton (Falkowski 2004; Quigg et al. 2003). Based on an analysis of available experimental data, Ho *et al*. (2003) deduced that phenotypic differences in elemental composition due to environmental conditions such as irradiance, macronutrient, and micronutrient concentration rarely result in more than 2 to 5 fold variability in element (E):P in response to an order of magnitude range in irradiance or macro-nutrient concentration, or

an order of magnitude variability for over 3 orders of magnitude variation in trace metal concentrations. On this basis Quigg *et al.* (2003) and Ho *et al.* (2003) hypothesize that phenotypic variation in elemental stoichiometry is much smaller than genetic differences between taxa, leading to the hypothesis that differences in elemental composition among species primarily represent phylogenetic differences in biochemical requirements and the ability of the organisms to take up and store these elements, not environmental or culture conditions.

Elemental stoichiometry can be strongly affected by irradiance and light regime. Light is expected to affect the cellular concentration of elements that are required for light harvesting and oxygenic photosynthesis: N, Fe and to a lesser extent Mn (Ho et al. 2003; Raven 1988; Raven 1990; Sunda and Huntsman 2004). Experimental studies on diatoms, prymnesiophytes and dinoflagellates indicate that a decrease in growth irradiance can result in an increase the cellular concentration of Fe and Mn which have a critical role in light harvesting and photosynthesis. Surprisingly few studies have been conducted to look at the change in elements other than C,N, P, or Fe as a function of growth irradiance. Recently Sunda and Huntsman (2004) found that the cellular concentration of Zn increased with decreasing light period in the coastal diatom *Thalassiosira pseudonana*. This suggests that elements not intimately associated with light harvesting may also be affected by irradiance. No work has simultaneously examined the effect of irradiance on a large range of major biologically required elements in phytoplankton. I analyzed the elemental composition, C, N, P, S, K, Mg, Ca, Sr, Fe, Mn, Zn, Cu, Co, Mo and Ni, of 5 marine phytoplankton species representing 4 major marine phyla over a light gradient to

test the hypothesis that irradiance is responsible for a relatively small proportion of the total variability in the elemental stoichiometry of phytoplankton.

Materials and methods

Culturing and sampling

Phytoplankton species investigated in this study included one nitrogen fixing cyanobacterium *Cyanothece* sp., one Prasinophyte (green) alga, *Pycnococcus provasolii* (CCMP 1203), one dinoflagellate, *Amphidinium carterae* (CCMP 1314), and two diatoms *Thalassiosira weissflogii* (CCMP 1336) and *Chaetoceros calcitrans* (CCMP 1315). The algae were grown at 19±1°C using a 12h:12h light dark cycle at five irradiances: 15 ,30, 100, 250, and 500 μmol quanta $m^{-2}s^{-1}$. Replicate culture samples (n>2) were maintained in exponential growth through a minimum of 6 generations before harvesting. Cell density and size were determined with a Coulter particle counter to calculate growth rates and cell volumes from the equivalent spherical diameters.

All apparatus for medium preparation, algal culturing and sampling, and elemental analysis was prepared according to rigorous acid cleaning procedures (Cullen et al. 2001). Cells were cultured in the medium Aquil prepared and sterilized according to Price *et al.* (1988, 1989). Synthetic ocean water (SOW) was enriched with sterile and metal free 150 μM $NaNO_3$, 10 μM Na_2HPO_4, and 40 μM Na_2SiO_3, plus 0.1 μM vitamin B_{12}, 0.1 μM biotin, 20 μM thiamin and 100 nM Na_2MoO_4. In the presence of 100 μM EDTA, at 250 μmol quanta $m^{-2}s^{-1}$, total trace metal concentrations were: Mn_T = 120 nM, Zn_T = 80 nM, Cu_T = 20 nM, Co_T = 50 nM and Cd_T = 15nM, calculated to yield unchelated concentrations of Mn′ = 10 nM, Zn′ = 20 pM, Cu′ = 0.2 pM, Co′ = 20 pM and Cd′ = 20

pM (Price et al. 1988/89; Westall et al. 1986). Further details of media preparation and sample digestion are provided in Ho *et al*. (2003).

Elemental analysis

All elements but carbon and nitrogen were assayed with a sector field HR-ICPMS (*Element 2*, ThermoFinnigan) fitted with a self-aspirating micro-flow Teflon nebulizer (PFA-100, Elemental Scientific Inc.) and a quartz Scott-type double pass spray chamber. Except for K, which was analyzed at high resolution ($m/\Delta m \cong 13000$), the analysis was conducted at medium resolution ($m/\Delta m \cong 5000$). Sensitivity and stability of the machine were adjusted to optimize conditions prior to sample analysis. The sensitivity was around $1\text{-}2\times10^6$ counts per second for 10 ppb under medium resolution. For the elements with more than one stable isotope, two isotopes were measured to confirm low interference: Mg 24/26, Ca 42/44, S 32/34, Fe 56/57, Cu 63/65, Zn 64/66, Sr 86/88, Mo 95/98, and Cd 110/111. The concentration differences between the two isotopes were less than 5 % for all these elements. Triplicate samples for carbon and nitrogen analysis were obtained by filtering 25-50 ml culture samples onto precombusted 13 mm GF/F filters or Gelman AE GF filters. These were analyzed for C and N content using a Carlo Erba elemental analyzer. Outliers were identified and removed if E:P was >1 order of magnitude larger than other replicates. Often Ni was below the detection limit of our method, and we were unable to get triplicate measurements for all irradiances for all species, but because Ni measurements are so sparse in the literature we decided to include the 36 successful measurements obtained but did not include Ni in many of the statistical analyses used to determine the proportion of the variance in E:P due to irradiance. Observations from 250

μmol quanta $m^{-2}s^{-1}$ treatment previously published in (Falkowski 2004; Ho et al. 2003; Quigg et al. 2003) are reported for comparison. All E:P ratios were log transformed to stabilize the variance.

Results

The anti-log of the mean of the log transformed E:P measured for the 5 different species of marine phytoplankton as a function of growth irradiance are presented in Table 3.1. Elemental ratios are only available for 3 irradiances, 15, 30, and 100 μE m^{-2} s^{-1} for *Chaetoceros calcitrans* because it could not tolerate 250 and 500 μE m^{-2} s^{-1}. As has been noted in previous studies, normalization per cell, cell volume, or nitrogen or carbon will change values and will quantitatively and sometimes even qualitatively alter trends. In this study, cellular phosphorus, nitrogen, carbon and cell volume are all highly correlated indicating most trends in E:P will be be common to E normalized to cell volume or carbon (Table 3.2). Normalization to P is preferred since it was measured simultaneously with the majority of the elements using ICPMS. Recent results on *Trichodesmium* spp. and two diatom cultures indicate that phosophorus can accumulate on the outside of phytoplankton cells (Sanudo-Wilhelmy 2004). If true for the phytoplankton in this study this suggests that E:P may be overestimated, but the correlation of cellular P with C, N and cell volume indicate all the trends among species and with irradiance are robust.

Table 3-1. Mean E:P of marine phytoplankton as a function of growth irradiance (*I*, μE m^{-2} s^{-1}). The units for C, N, S, K, Mg and Ca is mol:mol P, and for Sr, Fe, Mn, Zn, Cu, Co, Cd, Mo, and Ni is mmol:mol P with 1 standard error in % in brackets. Some of the data from the 250 μE m^{-2} s^{-1} treatment are from Quigg *et al*. (2003). If there was only one replicate no standard error is reported, * indicates two replicates, § indicates more than 3 replicates, and no symbol is used for three replicates.

Table 3-2. Correlations between cell size (cell volume, V in μm^3) and cellular C, N, and P (mol), all are highly significant, $p<<0.0001$.

Elements		R	n
P	C	0.80	94
P	N	0.79	94
P	V	0.86	94
V	C	0.89	94
V	N	0.87	94
N	C	0.98	94

Table 3-3. Multiplicative range (maximum/minimum) in E:P as a function of irradiance and taxonomic differences. Units are as defined in Table 3.1. I/T is the ratio of multiplicative ranges for Irradiance and Taxa.

		Multiplicative Range				
Me:P	**Median**	**Total**	**Irradiance**	**Taxa**	**I/T**	**n**
S:P	1.21E+00	7.5	4.7	4.1	1.1	64
K:P	7.96E-01	36	19	12	1.6	55
Mg:P	5.30E-01	43	13	43	0.3	60
Ca:P	2.18E-01	22	19	11	1.7	51
Fe:P	1.48E-02	900	87	250	0.3	73
Mn:P	4.12E-03	940	94	250	0.4	74
Mo:P	4.12E-03	380	70	80	0.9	67
Zn:P	2.05E-03	480	140	320	0.4	71
Sr:P	1.26E-03	57	21	57	0.4	58
Cu:P	4.35E-04	18000	2800	6000	0.5	70
Co:P	9.77E-05	350	64	54	1.2	63
Cd:P	2.31E-05	1200	590	70	8.5	73

Genetic differences versus phenotypic response in log E:P over a range of growth irradiance

A principal component analysis using the correlations between log E:P was used to visualize the relative effect of genetic differences and phenotypic response to growth irradiance on two groupings of elements, the trace metals, Fe:P, Mn:P, Zn:P, Cu:P, Cd:P, Co:P, and the alkali and alkaline earth metals, S:P, K:P, Mg:P, Ca:P, Sr:P (Figure 3.1). These two sets of elements were considered separately because observations of the two sets of elements were frequently not paired and an aggregate consideration would precipitously decrease the sample size. The first two principal components account for 87.6 % of the variance in transition metal data and 64.4% of the variance of the alkali and alkaline earth metal data.

The first principal component for the trace metals separates the observations by growth irradiance and accounts for 65% of the total variance in the data. Most metals are enriched relative to phosphorus, especially Fe, Mn and Cu and Zn under low light, 15 and 30 $\mu E\ m^{-2}\ s^{-1}$, and become increasingly depleted relative to phosphorus under irradiances saturating for growth, 250 and 500 $\mu E\ m^{-2}\ s^{-1}$. *Thalassiosira weissflogii* and *Pycnococcus provasolii* both have much lower metal enrichments at low light than the other species. The second principal component for the trace metals separates out species-specific differences, the relative enrichment of Cd and Co versus Zn separate out *Amphidinium carterae* which is enriched in Cd and Co and depleted in Zn relative to the other species especially at the highest and lowest irradiances. There is less spread in the observations over the second principal component at intermediate irradiances.

There are fewer observations for alkali and alkaline earth metals but the first

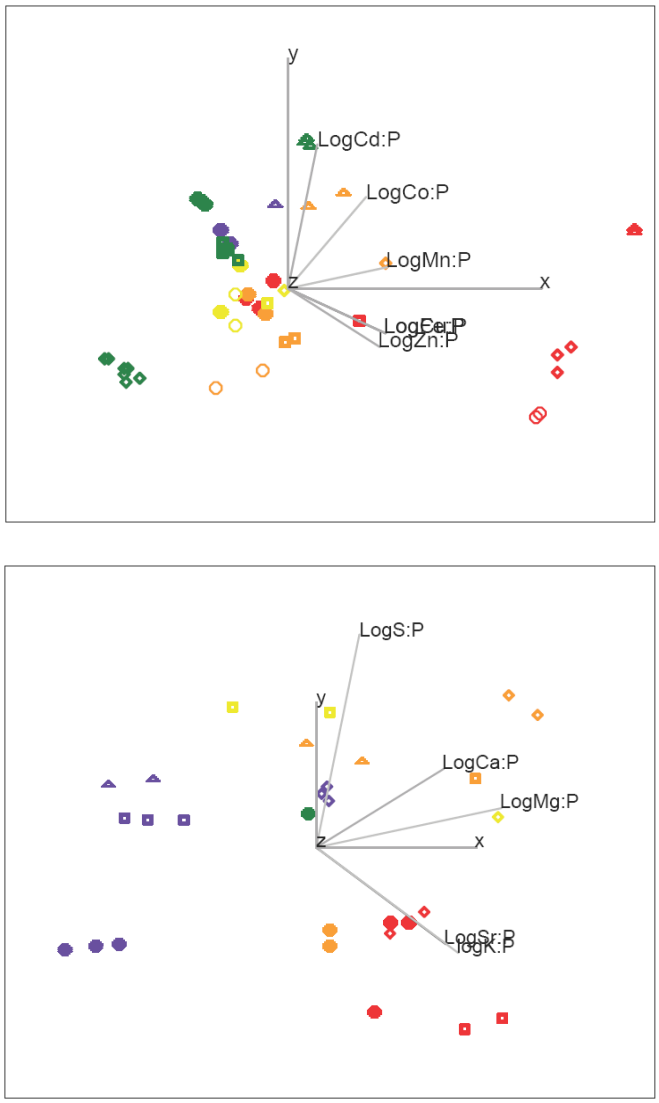

Figure 3-1. Principal component analysis on correlations for: Top panel (a) the transition metals Log Fe:P, Mn:P, Zn:P, Cu:P, Cd:P, Mo:P. The first 2 components account for 83.4 % of the data. Bottom panel (b) the macronutrients and alkali and alkaline earth metals, Log C:P, N:P, S:P, K:P, Mg:P, Ca:P, Sr:P. The first 2 principal components account for 61.3% of the variance. Colors represent light treatments: 500 (blue), 250 (green), 100 (yellow), 30 (orange), and 15 $\mu Em^{-2}s^{-1}$ (red), and shapes represent species: closed circles *T. weissflogii*, open circles *C. calcitrans*, squares *P. provasolii*, triangles *A. carterae*, and diamonds *Cyanothece sp.*.

principal axis also separates out different light treatments where all elements are relatively more enriched under low light, especially Mg:P and Ca:P. The other elements, S, K, and Sr, appear to reflect species-specific differences, for example high K:P or Sr:P relative to high S:P separates the diatoms *Chaetoceros calcitrans* and *T. weissflogii* from *A. carterae*.

The multiplicative range (maximum/minimum) of E:P is strongly correlated with its proportion of cell mass (Figure 3.2). Carbon, N and S all exhibit <8-fold range (Table 3.3), the alkali and alkaline earth metals have ~1 order of magnitude range, and the trace metals tend to have 2-3, and Ni and Cu exhibit >3 orders of magnitude variation in their multiplicative range. The variation in any given E:P is a function of both taxonomic differences and growth irradiance. Overall, irradiance and phylogenetic affiliation both accounted from 4 to 30-fold variation in the multiplicative range of E:P, depending on the particular element (Table 3.3). For the alkali and alkaline earth metals irradiance and phylogenetic differences tended to account for a large proportion or slightly more than the multiplicative range of the total dataset. For many of the transition metals, Fe, Mn, Mo, Cu, Co, and Cd, but not Zn, the range due to irradiance and taxonomic differences tended to be less than half of the multiplicative range of the whole dataset indicating that variation in E:P is a multiplicative function of both the species and growth irradiance. An analysis of variance supports the hypothesis that both taxonomic differences and irradiance are significant sources of variation in E:P (Table 3.4). Only log Mg:P and log Cu:P was not significantly different (ANOVA, $p<0.05$) between taxa, and only log Ca:P exhibited no significant change with growth irradiance. Although log Cd:P does not appear to vary with irradiance (Figure 3.3), individual species have opposite functional

responses, obscuring the pattern.

Table 3-4. Analysis of variance of E:P as a function of irradiance and taxonomic differences, showing proportion of variance explained by a linear model and significance level.

	TAXA		IRRADIANCE		
	r^2	p-value	R^2	p-value	n
LogS.P	0.27	0.001	0.34	<0.0001	64
logK.P	0.34	0.0003	0.29	0.0018	55
LogMg.P	0.13	0.09	0.53	<0.0001	60
LogCa.P	0.46	<0.0001	0.06	0.56	51
LogSr.P	0.19	0.02	0.30	0.0006	58
LogFe.P	0.22	0.002	0.57	<0.0001	73
LogMn.P	0.17	0.01	0.45	<0.0001	73
LogZn.P	0.17	0.01	0.71	<0.0001	71
LogCu.P	0.11	0.09	0.66	<0.0001	70
LogCo.P	0.39	<0.0001	0.22	0.005	63
LogMo.P	0.19	0.01	0.49	<0.0001	68
LogCd.P	0.62	<0.0001	0.40	0.6	73

Functional response in E:P as a function of growth irradiance

In general most macronutrient:P did not change consistently with irradiance across the different species examined: C:P was high at high light for *A. carterae* and high at low light for *T. weissflogii* and *Cyanothece.* sp.; N:P tended to decrease with irradiance for *T. weissflogii*, *Cyanothece sp.* and *A. caterae* but did not significantly change for *C. calcitrans* or *P. provasolii*; and although the standard error on Log Ca:P is only ~10% of the mean and is generally depleted at high irradiance, Ca:P increases with irradiance for *Cyanothece*. sp.. Log S:P is the exception, for the species with observations for more than 3 irradiances, Log S:P has a weakly unimodal relationship with irradiance (Figure

3.4). Most of the trace elements, Fe, Mn, Zn, Cu, Co, S, Mo and Ni, and the macronutrients, K and Mg, are enriched relative to phosphorus under irradiances that are limiting for growth (Figure 3.3). For some species, a select number of elements are enriched relative to phosphorus at saturating irradiances including Fe, Mn and Zn in *T. weissfloggi*, and Co in *Cyanothece* sp. and *P. provasolii*, suggestive of an increased requirement for these elements under saturating irradiance and high growth rates (Figure 3.3). Cadmium is a special case; the diatoms become enriched in Cd:P with irradiance while *Cyanothece* became depleted in Cd:P with increasing irradiance.

Functional response in net steady state uptake rate as a function of growth irradiance

In the case of Fe, previous studies have found that steady state iron uptake is a Michaelis-Menton function of free iron availability in the media, and that increases in growth rate, as would occur with an increase in irradiance can dilute Fe:P or Fe:C (Sunda and Huntsman 1997). The steady state uptake rate (V_{ss} = E:P · μ, in mol E/ mol P h) for almost all elements is a function of irradiance, indicating that elemental composition is not only due to dilution by growth, but that steady-state nutrient uptake is actively regulated as a function of growth and irradiance (Figure 3.5 & 3.6). For all species except *T. weissflogii*, steady-state trace element uptake rate, Fe, Mn, Cu, Co, Mo and Mg, is much higher under low irradiance (15 and 30 μE m^{-2} s^{-1}). As a result Mn:P, Fe:P, Zn:P, Mo:P, Co:P can reach ~ 1 order of magnitude and Cu:P more than 3 orders of magnitude higher under low versus high growth irradiance. In *T. weissflogii* uptake for Fe, Mn, Zn, Cu, Co all increase at 500 μE m^{-2} s^{-1} relative to 250 μE m^{-2} s^{-1}. The uptake

rate of alkali and alkaline earth metals tends to be unimodal, but not for all species.

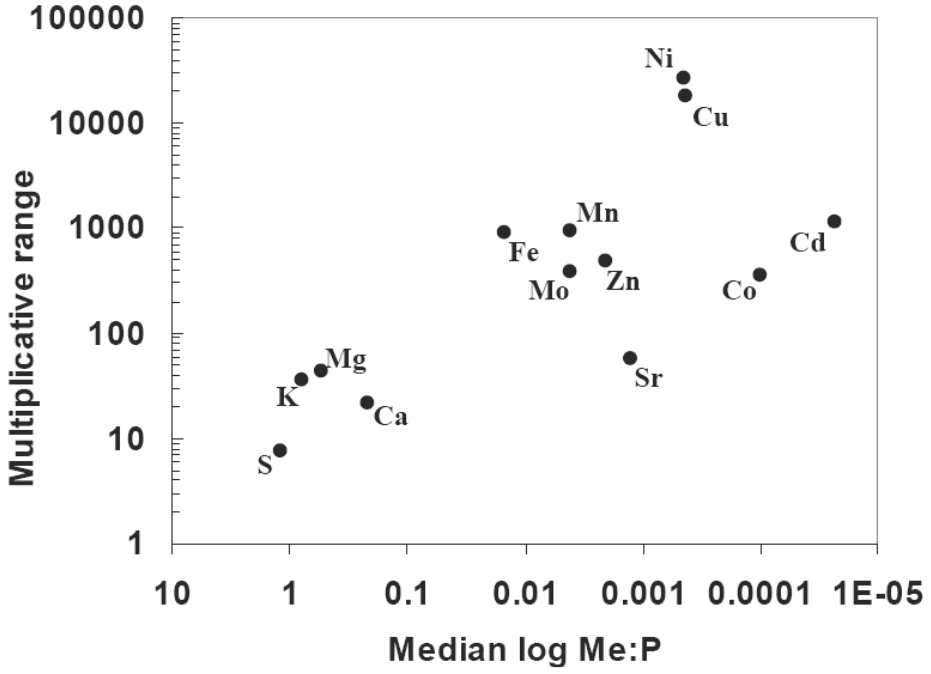

Figure 3-2. Multiplicative range (maximum/minimum) in E:P as a function of total contribution to cellular biomass (Median E:P). Macronutrients are reported as mol/mol, micronutrients mmol/mol.

Elemental correlations as a function of irradiance

Many of the Log E:P are correlated. The pairwise correlations between log E:P at each growth irradiance indicated a shift in the elements that are significantly ($p<0.05$) and highly correlated ($r^2>0.8$) at different irradiances unless otherwise indicated (Figure 3.7). The overall number of and type of elements correlated is related to irradiance, the largest number of correlations occurs at the highest growth irradiance, very few significant correlations at intermediate irradiance. The correlations at low irradiance are predominantly trace metals, many of which are involved in photosynthesis. At saturating

irradiances a mix of alkali and alkaline earth metals and S are correlated with trace elements that appear to be needed for high growth at high irradiance, Co, Mn, Fe and Mo.

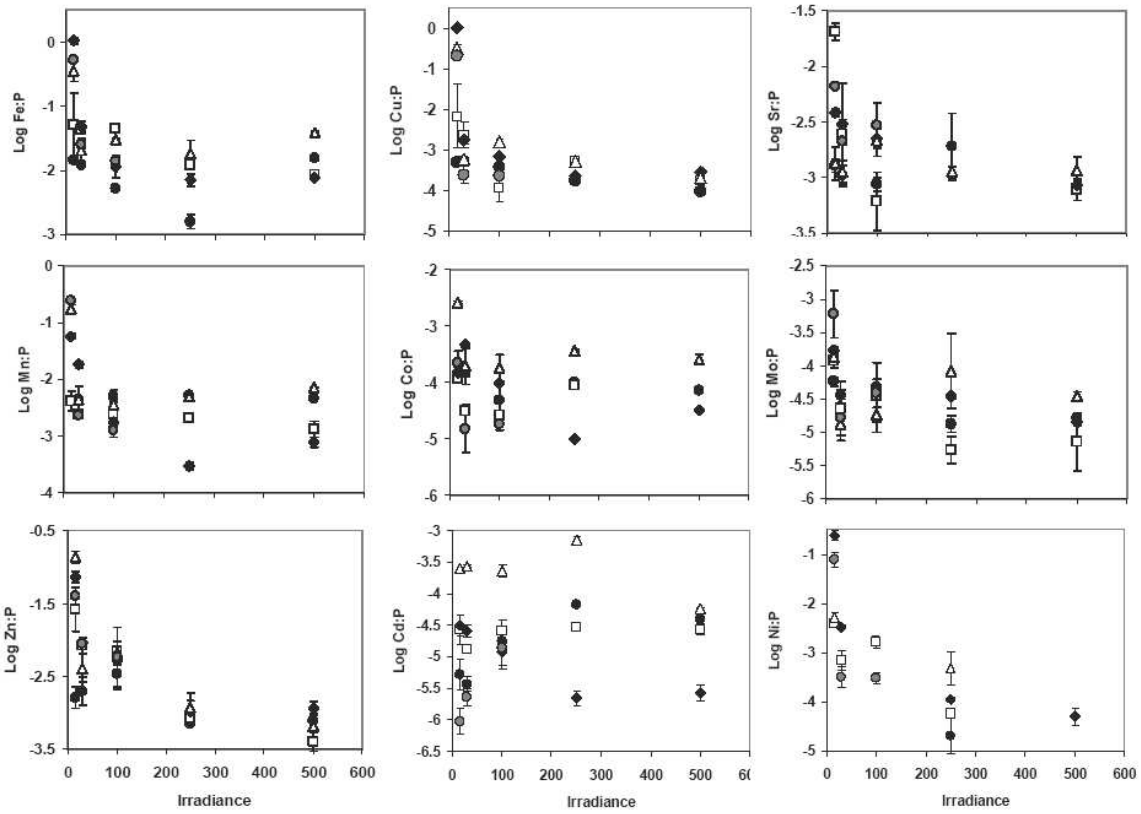

Figure 3-3. Log E:P and one standard error as a function of growth irradiance: transition metals. The different species are denoted by symbols: black circles *Thalassiosira weissflogii*, gray circles *Chaetoceros calcitrans*, open squares *Pycnococcus provasolii*, open triangles *Amphidinium carterae*, and black diamonds *Cyanothece sp.*.

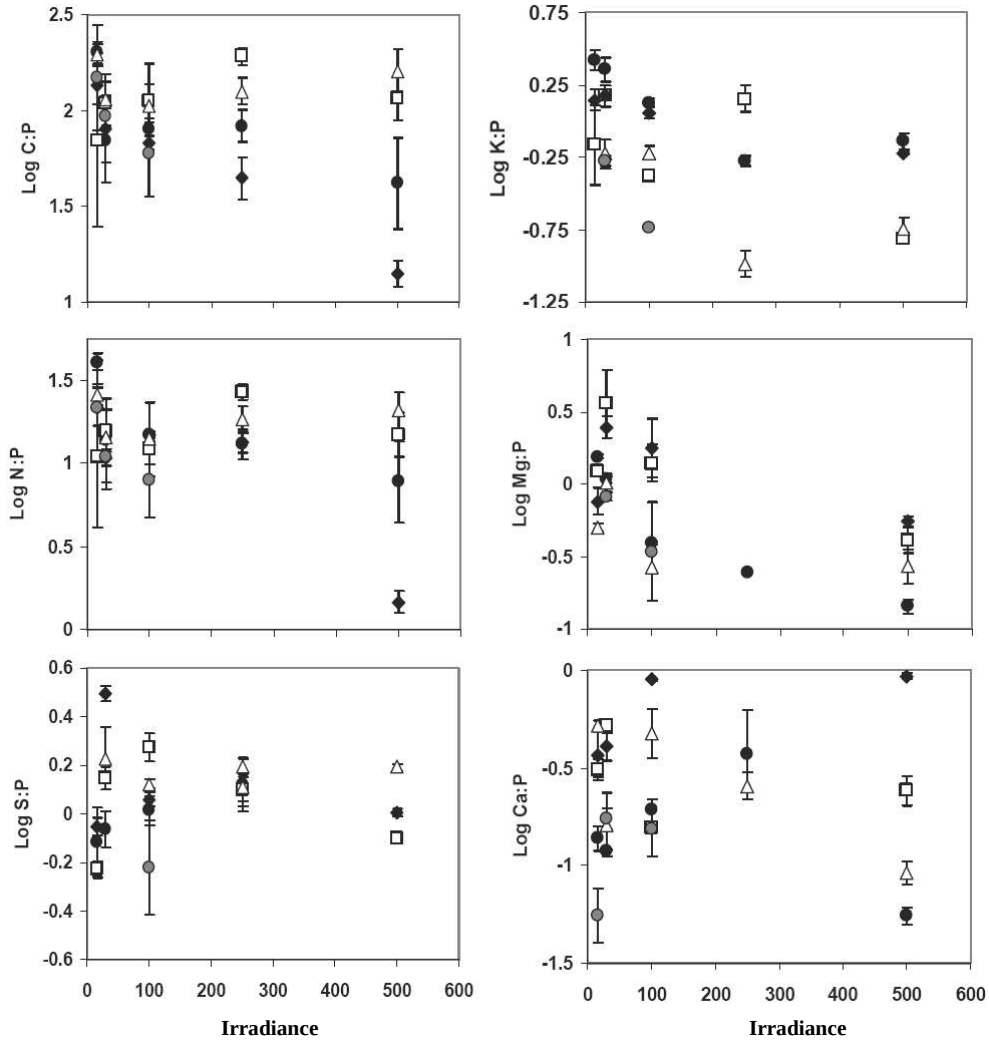

Figure 3-4. Log E:P and one standard error as a function of growth irradiance: macronutrients and alkali and alkaline earth metals. The different species are denoted by symbols: black circles *Thalassiosira weissflogii*, gray circles *Chaetoceros calcitrans*, open squares *Pycnococcus provasolii*, open triangles *Amphidinium carterae*, and black diamonds *Cyanothece sp*..

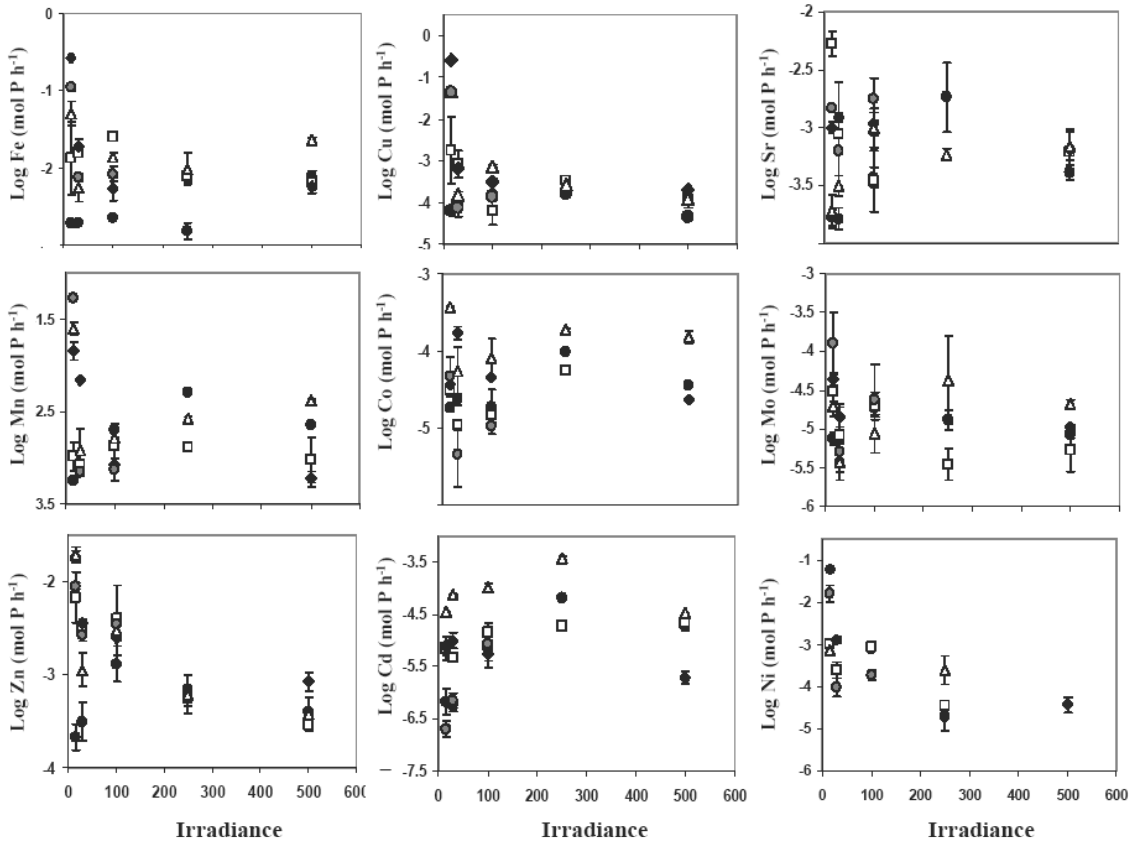

Figure 3-5. Log steady state net uptake rate for each element (mol) as a function of cellular P as a function of growth irradiance (Log mol E/ mol P h). Macronutrients and the alkali and alkaline earth metals. The different species are denoted by symbols: black circles *Thalassiosira weissflogii*, gray circles *Chaetoceros calcitrans*, open squares *Pycnococcus provasolii*, open triangles *Amphidinium carterae*, and black diamonds *Cyanothece sp*..

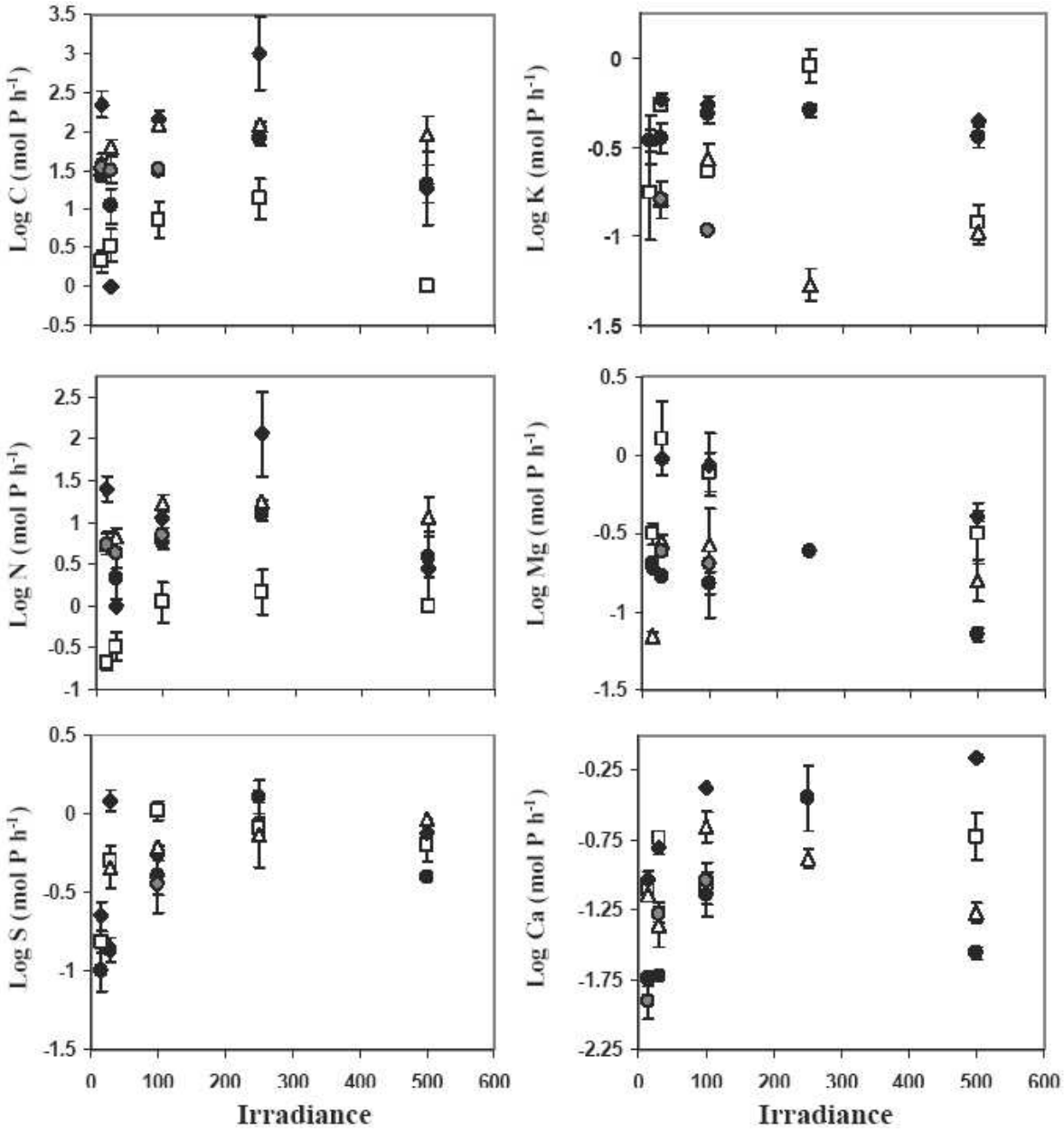

Figure 3-6. Log steady state net uptake rate for each element (mol) as a function of cellular P as a function of growth irradiance (Log mol E/ mol P h). Transition metals. The different species are denoted by symbols: black circles *Thalassiosira weissflogii*, gray circles *Chaetoceros calcitrans*, open squares *Pycnococcus provasolii*, open triangles *Amphidinium carterae*, and black diamonds *Cyanothece sp*..

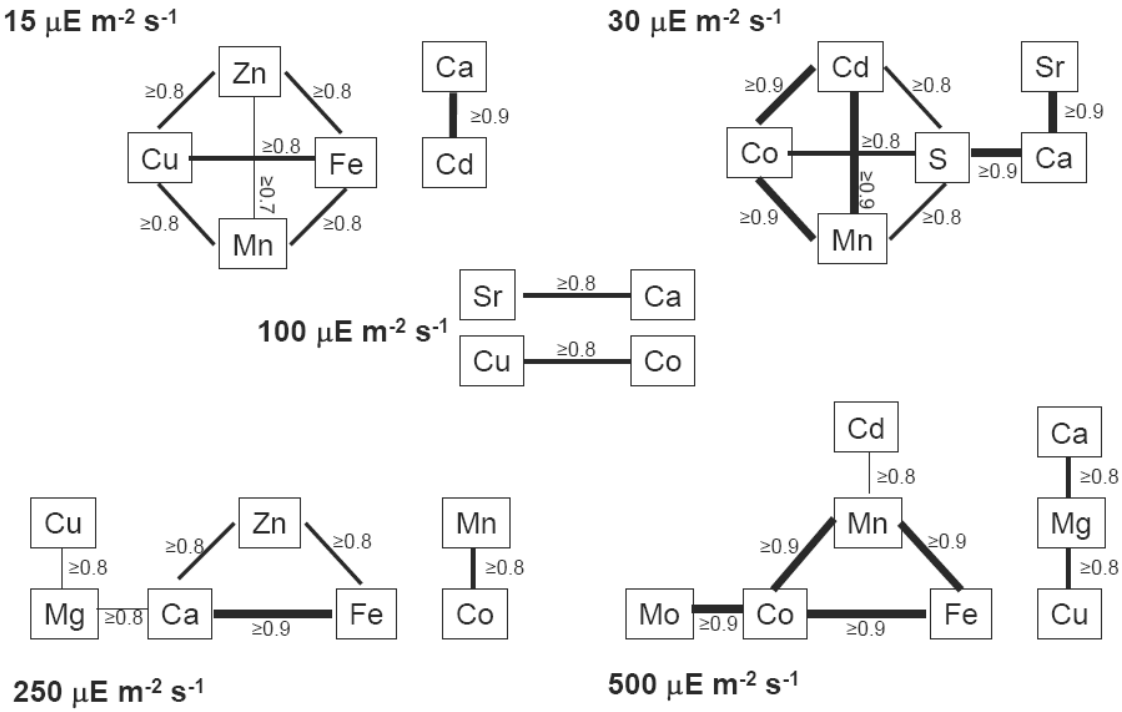

Figure 3-7. Correlation between Log E:P as a function of growth irradiance for $r > 0.8$, unless otherwise noted by the number on the lines. The thickness of the lines represents the strength of the correlation.

Discussion

Differences in elemental stoichiometry have been identified between distinct taxonomic groups grown under comparable environmental conditions (Falkowski 2004; Geider and LaRoche 2002; Ho et al. 2003; Quigg et al. 2003). Ho *et al*. (2003) defined the elemental stoichiometry of nutrient saturated marine phytoplankton grown at 250 μE m^{-2} s^{-1} as:

$$(C_{124}N_{16}P_1S_{1.3}K_{1.7}Mg_{0.56}Ca_{0.5})_{1000}\ Sr_{5.0}Fe_{7.5}Mn_{3.8}Zn_{0.80}Cu_{0.38}Co_{0.19}Mo_{0.03.}$$

Based on the 5 species examined over 15 to 500 500 μE m^{-2} s^{-1}, phenotypic responses to irradiance is responsible for <1 order of magnitude to >3 orders of magnitude in E:P within species, comparable to phylogenetic differences. A change in irradiance changes the relative order of many of these elements (Figures 3.1, 3.3, 3.4 and Table 3.1). In particular, many of the trace metals are highest at very low irradiance, Fe:P, Mn:P, Zn:P, Cu:P Co:P and Mo:P, while S:P, K:P, Mg:P and Ca:P tend to be highest at intermediate irradiances. Irradiance has different effects on E:P in different species, often magnifying between species differences in elemental stoichiometry. This indicates elemental stoichiometry of phytoplankton biomass may differ significantly between light-limited and light-saturated regions due to both the phenotypic response to light and taxonomic composition of the communities.

The role of photoacclimation in variation in E:P

Phytoplankton regulate their metabolic rates in response to changes in incident irradiance through a variety of plastic physiological responses broadly referred to as photoacclimation (Richardson et al. 1983). Although there are taxonomic differences in acclimation strategies there are some general phenotypic physiological responses that are common to all taxa, for example cellular pigment concentration tends to increase with decreases in irradiance (Falkowski and LaRoche 1991; MacIntyre et al. 2001; Richardson et al. 1983). Many cellular components associated with photoacclimation have unique elemental stoichiometries that can alter the overall elemental stoichiometry of cells over a light gradient (Raven 1988; Raven 1990). For example, each chlorophyll-*a* molecule has a Mg atom, so the change in pigment with irradiance results in a shift in Mg:P (Table 3.1). Based on the decreasing efficiency of exciton transfer with the size of the light harvesting antennae, Raven (Raven 1988; Raven 1990) estimates that photoacclimation to low irradiance will trigger the increased requirements for cellular Fe:P and Mn:P due to their participation in the photosynthetic reaction centers, photosynthetic electron transport and water splitting capacity, in agreement with field and laboratory measurements. Increases in nitrogen (N:P) have also been observed and attributed to increased apo-protein associated with increased cellular pigment (Flynn et al. 2001; Sciandra et al. 1997; Sciandra et al. 2000). For some species a select number of elements became enriched relative to phosphorus at saturating irradiances including Fe, Mn and Zn in the coastal diatom *Thalassiosira weissfloggi*, and Co in the diazotroph, *Cyanothece* sp. and the Prasinophyte, *Pycnococcus provasolii*, indicating an increased requirement for these elements under saturating irradiance and high growth rates (Figure 3.3).

Mechanistic models for E:P

Sterner and Elser's (2002) growth rate hypothesis predicts a decrease in N:P with increased growth rate due to an increased cellular allocation to RNA necessary to meet the protein synthesis demand regardless of the environmental conditions (Elser et al. 2000; Sterner and Elser 2002). Most of the evidence for this relationship between growth rate and N:P comes from freshwater phytoplankton and zooplankton, and accumulating evidence suggests the growth rate hypothesis may not apply to all organisms and may break down under limitations by light or elements other than phosphorus (Elser *et al*., 2003). The interspecific relationship between N:P and growth rate is weak for marine phytoplankton growing near μ_{max} or limited by light (Table 3.1). The growth rate hypothesis is based on the inference that an increase in growth requires an increase in the pool of cellular phosphorus; this differs from the theoretical calculations of Raven which explicitly consider the moles of element required to make a reaction run at a specific rate (but see Klausmeier et al. (2004). Different elements, especially nitrogen and phosphorus are required in different ratios for a large number of different processes in phytoplankton making it difficult to observe a change in stoichiometric requirements associated with one particular metabolic process in total cellular biomass.

Sunda and Huntsman (Sunda and Huntsman 2004; Sunda and Huntsman 1997; Sunda and Huntsman 1998a) propose that

$$E{:}P = V_{ss} / \mu, \qquad (3.1)$$

where the steady-state nutrient uptake rate ,V_{ss}, is a Michaelis-Menton function of available limiting nutrient (Sunda and Huntsman 2004; Sunda and Huntsman 1998a), while growth rate, μ, is influenced by the cell quota (E:P) of the limiting nutrient and environmental conditions such as growth irradiance. Sunda and Huntsman (1998) suggest E:P is generally controlled by a natural feedback, where uptake is influenced by increasing nutrient availability resulting in increased cellular quota which leads to increased growth and decrease in E:P, where competitive inhibition of multiple trace metals for surface transport sites can alter quota and growth. As a result this model predicts that under nutrient saturating conditions an increase in growth rate due to irradiance will result in an decrease in cellular E:C or E:P due to the dilution of E by growth rate. For *Thalassiosira pseudonana* and *Prorocentrum minimum* (Fe only), Sunda and Huntsman (1997, 1998) found V_{ss} for Mn and Fe was independent of irradiance between 50 and 500 μE m^{-2} s^{-1}, and that changes in E:P were primarily due to biodilution.

Re-evaluating the affect of irradiance on the mechanistic model for E:P

For 5 different taxa we find that below 50 μE m^{-2} s^{-1} the steady state uptake rate (V_{ss}, Figure 3.5 & 3.6) for Mn and Fe and Zn, Cu, Co, Mo, Sr, Mg, are strongly affected by irradiance, resulting in a large accumulation of E:P under low irradiance (Figure 3.3 & 3.4). This has been previously observed for Fe in *Thalassiosira weissflogii* (Strzepek and Price 2000). This is not likely due to the effect of irradiance on the availability of free metal because an increase in irradiance would only increase the availability of Fe and Mn and the steady state uptake, underestimating, V_{ss} (Sunda 1994; Sunda and Huntsman 1997; Sunda and Huntsman 1998a; Sunda and Huntsman 1998b). The steady-state uptake

rate for many of the observed elements relative to phosphorus were nearly independent of irradiance between 50 and 500 μE m^{-2} s^{-1}, but below this irradiance there is a steep increase in V_{ss} and E:P of Mn, Fe, Zn, Cu, Co, Mo, Sr. Mg with decreasing irradiance.

Previously, increases in cellular Fe:P and Mn:P have been attributed to an increased requirement under low light (Raven 1988; Raven 1990; Sunda and Huntsman 2004). Although increased requirements for Fe:P and Mn:P are predicted on the basis of increased cellular concentrations of Fe and Mn-rich photosynthetic machinery, total cellular Fe:P and Mn:P does not necessary reflect biochemical need. For most of the trace elements only a small proportion of their total concentration are identified in known metabolic processes (Hewitt 1983). Substantial storage could obliterate any patterns in requirements in total cellular ratios. Based on experimental data on storage of C, N, and P, Fogg and Thake (1987) hypothesized that storage ability for a given nutrient will increase as its proportion of total cell mass decreases. For the species examined, the log multiplicative range in E:P is correlated with log median E:P in biomass suggesting a increased storage capacity for nutrients that make up a small proportion of cell biomass (Figure 3.2).

Storage is in part a function of V_{ss}, but more specifically it is determined by the rate of uptake of E relative to P into the cell (V), the exudation of E relative to P, and the requirements of E:P for growth. Equation 3.1 can be parameterized to consider the effect of storage and requirements separately and highlight the importance of exudation:

$$E{:}P_{Cellular} = E{:}P_{Storage} + E{:}P_{Requirement} = (V - \text{Exudation}) / \mu. \qquad (3.2)$$

To understand why $E:P_{Cellular}$ increases under low irradiance, we need to determine how each of the parameters in Eq. 3.2 change with irradiance. There is comparatively little information on how irradiance affects the exudation and uptake rates for different elements. Experimental studies of uptake of C, N and P, indicates increases in light can stimulate an increase in maximum rate of uptake (V_{max}) and decrease in the half saturation constant (k_m), but based on the information available the observed increase in E:P under low growth irradiance is as likely due to a decrease in exudation of E relative to P as to an increase in uptake of E relative to P. Exudation of organic carbon can be highly variable, and high rates have been related to factors that cause physiological stress including high irradiance (Fogg 1977; Sharp 1977; Verity 1981; Zlotnik and Dubinsky 1989), suggesting exudation has the capacity to be an important physiological factor in the control of elemental stoichiometry, and since phytoplankton exudates have the ability to bind trace metals, may change the bioavailability of a variety of elements to other phytoplankton (Vasconcelos et al. 2002).

Oceanographic implications

The taxonomic and phenotypic variability in the elemental stoichiometry of phytoplankton biomass in response to irradiance suggests that the elemental stoichiometry of phytoplankton biomass will significantly differ between light-limited and light-saturated regions due to both the phenotypic response to light and taxonomic composition of the communities. Mesoscale eddies are responsible for 35-50% of new production, ~0.5 mol N m^2 per year (McGillicuddy et al. 1998). These eddies lift micro- and macronutrients into the lower portions of the euphotic zone often stimulating blooms

and export of light limited phytoplankton, especially diatoms (Goldman 2003; Sweeney et al. 2003). Our experimental data indicate that light limited phytoplankton accumulate large concentrations of Fe, Mn, Zn, Cd, and Cu, consistent with the observed depletion of Cu^{+2} and Mn^{+2} reported in deep chlorophyll maxima (Moffett 1995; Sunda and Huntsman 1998a). This indicates that the fractionation of Fe, Mn, and Cu relative to P in light-limited, nutrient-saturated phytoplankton may be a very important and previously unrecognized component of the biogeochemical cycling of these elements in the ocean.

Chapter 4. Scaling-up from size-dependent physiology to the size structure of phytoplankton communities over a resource gradient

Abstract

In many community assemblages, the abundance of organisms is a power-law function of body size. In phytoplankton communities, increases in total biomass are often associated with a shift in the proportion of the biomass in different size classes and an increase in the size of the largest cell present, indicating that nutrient availability influences both the total abundance and the relative numbers of large versus small cells in phytoplankton communities. Changes in plankton community size structure with nutrient availability are often interpreted as indicating deviations from steady state. We show that a steady-state physiological null model with size scaling of cellular nutrient requirements and growth, and no competitive interactions, can reproduce the power-law relationship between cell size and abundance and the dominance of small phytoplankton cells under oligotrophic conditions, and relative increase in abundance of larger phytoplankton cells under eutrophic conditions. If physiological differences associated with the taxonomic composition of different community size fractions is considered, then the null model can replicate more detailed field observations such as the absence of small, slow growing *Prochlorococcus* spp. and the relative dominance of large diatom species in nutrient-rich, upwelling regions of the ocean. These predictions depend on the assumption that the size-dependence of species diversity is independent of cell size. If species diversity is a

log-normal function of body size the size scaling of log abundance exhibits a similar response to nutrient availability but is no longer a linear function of log cell size. Deviations from the patterns predicted by the physiological null model can be used to identify if extrinsic processes such as competition or loss rates through grazing or aggregation and sinking become the dominant forces shaping phytoplankton community size distributions.

Introduction

The size structure of phytoplankton communities strongly influences the function of aquatic ecosystems. Large phytoplankton cells tend to be grazed by large zooplankton, resulting in shorter, simpler food webs which results in more efficient matter and energy transfer (Ryther 1969). Large and dense phytoplankton cells are responsible for the majority of exported production (Laws et al. 2000; Legendre 1981; Michaels and Silver 1988). This flux of fixed carbon and nutrients from the surface into the deep ocean sequesters carbon from the ocean-atmosphere system for hundreds to thousands of years (Eppley and Peterson 1979; Falkowski et al. 2000). Therefore understanding the mechanisms controlling the size structure of the phytoplankton community in response to environmental forcing is essential to understanding temporal and spatial fluctuations in food web structure, the regulation of the biological pump, and the ability of the ocean to act as a long-term sink for atmospheric carbon dioxide.

It is difficult to reconcile the existence and success of large cells using steady-state growth models. From bacteria to large mammals, body size is a predictor of metabolic rate:

$$M = c_1 V^{b}, \quad (4.1)$$

where c_1 is a group-specific coefficient and b is the size scaling exponent of the relationship between the metabolic rate (M, for example growth rate) and a dimensionless measure of organism size (V, for example total carbon content, or bio-volume, normalized by a reference size). While c_1 is variable, b is commonly ¾ for organism-specific metabolic rates due to fundamental geometric constraints (Banavar et al. 2002; West et al. 1999). Assuming organism mass is linearly related to cell volume, the size-scaling exponent of mass-specific metabolic rates is ¾ - 1 = -¼. Deviations in the ¾ size-scaling exponent have been associated with sub-optimal environmental conditions, such as extremes in temperature and irradiance (Banse 1976; Finkel 2001; Gillooly et al. 2001a; Peters 1983a; Sommer 1989). Resource limitation by light or nutrient availability can alter the size scaling of metabolic rates, resulting in a decrease in the size-scaling exponent (Finkel 2001).

Light harvesting and nutrient uptake by phytoplankton is size-dependent. Light absorption is a function of the pigment composition, concentration and cell size (Duysens 1956; Kirk 1975). Assuming all cells have similar pigment concentration and composition, larger cells will absorb fewer photons per chlorophyll-*a*. Experimental data support the theoretical predictions of a general decrease in intracellular pigment concentration with increasing cell size, which will alter the size scaling of light limited photosynthesis and growth (Finkel 2001; Finkel and Irwin 2000; Finkel et al. 2004). Experimental and theoretical evidence also demonstrates that smaller cells have higher rates of nutrient uptake per unit biomass and lower half-saturation constants due to their higher surface area to volume (SA/V) ratios (Aksnes and Egge 1991; Eppley and Thomas

1969; Hein et al. 1995). Furthermore, small cells have a lower minimum metabolic requirement that selectively allows them to survive at much lower resource concentrations than larger cells (Grover 1991; Shuter 1978). For example, if we consider that nutrient flux to a phytoplankton cell depends on diffusion, and growth is a function of uptake and cell quota, then the resource concentration required to maintain a specific percentage of the maximum growth rate (if maximum growth rate $\propto V^{-0.25}$) will scale as $V^{1/3}$ (Finkel et al. 2004; Hudson and Morel 1993; Pasciak and Gavis 1974). Lower resource requirement per individual supports higher population densities, reducing the likelihood of genetic bottlenecks and chance stochastic extinction events (Fenchel 1993). As a result, small phytoplankton cells have significant advantages over larger phytoplankton cells under steady state environmental conditions (Grover 1989; Grover 1991).

Despite all the advantages of small size, phytoplankton cells span over ten orders of magnitude in cell volume and phytoplankton communities often exhibit a characteristic size structure. The majority of field data suggests that small phytoplankton cells dominate in stable, oligotrophic environments such as the open ocean while larger cells can dominate biomass in variable, eutrophic environments such as coastal areas (Ahrens and Peters 1991; Chisholm 1992; Sprules and Munawar 1986). A complementary rule, also generated from field observations, is that cell abundance (A) per unit volume is inversely related to organism size:

$$A = c_2 V^{\xi}, \qquad (4.2)$$

where the size scaling exponent (ξ) is often –1 (Sheldon and Kerr 1972; Sheldon and Parsons 1967; Sheldon et al. 1972). Subsequent studies have found considerable

variability in ξ which often ranges between -2/3 to -5/3 (Boss et al. 2001; Peters 1983b; Sprules and Munawar 1986). In some local studies, predominantly from terrestrial systems, the relationship between abundance and body size more closely resembles a triangle where minimum abundance is fairly uniform across body size, and maximum abundance occurs for intermediate sized species (Blackburn 1996; Gaston 2000; Lawton 1990), or multiple peaks are present (Griffiths 1986).

Hypotheses for the abundance-body size relationship, such as size-dependent differences in energy use (Damuth 1981), competitive interactions (Grover 1989; Nee 1991), or the scale-free self-organization of complex adaptive systems (Rinaldo et al. 2002) do not explain why nutrient limitation alters the size structure of phytoplankton communities, although Sprules and Munawar have hypothesized that variations in c_2 and ξ indicate a deviation from steady state (Sprules and Munawar 1986). Food web models that include several trophic levels (often autotrophs, heterotrophs and detritivores) and many size-dependent processes (uptake, respiration, sinking rate, grazing rate etc.) have successfully simulated a large number of population and community level patterns, but due to a large number of parameters it can be difficult to attribute any particular pattern to any specific mechanism (Kerr 2001; Moloney and Field 1991; Moloney et al. 1991). The physical constraints body size places on metabolic rate and resource acquisition ability has been largely neglected and has not fully analyzed in the attempt to understand this general relationship between abundance and body size. Here we employ a size-resolved physiological null model to solve for steady-state numerical abundance that allows us to predict the size structure of phytoplankton communities as a function of physiological constraints and resource availability.

Materials and Methods

The physiological model

To determine the size structure of biomass and numerical abundance we use a standard internal stores or Droop formulation to describe the growth rate of phytoplankton as a function of the internal nutrient content in response to a continuous inflow of nutrient and outflow of both nutrient and cells (Grover, 1991). The three state variables are concentration of cells (X, cells/L), cellular nutrient content (Q, μmol of nutrient/cell), and the nutrient concentration in the environment (R, μmol/L):

$$dX/dt = X(\mu - D) \quad (4.3a)$$

$$dQ/dt = \rho - \mu Q \quad (4.3b)$$

$$dR/dt = D (R_0 - R) - \rho X \quad (4.3c)$$

where D is the dilution rate (h^{-1}), and R_0 is the concentration of nutrient introduced into the system (μmol/L). Growth rate (μ) and uptake (ρ) are defined as:

$$\mu = \mu'_{max} (1 - Q_{min} / Q) \quad (4.4a)$$

$$\rho = \rho_{max} R / (K_m + R). \quad (4.4b)$$

where μ'_{max} is the maximum potential growth rate obtained at infinite nutrient quota, ρ_{max} is the maximum uptake rate, and k_m is the nutrient concentration where $\rho = \rho_{max}/2$.

The dilution rate can be interpreted as a volume flux into a patch of the surface

ocean that is balanced by an equal flux out of the patch. If the volume flux is predominantly vertical then the in-flowing water will be nutrient rich and the out-flowing water will be relatively deplete of inorganic nutrient and rich with cells that will be eventually transported into the deep ocean and recycled back into inorganic nutrients. The vertical extent of the surface patch is set by physical mixing and will determine the dilution of the upwelling flux of nutrient and the average irradiance. High dilution rates describe upwelling zones and low dilution rates represent shallow stratified open ocean environments. In this model, dilution rate is an alternate analog of Margalef's concept of energy (turbulance) as a driving factor controlling phytoplankton community composition (Margalef 1978).

At steady state, the following equilibria are predicted:

$$Q^* = Q_{min} / (1 - D / \mu'_{max}) \quad (4.5a)$$

$$R^* = K_m / (\rho_{max} / (D\,Q^*) - 1) \quad (4.5b)$$

$$X^* = (R_0 - R^*) / Q^*. \quad (4.5c)$$

Generally this model is used to simulate and predict the growth rate of phytoplankton in response to changes in external nutrient concentration and to calculate the relative competitive ability, R*, of organisms under equilibrium conditions (Ducobu et al. 1998; Grover 1991; Tilman 1977). All of the parameters in the Droop model depend on cell size, with the exception of D and R_0. Based on extensive experimental observations we express the size dependence of Q_{min}, Q_{max}, μ'_{max}, K_m, and ρ_{max} by a power-law dependence on cell volume (Table 3.1). The size scaling of ρ_{max} is estimated from the

product of the internal nutrient requirement at μ'_{max} (Q_{max}) and the maximum growth rate. Instead of solving for R^* to determine competitive ability under equilibrium conditions we explicitly assume no competitive interactions and solve for X^*, a measure of the ability of a species to convert nutrients into cells and biomass.

Table 4-1. Volume (μm^3) scaling of physiological parameters, aV^b, used in the physiological null model.

Physiological parameter	Symbol	Units	b	a
[a]**Maximum growth rate**	μ_{max}'	day^{-1}	-0.25	5.37
[b]**Maximum uptake rate**	ρ_{max}	$\mu mol\ N\ (cell\ day)^{-1}$	0.66	μ
[c]**Half saturation constant**	k_m	$\mu mol\ N$	0.33	1.00
Minimum cell quota	Q_{min}	$\mu mol\ N\ (cell)^{-1}$	0.72±0.06 [d]	1.50E-09 [d]
Maximum cell quota	Q_{max}	$\mu mol\ N\ (cell)^{-1}$	0.85 [e]	3.60E-09 [e]

a. Maximum growth rate, size scaling exponent based on theoretical considerations (see text), the intercept is the extrapolated growth rate of a $1\mu m^3$ cell based on data compilation by Tang (1995).

b. Uptake rate, size scaling exponent set based on theoretical considerations of diffusion (Aksnes and Egge 1991), the intercept is set by the model.

c. The half saturation constant, size scaling exponent based on theoretical considerations of diffusion and size-dependent nutrient requirements (Aksnes and Egge 1991), the intercept is from nitrogen uptake measured by Eppley and Thomas (1969) as interpreted by Stolte and Riegman (1995).

d. Shuter (1978), e. Montagnes and Franklin (2001).

Scaling-up from physiological rates to the size scaling of abundance and biomass

Computing the density of cells for species of different sizes in a community requires not only knowledge of X^* but also the relationship between cell size and species diversity and the controls on the distribution of the species in habitable space. We assume the surface ocean is divided into a very large number of patches, and there is no competition for resources among patches, so species diversity as a function of size governs their appearance in the habitat. Species diversity (*S*, number of species/L) is often a skewed log-normal (*SLN*) function of body size (Brown 1995; Fenchel 1993; Gaston 2000; May 1978; Van Valen 1973),

$$S(d) \propto f_{SLN}(d) = 2 f_{LN}(d;\bar{d},\sigma) \int_0^{d^\alpha} f_{LN}(x;\alpha\bar{d},\sigma)\, dx \qquad (4.6a)$$

where α is the shape parameter and f_{LN} is the log-normal distribution

$$f_{LN}(d;\bar{d},\sigma) = \frac{1}{\sqrt{2\pi}\sigma d} e^{-(\log d - \bar{d})^2/2\sigma^2} \quad . \qquad (4.6b)$$

Maximum species diversity for the log normal distribution occurs at an intermediate cell size of $\exp(\bar{d} + \sigma^2/2)$, and $\exp(2\bar{d} + \sigma^2)(e^{\sigma^2} - 1)$ is the variance around the intermediate cell size (Azzalini 2003; Azzalini 1996). We constrain the range of cell sizes from a minimum diameter of 0.6 μm to the maximum size that can survive in a given habitat. The species diversity-body size relationship is not always skewed log-normal but can have multiple peaks, or can be independent of cell size (Gaston 2000). Given the little information available for the relationship between phytoplankton species diversity and cell size at different spatial and temporal scales we also consider that species diversity may be independent of cell size ($S(d) = 1$).

Species diversity and cell abundance (X^*) are functions of *d* defined on a

continuum, which is convenient mathematically, but awkward for comparison to empirical measurements which measure quantities over discrete size classes. We define N as the number of cells in the community of diameter less than d,

$$N(d) = \int_{d_{\min}}^{d} X^{*}(x)\ S(x)\ dx \Big/ \int_{d_{\min}}^{d_{\max}} S(x)\ dx\ . \qquad (4.7)$$

The abundance (A, cells/L) of cells in the community of diameter $d \pm \Delta d/2$ is

$$A(d) = \mathrm{d}N/\mathrm{d}d\ \Delta\mathrm{d} = X^{*}(d)S(d)\Delta d \Big/ \int_{d_{\min}}^{d_{\max}} S(x)dx\,, \qquad (4.7a)$$

which are computed for Δd = 1μm. The biomass (B) of cells less than diameter d is defined as

$$B(d) = \int_{d_{\min}}^{d} X^{*}(x)\ S(x)\ V(x)\ dx \Big/ \int_{d_{\min}}^{d_{\max}} S(x)\ dx \qquad (4.8)$$

where $V(d)$ is the volume of a cell of diameter d. Often cellular carbon content is a power function of cell volume with an exponent between 0.75 to 1 (Menden-Deuer and Lessard 2000). Our *a priori* assumption is that the carbon content per cell is equal to cell volume, but if cellular carbon is $\propto V^{3/4}$ then there will be less biomass in the larger size fractions and a lower size scaling exponent on biomass than predicted.

The size-constrained Droop model can predict the relative number of cells of different sizes in phytoplankton communities and the size ranges present. The diameter of

the largest cell present is d_{max} = max { d | min (X^*, Q^*, R^*) > 0 }, the biggest diameter for which the equilibrium values of X, Q, and R are all physically reasonable. For simplicity it is assumed that all cells are spherical, although large cells are often highly prolate in shape (Grover 1989). Although taxonomic differences in nutrient requirements and acquisition are well documented, for example *Prochlorococcus* has lost the ability to take up nitrate and depends on ammonium and organic nitrogen to fulfill its nitrogen (N) requirements (Garcia-Fernandez et al. 2004), we initially assume all cells have the same type of nutrient uptake systems and selected an unspecified form of nitrogen as the limiting nutrient to reduce complexity and because it is often the proximate limiting nutrient for marine phytoplankton growth (Falkowski 1997b).

Results

Environmental regulation determines the maximum cell size in the community

The physiological null model predicts an increase in the abundance of large cells relative to smaller cells with increasing nutrient availability, resulting in an increase in the maximum size of the cells present and average cell size of the phytoplankton community (Figure 4.1). As a result, as total phytoplankton biomass increases with increasing nutrient availability the fraction of the biomass contributed by the ≤2μm size fraction, the picoplankton, decreases, in qualitative agreement with field observations from marine (Figure 4.2) and aquatic ecosystems (Ahrens and Peters 1991; Sprules and Munawar 1986). For any nutrient concentration an increase in dilution rate decreases the size of the largest cell present in the community.

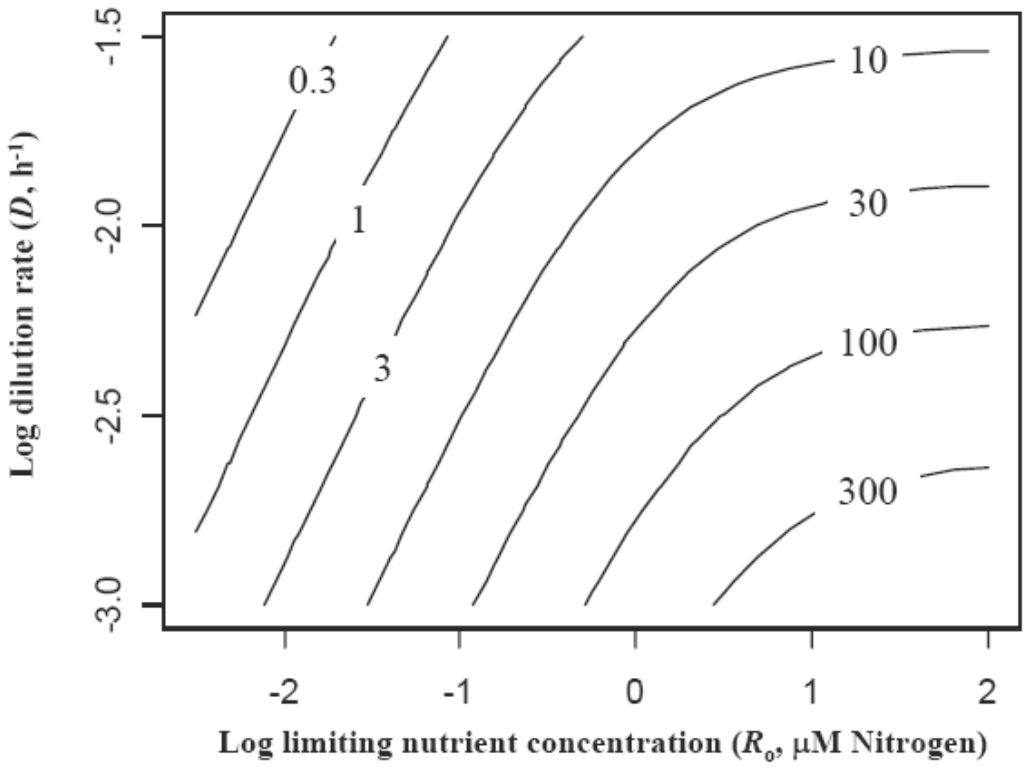

Figure 4-1. Maximum cell diameter (μm) present in the community as a function of $\log_{10}$ limiting nutrient availability (μM nitrogen) and $\log_{10}$ dilution rate (h^{-1}).

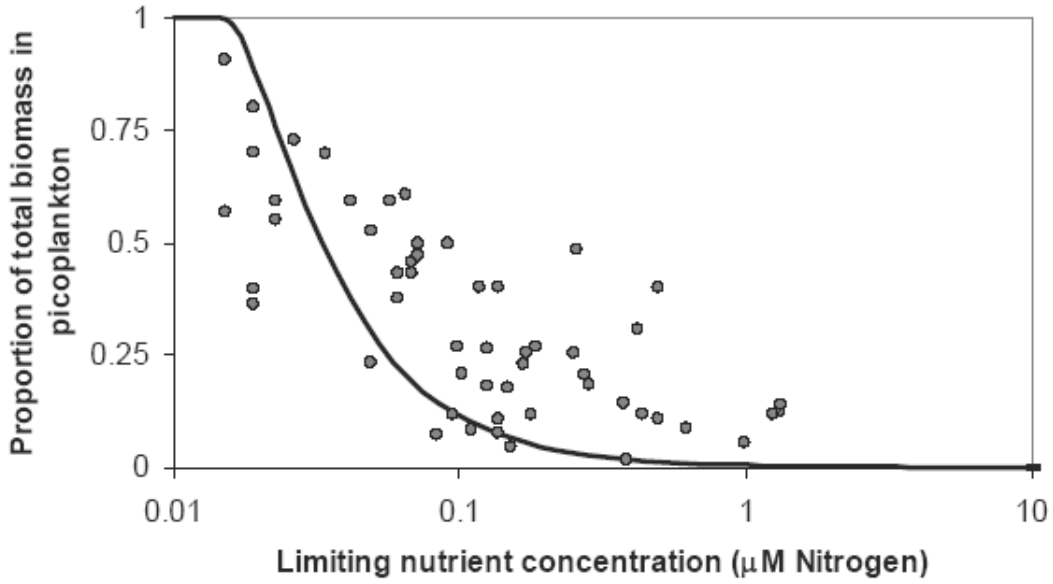

Figure 4-2. Percentage of total biomass in the picoplankton size fraction (<2 μm in diameter) as a function of nutrient availability (μM nitrogen) for a dilution rate (D, h^{-1}) of 10^{-2} predicted by physiological null model and compared with field data of microbial size spectra compiled by Chisholm (1992). Total biomass is calculated assuming total biovolume is linearly proportional to carbon. Field data compiled by Chisholm (1992) was compared with the model predictions by converting μg Chl-*a*/L to μM nitrogen using C/Chl (wt/wt) = 10 and assuming C:N in biomass is in Redfield proportions.

Consequences of the species diversity-body size relationship for the size scaling of abundance

The size scaling of abundance requires a description of the partitioning of space by species of different sizes. The assumption that every species has an equal probability of inhabiting each patch means that the relationship between body size and species richness will have a strong influence on the size scaling of abundance. When species richness is a skewed log-normal function of V then cell density is concave down with respect to V (Figure 4.3a), but when species richness is a linear function of V then cell density is approximately a power-law function of V (Figure 4.3b). If species diversity is a skewed log-normal function of cell size, then ξ can be quite variable and much flatter than when $S(d) = 1$, depending on resource concentration, dilution rate, and the size of the species with maximum abundance, and the range of cell sizes sampled. As nutrient concentration decreases, overall cell density (cells/L) decreases, until a threshold is reached (0.1 μM N), and then further decreases in nutrient concentration results in an overall increase in abundance due to the decrease in the number of species in the community. If $S(d) = 1$ then the null model predicts a power-law decrease in relative abundance of small versus larger cells that is uniform except at the largest sizes supported by the community, which exhibit a rapid decrease in cell density as they approach washout. Subsequent calculations assume $S(d)=1$ because $A(d)$ then more closely matches field observations.

Relative abundance of large versus small cells (ξ)

The size-scaling exponent (ξ) of abundance $A(d) \propto V^{\xi}$, is estimated by fitting predictions of relative abundance from cells 0.6 μm in diameter to the largest cell

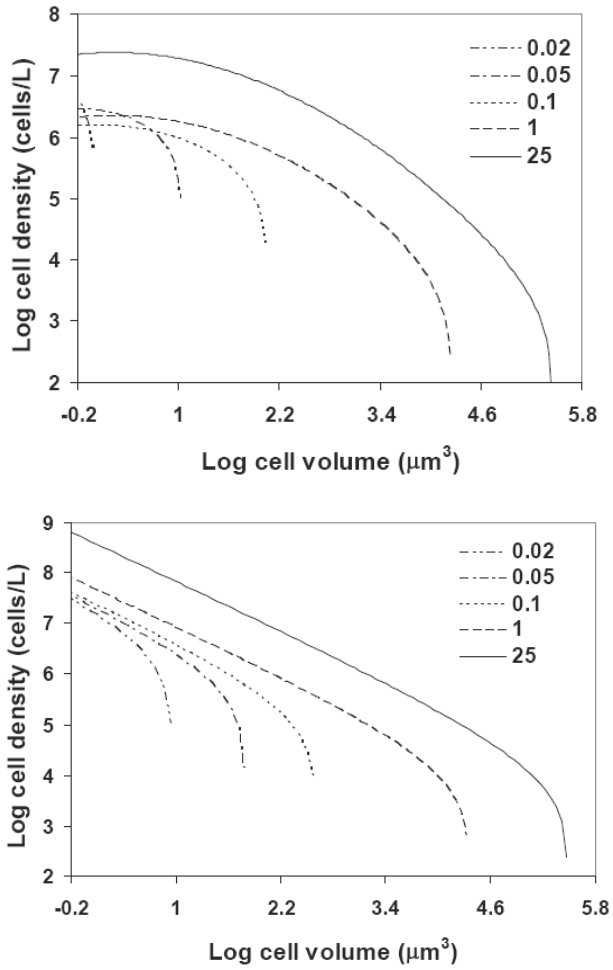

Figure 4-3. Predicted relative abundance (*A*, Eq. 3.7a) of cells (L^{-1}) of different sizes (volume, μm^3) at a dilution rate of 1 $week^{-1}$ for (top panel, a) a skewed log-normal relationship between species richness and cell size for five limiting nutrient concentrations (μM nitrogen): 0.02 (dotted-dotted dash), 0.05 (dotted-dash), 0.1 (small dash), 1 (large dash), and 25 (solid line). The skewed log-normal distribution is defined in Equation 3.6, with $\sigma = -3.5$, $\alpha = 4$ and $\bar{d} = -11.4$, for a community with cells ranging from 0.6 – 1000 μm diameter with maximum diversity at $d = 10$ μm, and (bottom panel, b) a uniform relationship between species richness and cell size for five limiting nutrient concentrations (μM nitrogen) as labeled in previous figure.

supported. We find ξ=-1.6 to -0.74, depending on the nutrient concentration of the input media and the size scaling of Q_{min} (Figure 4.4), note this is in remarkable agreement with observations from phosphorus limited lakes (see Figure 4 in (Sprules and Munawar 1986)). At high nutrient supply concentrations (R_0), $R^* << R_0$ so ξ is approximately the size scaling exponent of $1/Q^*$, and as a result if $Q_{min} \propto V^{0.72}$ then $\xi \rightarrow$ -0.72 under high R_0, and if $Q_{min} \propto V^1$ then $\xi \rightarrow$ -1 under high nutrient concentrations (Figure 4.4a). As R_0 decreases this simplification becomes increasingly inaccurate and ξ decreases. When R_0 is very close to R^*, the cells approach wash-out and X^* drops rapidly. Sampling cellular abundance for size fractions that are close to wash-out will be difficult because as abundances drop ever increasing effort is required to observe the larger cells. As a consequence, several of the phenomena plotted here are difficult to observe empirically. Increases in dilution rate result in decreases in ξ, except at extremely low R_0 where only small cells have viable population abundances (Figure 4.4b).

Discussion

R.W. Sheldon's pioneering work on particle distributions in the surface waters across the Atlantic and Pacific Oceans in the 1960-70s led to the general conclusion that there is roughly equal biomass for all particle sizes (Kerr 2001; Sheldon and Parsons 1967; Sheldon et al. 1972). This work was followed by the discovery that ubiquitous, abundant, and extremely small photosynthetic picoplankton (<2 μm in diameter), *Prochlorococcus* spp., contribute significantly to primary production and biomass in many oligotrophic regions of the world's oceans (Chisholm et al. 1988; Li and Wood 1988; Zubkov et al. 1998). This has been followed by an increasing awareness of

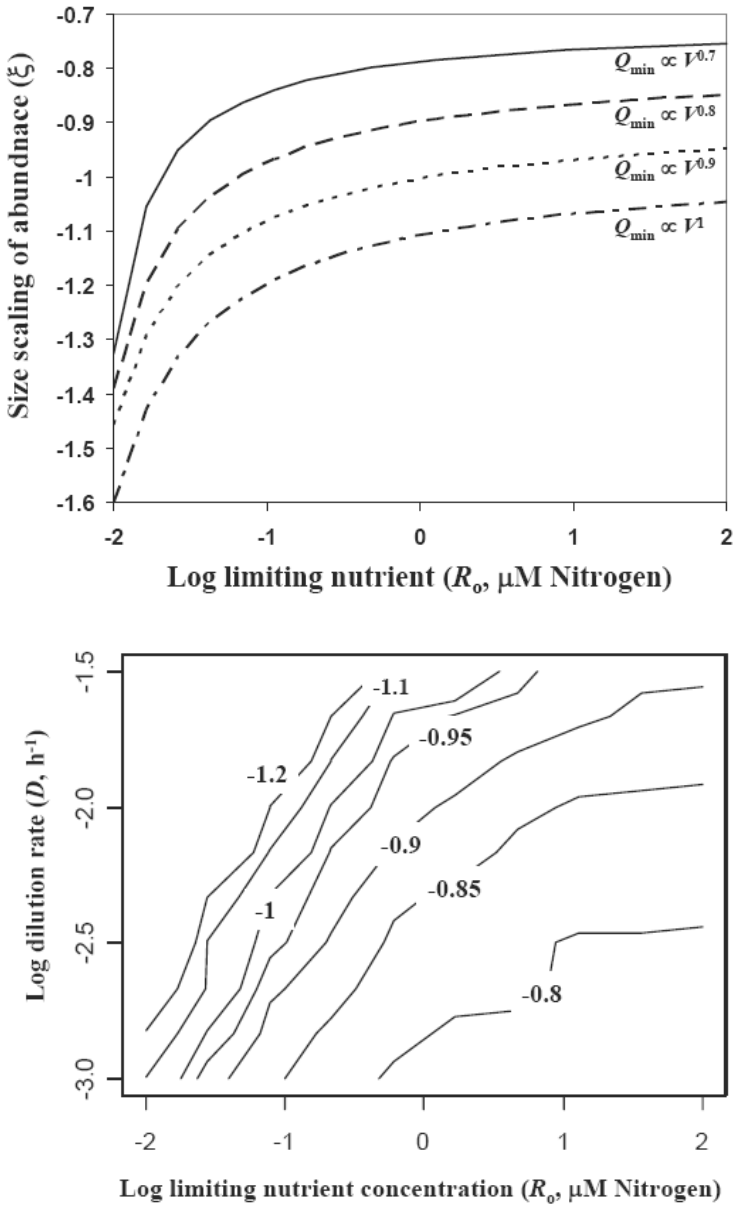

Figure 4-4. Size scaling of abundance (cells L^{-1}) as a function of nutrient concentration (μM nitrogen) for (a, top panel) a range of size scaling exponents for minimum cell quota for nitrogen: $Q_{min} \propto V^{0.7}$ (dotted lines), $Q_{min} \propto V^{0.8}$ (dashed line), $Q_{min} \propto V^{0.9}$ (dashed-dotted line), $Q_{min} \propto V^{1}$ (solid line), and (b, bottom panel) dilution rate (D, h^{-1}).

pervasive populations of picoeukaryotes from a wide variety of taxonomic groups (Moon-Van Der Staay et al. 2001). These observations have contributed to the paradigm that the euphotic zone of the ocean is often inhabited by a background of very abundant small phytoplankton cells that are accompanied by larger cells as nutrient availability increases (Ahrens and Peters 1991; Chisholm 1992; Sprules and Munawar 1986).

There are many factors that affect the size structure of phytoplankton communities including: competitive interactions among phytoplankton taxa (Grover 1989; Tilman 1977), grazing (Armstrong 1994 ; Gonzalez et al. 1990; Kerr 2001; Kiorboe 1993), sinking (Gavis 1976; Kiorboe 1993; Munk and Riley 1952) and physical aggregation (Burd and Jackson 2002; Jackson 1990), and sampling or analysis bias (Blackburn 1996; Griffiths 1992; Sheldon et al. 1972). Regardless of the degree to which these or any other factors contribute to the actual size structure of phytoplankton communities, the aggregate behavior of the individual phytoplankton cells inherently shapes the size structure of phytoplankton communities. Considering the size-dependence of nutrient requirements, nutrient uptake and growth, we have constructed a series of predictions for how phytoplankton community size structure will change as a function of nutrient availability and dilution rate under steady state:

I. The existence of a population of large cells requires a minimum concentration of supplied nutrient. An increase in the concentration of the limiting nutrient results in an increase in the maximum cell size present, the range of cell sizes present in the community, and an increase in the proportion of total biomass present in the larger size fractions, in agreement with field observations (Chisholm 1992).

II. Communities are predicted to be characterized by a logarithmic decrease in cell

density with increasing cell size and the relative numbers of large and small cells (ξ) change with the concentration of limiting nutrient (R_o) such that ξ is low under low nutrient concentration and highest under high nutrient concentration. The actual value of ξ depends on D and the size scaling of Q_{min}.

III. Dilution rate determines the size scaling of μ/μ_{max} and therefore the size scaling of abundance under any given nutrient concentration. Fast dilution rates will tend to wash out large, slow growing cells ($D > \mu_{max}$), while under low dilution rates cells of all sizes will be supported.

Most of these predictions, specifically the logarithmic decrease in cell density with the logarithmic increase in cell size with a slope of -1.6 to -0.75 are in remarkable agreement with the range of values observed in field observations for phytoplankton and other autotrophs as well as range of heterotrophs (Belgrano 2002; Bonner 1988; Boss et al. 2001; Cavender-Bares et al. 2001; Damuth 1981; Damuth 2001; Tittel et al. 1998). The model predicts that the size scaling of biomass in the water column (bulk phytoplankton carbon/L) ranges from $V^{-0.85}$ to $V^{0.25}$ if the size scaling of carbon quota ranges between $V^{3/4}$ to V^{1}, also in agreement with field observations (Ahrens and Peters 1991; Rodriguez and Mullin 1986; Sprules and Munawar 1986). The trended change in ξ in response to R_o and D are in accord with observed changes in size structure with bulk chlorophyll concentrations (Li 2002; Tremblay 1994) and phosphorus concentrations (Ahrens and Peters 1991; Sprules and Munawar 1986), but the trended change with nutrient concentration have not always observed in marine systems (Cavender-Bares et al. 2001). Application of this general theoretical framework can replicate a range of patterns in the size structure of phytoplankton that have been previously explained by a

number of different theories including deviations from steady state (Sprules and Munawar 1986), size-dependent grazing (Armstrong 1994; Kerr 2001), size-dependent physiological properties (Stolte and Riegman 1995; Tozzi et al. 2004), and the intermediate disturbance hypothesis (Li 2002).

Big cells can dominate numerically under steady state conditions

Steady state measurements of resource acquisition and growth indicate that smaller phytoplankton species generally have a competitive advantage over larger species, making it difficult to explain the persistence of large phytoplankton cells (Grover 1989). Invoking no competitive interactions, at steady state the physiological null model allows the co-existence of species covering a wide range of sizes with abundance $\propto V^{1.6 \text{ to } -0.75}$ depending on R_o, D and the size scaling of minimum quota. A number of field observations suggest that under certain environmental conditions small phytoplankton cells are rare and large cells dominate (Furnas 1991; Li 2002; Partensky et al. 1999; Zubkov et al. 1998). For example, small *Prochlorococcus* species are geographically limited between 50° N and 50° S (Zubkov et al. 1998), and large diatoms often dominate in upwelling regions characterized by high nutrient, and high bulk chlorophyll concentrations (Li 2002; Margalef 1978). Deviations from steady state, nutrient pulsing, nutrient storage, and surge uptake abilities have been proposed to explain the dominance of large phytoplankton species (Sprules and Munawar 1986; Stolte et al. 1994; Stolte and Riegman 1995; Tozzi et al. 2004). Repeated observations of extraordinarily high growth rates and chlorophyll-*a* normalized primary production in the microplankton size fraction under high nutrient, and high flow rates, such as upwelling

conditions (Froneman et al. 2001; Furnas 1991; Li 2002; Tremblay 1994) hint at an alternate, steady state explanation. A positive co-variance between cell size, taxonomic groupings and μ'_{max} could explain the observations of high biomass and high rates of chlorophyll-*a* normalized primary production in microplankton size fractions.

Picoplankton assemblages are often dominated by *Prochlorococcus* spp. and *Synechococcus* spp., which have maximum growth rates of ~1-1.4 and ~1-2 divisions per day, respectively (Kana and Glibert 1987; Partensky et al. 1999; Shalapyonok et al. 1998). The nanoplankton, typically defined as 2-20 μm, include species from most of the dominant eukaryotic taxonomic groups. A common and often dominant constituent of the lower range of the nanoplankton size fraction is *Emiliania huxleyi*, a Prymnesiophyte, with a maximum growth rate that ranges from 1.3-2.8 divisions per day (Brand 1981; van Bleijswijk et al. 1994). Although there are a few dinoflagellate and diatom species that are in the nanoplankton size range, most are >10 μm, and tend to dominate in the microplankton, 20-1000 μm, size fraction. It is widely recognized that diatoms have growth rates considerably higher than dinoflagellates of the same size (Chan 1978; Falkowski et al. 1985; Geider and Osborne 1992; Langdon 1987; Tang 1995). Due to their high nutrient requirements and a high half saturation constant for nutrient uptake, large cells can only grow rapidly under high nutrient conditions. In contrast, smaller cells are physiologically adapted for rapid growth under low nutrient conditions, and can grow at their maximum inherent growth rate at nutrient concentrations under which larger cells are seriously nutrient limited. As a result we hypothesize that there is increasing evolutionary pressure for large species to increase their maximum growth rate under high nutrient conditions. This idea is supported by a comparison of the maximum growth rate

for a number of ecologically important taxonomic groups at a reference size of $1\mu m^3$ that indicates that except for dinoflagellates, larger phytoplankton taxa generally have inherently larger maximum growth rates per unit volume (Table 4.2).

There is a 16-fold difference in the maximum growth rate between the major taxonomic groups with the diatoms having the fastest and the picoplankton the smallest maximum growth rates. If this co-variation between the change in taxonomic group with a change in the size range of organisms present and their size-dependent physiology is represented as a difference in the intercept on the allometric relationship between maximum growth rate and organism size (Eq. 4.1), then the physiological null model can reproduce an even larger range of patterns in abundance (Figure 4.5). For example, a phytoplankton community with picoplankton dominated by slow growing *Prochlorococcus* and *Synechococcus* spp. and nanoplankton dominated by *E. huxleyi*, and microplankton dominated by fast growing diatoms results in increases in the expected abundance of large cells under medium to high nutrient concentrations, and decreases in the abundance of small cells under high nutrient concentrations and dilution rates, consistent with the chemical and physical conditions and community size structure observed in upwelling regions (Li 2002; Tremblay 1994). An incorporation of the change in maximum growth rate with size range into the physiological model replicates the washout of the small, relatively slow growing picoplankton cells under high dilution rates while large fast growing diatom cells will persist if nutrient concentrations are high (Figure 4.5). Note that these patterns are dependent on a co-variation between nutrient availability and dilution rate, which is consistent with the effect of mixing, turbulence and upwelling that introduces nutrients into the euphotic zone in freshwater and marine

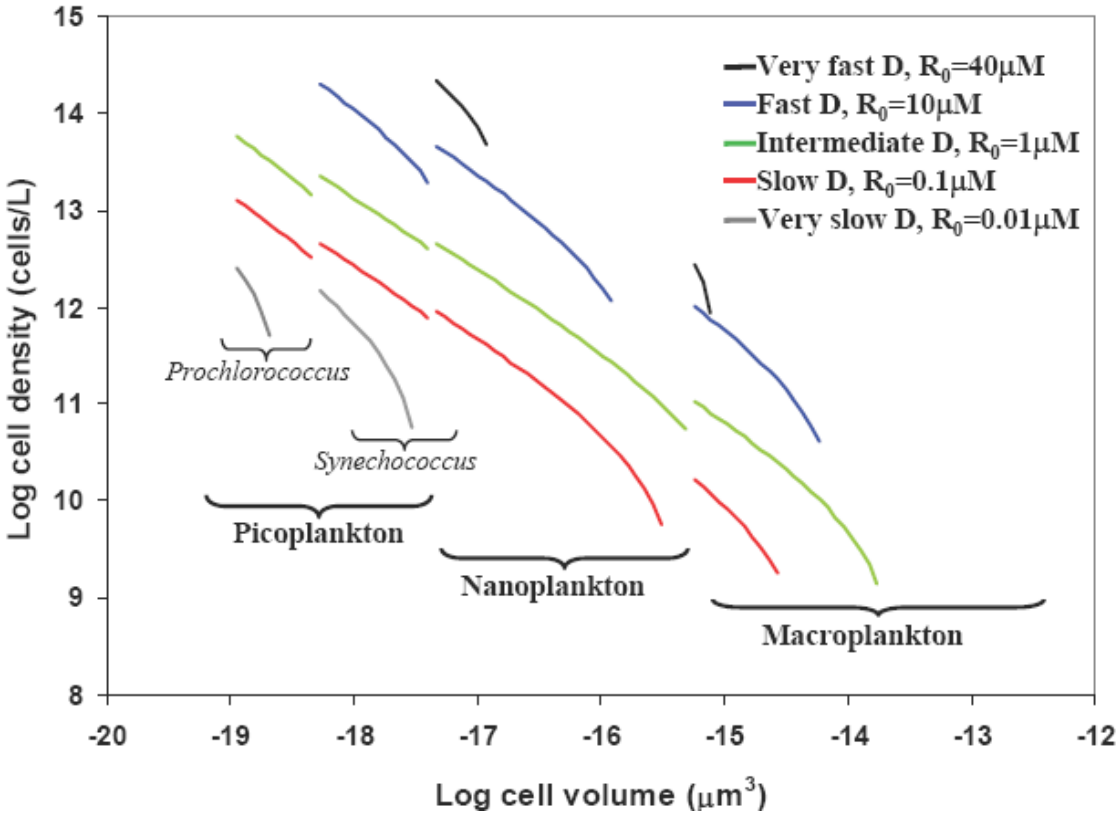

Figure 4-5. Predicted cell densities in pico-, nano-, and microplankton size fractions as a function of limiting nutrient concentration (μM nitrogen) where nutrient concentration co-varies with dilution rate (log D = ((log R + 2)/2) -3), and assuming that picoplankton are dominated by *Prochlorococcus* and *Synechococcus* spp, the nanoplankton are dominated by the coccolithophorid *Emiliania huxleyi*, and the microplankton are dominated by fast growing diatoms with growth rates and size ranges as provided in Table 4.2.

Table 4-2. Inherent taxonomic differences in growth rate estimated for a 1 μm^3 cell and assuming the size scaling of growth follows the 3/4 rule (*b*=-0.25).

	Relative μ_{max}	**Size range diameter (μm)** [f]	**Observed μ_{max}** [g] **day^{-1}**
Prochlorococcus spp.	1.00 [a]	0.6 to 1	1 to 1.42 [b]
Synechococcus spp.	2.89	1 to 2	1.97[c]
Emiliania huxleyi	6.38	2 to 10	1.3[d]
Dinoflagellate spp.	7.93	5 to 10^3 (x = 20)	1.41[e]
Diatom spp.	16.39	5 to 10^3 (x = 15)	2.92 [e]

a. The predicted maximum growth rate (divisions/day) for a *Prochlorococcus* cell with a cell volume of 1 μm^3 is 0.58 when b = -0.25. b. Partensky et al. (1999); Shalapyonok et al. (1998), c. Kana and Glibert (1987), d. van Bleijswijk et al. (1994)

e. The maximum growth rate for the dinoflagellates and diatoms was estimated from Tang (1995), using an estimate of average cell volume of the phytoplankton data from Figure 2, Tang (1995), and then calculating the maximum growth rate of the diatoms and dinoflagellates with *b* = -0.25 and a cell volume of 1 μm^3.

f. The diameter of the different groups are estimates based on an examination of the size of species in the CCMP culture collection and reports in the literature.

g. Observed μ_{max} is a measured growth rate of a particular species from the taxonomic group.

ecosystems. This shift in growth rate, phytoplankton size and taxonomic structure is consistent with the high chlorophyll-normalized photosynthetic rates that have been reported for diatom enriched macroplankton size fractions versus smaller size fractions from tropical (Furnas 1991; Malone 1993; Maranon 2001), temperate (Tamigneaux 1999) and polar regions (Legendre 1993).

Conclusions

Field observations indicate phytoplankton community size structure varies with resource availability and hydrographic conditions (Ahrens and Peters 1991; Chisholm 1992; Li 2002; Sprules and Munawar 1986; Tremblay 1994). Hypotheses that have been proposed to account for the size structure of phytoplankton communities include: size and density dependent grazing (Armstrong 1999), particle sinking and coagulation dynamics (Burd and Jackson 2002), size-dependent niche breadth (Brown 1995; La Brecque 1992), and size dependent physiological strategies such as surge uptake or storage abilities (Stolte et al. 1994; Stolte and Riegman 1995; Tozzi et al. 2004). We have shown that a size-resolved physiological model that describes growth rate as a function of the supply of nutrient with no competitive interactions can replicate the characteristic inverse power-law relationship between the abundance of phytoplankton cells and cell size, and the relative dominance of small phytoplankton cells observed under stratified, oligotrophic conditions, and the increase in the abundance of larger phytoplankton cells under well mixed, eutrophic conditions. Furthermore this equilibrium model predicts that taxonomic and size diversity is a unimodal function of limiting nutrient concentration when it co-varies with dilution rate providing an alternate hypothesis to Li's (2002) proposal that the

frequency of disturbance shapes the abundance and diversity of phytoplankton communities. The ability of the physiological null model to replicate large trends in community size structure indicates that resource availability and volume flux may often be the primary controls on the size structure of phytoplankton communities. Including a consideration of changes in the size normalized maximum growth rate of different taxonomic groups of phytoplankton, and that dilution rate likely increases with nutrient concentration further increases the match between the physiological model and field observations. The size scaling of phytoplankton physiology, growth and photosynthetic rate, nutrient quotas, and rates of resource acquisition, will always inherently shape the size structure of the phytoplankton community. Deviations from the physiological model can be used to highlight conditions where competition or loss rates through processes such as grazing or sinking become the dominant forces shaping phytoplankton community size distributions.

Chapter 5. Climatically-driven macroevolutionary patterns in the cell size of marine diatoms over the Cenozoic

Abstract

The size structure of marine phytoplankton communities strongly affects food web structure and influences the efficiency of organic carbon exported into the ocean interior. Many taxonomic groups exhibit evolutionary change in body size, yet macroevolutionary patterns in the size structure of phytoplankton communities have not been previously investigated. To examine the historical pattern of size structure in phytoplankton communities, we constructed a database of the size of the silica frustule of the dominant fossilized marine planktonic diatom species over the Cenozoic. We found the minimum and maximum size of the diatom frustule of the marine planktonic community has expanded in concert with species diversity. In contrast, the mean area of the diatom frustule is highly correlated with vertical and latitudinal temperature gradients inferred from the $\delta^{18}O$ of foraminiferal calcite. This is consistent with the hypothesis that climatically induced changes in oceanic mixing have altered nutrient availability in the euphotic zone and driven macroevolutionary shifts in the size of marine pelagic diatoms through the Cenozoic.

Introduction

Diatoms are a group of eukaryotic oxygenic photoautotrophs characterized by an opaline silica frustule that can be preserved in the fossil record. The oldest unequivocal fossil diatoms are found in the middle Cretaceous (Gersonde and Harwood 1990;

Harwood and Gersonde 1990), but molecular clock estimates indicate they may have originated as early as 165-240 million years ago (Kooistra and Medlin 1996; Medlin and Kaczmarska 2004; Medlin 1997). The fossil record indicates that diatom diversity and evolutionary tempo (Barron 2003; Katz et al. 2004) has increased over most of the Cenozoic. The general increase in the diversity of diatoms, in conjunction with the decreasing diversity of fossil calcareous nannoplankton and dinoflagellate cysts, has been cited as evidence for an increase in the relative importance of diatoms to the oceanic carbon cycle through the Cenozoic (Falkowski 2004; Katz et al. 2004). In the contemporary ocean, diatoms account for a large proportion of oceanic primary and export production (Smetacek 1999).

The size structure of the phytoplankton community is correlated with food web dynamics and export production (Laws et al. 2000). Small cells are much more likely to be rapidly recycled within the upper ocean in a microbial "loop"(Azam et al. 1983), while communities dominated by large cells tend to be associated with an increasing efficiency of trophic transfer to metazoans (e.g., fish) and export of photosynthetically fixed carbon into the deep sea. The export of carbon, commonly referred to as the biological pump, contributes to the ocean's capacity to act as a sink for atmospheric carbon dioxide (Falkowski 1998). Changes in nutrient availability are associated with shifts in the size structure of phytoplankton communities and the magnitude and efficiency of the biological pump. Typically, phytoplankton communities are dominated by small phytoplankton cells under oligotrophic conditions such as the oceanic gyres, while larger phytoplankton cells are more abundant along continental margins and in upwelling zones, where nutrient concentrations tend to be higher and more variable (Chisholm 1992).

Evolutionary shifts in the size of phytoplankton cells would have had a profound influence on oceanic food web dynamics (Laws et al. 2000), carbon cycling, and the interpretation of $\delta^{13}C$ of organic carbon over the Cenozoic (Hayes et al. 1999). Several studies on a few single, morphologically defined species of marine diatoms have documented size shifts in response to temperature and upwelling zones over hundreds of thousands to several millions of years (Burckle 1977; Sorhannus et al. 1991; Wimpenny 1936). These observations suggest that environmental factors could drive evolutionary change in phytoplankton cell size, but macroevolutionary changes in the average size of the cells within phytoplankton communities have not been investigated over the Cenozoic.

Macroevolutionary change in body size has been documented in unicellular foraminifera (Schmidt et al. 2004), as well as a variety of aquatic and terrestrial metazoans (Alroy 1998; Hallam 1975). A combination of size bias in origination or extinction, physiologically imposed boundaries on minimum and maximum size, and active selection pressures can result in complex temporal patterns in the evolution of body size. In conjunction with species radiation, passive evolutionary mechanisms tend to result in increases in both the maximum and minimum size with no change in the mean body size of the group (Gould 1997; Stanley 1973). Bias towards the survival of small species after mass extinction events, and a physiological boundary on minimum body size often results in increases in both the maximum and mean size within a taxonomic group, referred to as Cope's rule (Kitchell 1986; McShea 1994b; Stanley 1973). Active selection pressures, such as trended changes in resource availability or predation pressure, can result in shifts in the size of taxonomic groups towards a particular size with

a contraction in the size range (McShea 1994b). Different selection pressures may act on individuals of different size, resulting in a large variety of size distributions.

Variations in the concentration of atmospheric CO_2 and other greenhouse gases can alter nutrient concentrations in the upper ocean through two basic mechanisms. First, greenhouse forcing of planetary temperature influences the equator-to-pole (horizontal) and surface-to-deep (vertical) temperature gradients in the ocean. These two thermal gradients determine the energy required to mix nutrients from the ocean interior to the euphotic zone. Second, the concentration of CO_2 and surface temperatures influence the rate of rock weathering, which affects the flux of nutrients from cratons to the ocean. Resource availability in the euphotic zone affects phytoplankton community size structure, which in turn can alter the biological pump and the rate of burial of organic matter along continental margins. Thus, climate-induced environmental changes in nutrient availability have the potential to result in climatic feedbacks through ecological and evolutionary shifts in phytoplankton community size structure and the efficiency of the biological pump (Figure 5.1).

Here we present the first record of macroevolutionary change in the size structure of marine phytoplankton communities with a focus on the frustule size of planktonic diatoms over the Cenozoic. Using this dataset, we quantify evolutionary change in the size of diatoms over the last 65 million years and determine if the change in the size structure of the diatom community is a passive evolutionary trend or is caused by climatically-driven change in environmental conditions.

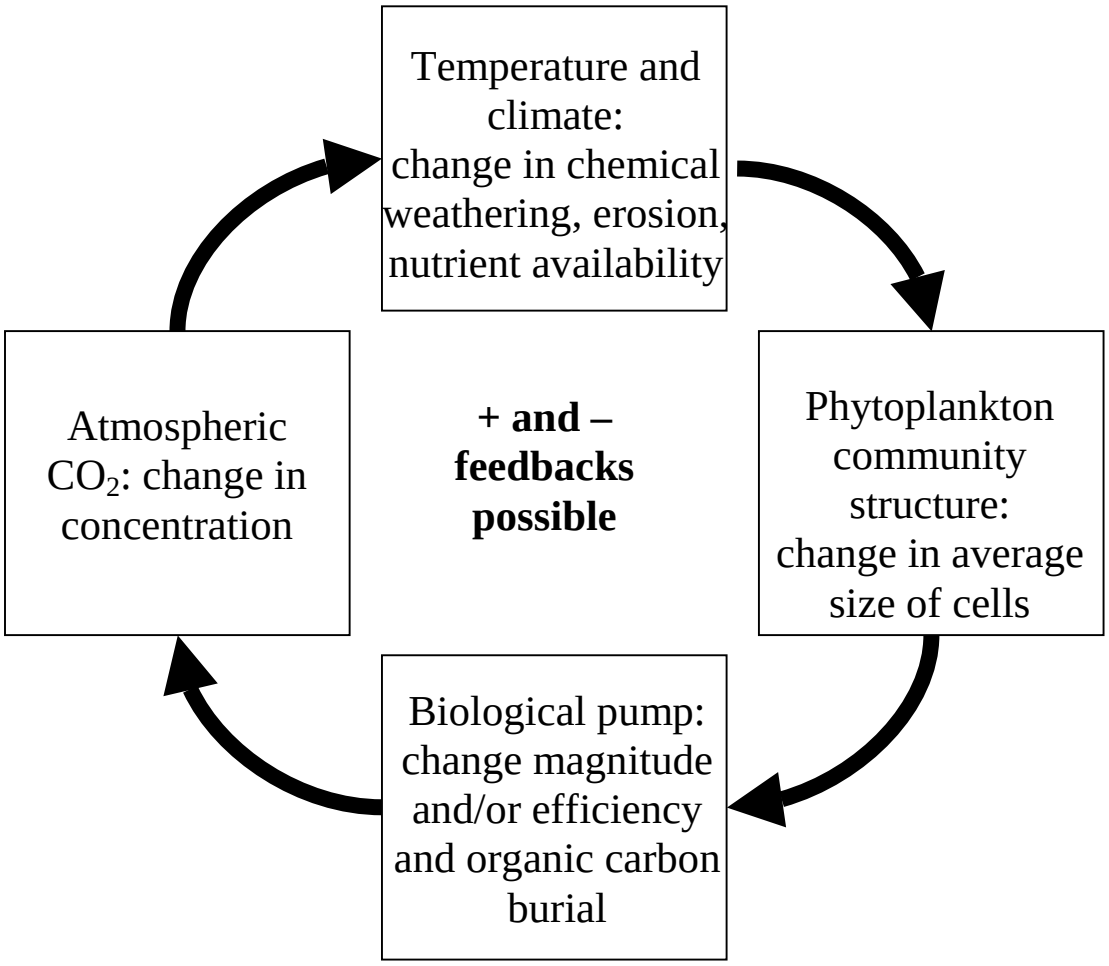

Figure 5-1. Potential feedbacks between climate and macroevolutionary change in the size structure of phytoplankton communities through changes in the biological pump and the sequestration of atmospheric CO_2.

Methods and Materials

Diatom frustule size database

A Cenozoic database of marine diatom frustule size and associated geographic and stratigraphic information was compiled from a combination of measurements of light and scanning electron micrographs and floral descriptions from a variety of literature sources, with an emphasis on reports from the Deep Sea Drilling Project (DSDP) and Ocean Drilling Program (ODP). Diatoms are primarily represented in the fossil record by their silica frustules. In living diatoms, the frustule is composed of an epitheca which overlays the hypotheca and is held together by concentric girdle bands. These components are often separated during preservation or preparation of samples, making the construction of a database of frustule volumes impractical. To compare the size of species with different basic morphologies, the size for each diatom species was estimated as the median of the largest observable projected area (valve or girdle view) of the measured theca. The average size of the frustule of the diatoms making up an assemblage was estimated as the community mean of the median size of the extant species within a particular time interval or geographic region without regard to relative abundance. Diatom species found only as fragments of the theca, for example *Rhizosolenia* and *Neobrunia* spp., have been excluded from the database. This analysis provides low temporal resolution but large sample sizes that enable a broad comparison of the average frustule size within the diatom community between ocean basins (Atlantic and Pacific) and broad latitudinal bands.

Construction of a higher resolution temporal record of frustule size of the diatom community

To construct a higher-resolution temporal record of change in the frustule size of the dominant diatom community through the Cenozoic, the median size of species was matched to the stratigraphic ranges of the dominant marine diatom species provided by the Neptune database (Appendix I, and Figure 5.2). Neptune is a global compilation of micropalaeontological data, including 389 species of diatoms, from 165 drill holes from Legs 1-135 of the DSDP and ODP, adjusted to a uniform taxonomic system correcting for synonyms and a common time scale (Spencer-Cervato 1999). Neptune represents the largest, most comprehensive database of the dominant marine fossil diatoms currently available, providing unprecedented spatial and temporal coverage. Nonetheless interpretations must consider the decrease in species diversity in the older part of the record.

The minimum and maximum size of the diatoms was estimated from the species within the community with the most extreme areas for each one million year time interval. These estimates were then used to calculate the % rate of change in frustule area per one million years (Darwins).

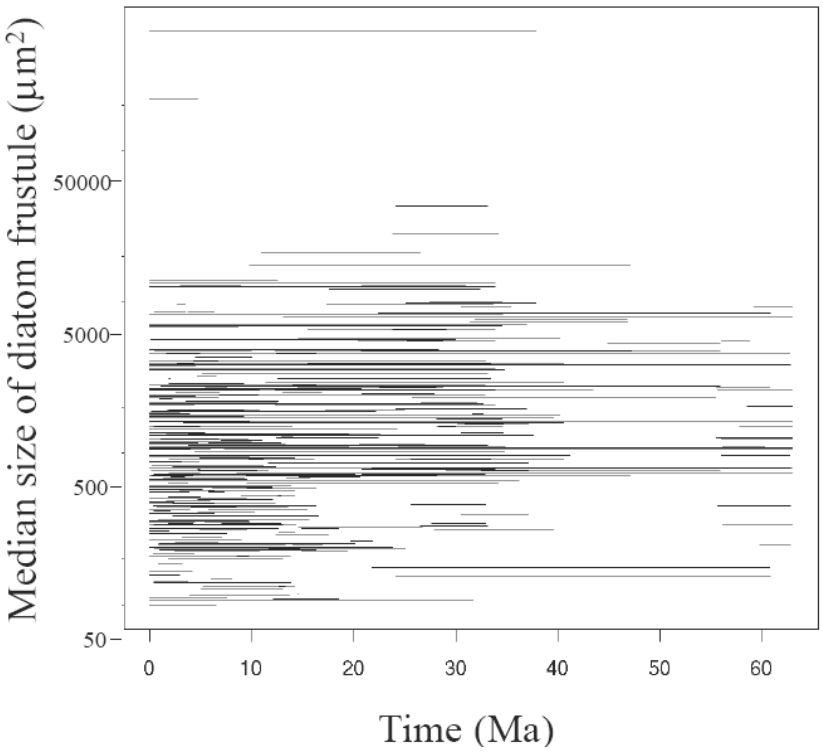

Figure 5-2. Line plot of median frustule size of diatom species in the Neptune database.

Since the change in minimum and maximum size depends on the origination of rare large or small species, and is static over many millions of years, an average rate of change was estimated for 0-35 and 35-65 Ma. The multiplicative size range was estimated as the maximum size divided by the minimum size. To reduce the effect of a few extremely small or large species, the average frustule size of the diatom community was determined from the 90% trimmed mean of the species areas for centric species, pennate species, and all species present, in each one million year time interval.

The mean size of the diatom frustule was compared with paleoenvironmental indicators: global sea level (Haq et al. 1987), % flooded continental area (Ronov 1994), $\delta^{18}O$ of tropical benthic foraminifera (indicator of deep sea temperature) (Wright 2001),

difference in $\delta^{18}O$ of tropical planktonic and benthic foraminifera (indicator of oceanic thermal gradients) (Wright 2001), and $\delta^{13}C$ of organic matter in marine sediment (Hayes et al. 1999). When data sets were not temporally commensurate they were interpolated using the lowest resolution time scale.

Testing the significance of temporal changes in average size of frustule in the diatom community

Permutation tests were used to ensure that changes in the variance in mean size, due to the temporally varying sample size, did not create a false impression of temporal changes in the size distribution. Our statistic of temporal variation was the sum over time of the squared differences between the time-resolved and time-independent size histograms. We generated 999 samples from two different null distributions: the first by permuting the species present in each 5 myr interval, and the second by permuting sizes among species and computing the temporally-resolved size distributions. In both cases, the sample sizes in each time interval were unchanged.

Results and discussion

Macroevolutionary change in the size of the diatom frustule over the Cenozoic

Over the Cenozoic, the minimum size of the frustule decreased, and the maximum size increased, resulting in a 100-fold increase in the multiplicative range (maximum/minimum) in frustule size (Figure 5.3) in concert with increasing species diversity (Spencer-Cervato 1999; Tappan 1980). Contemporaneous with the increase in the range of frustule size, there is a 2.5-fold decrease in mean frustule size (Figure 5.3).

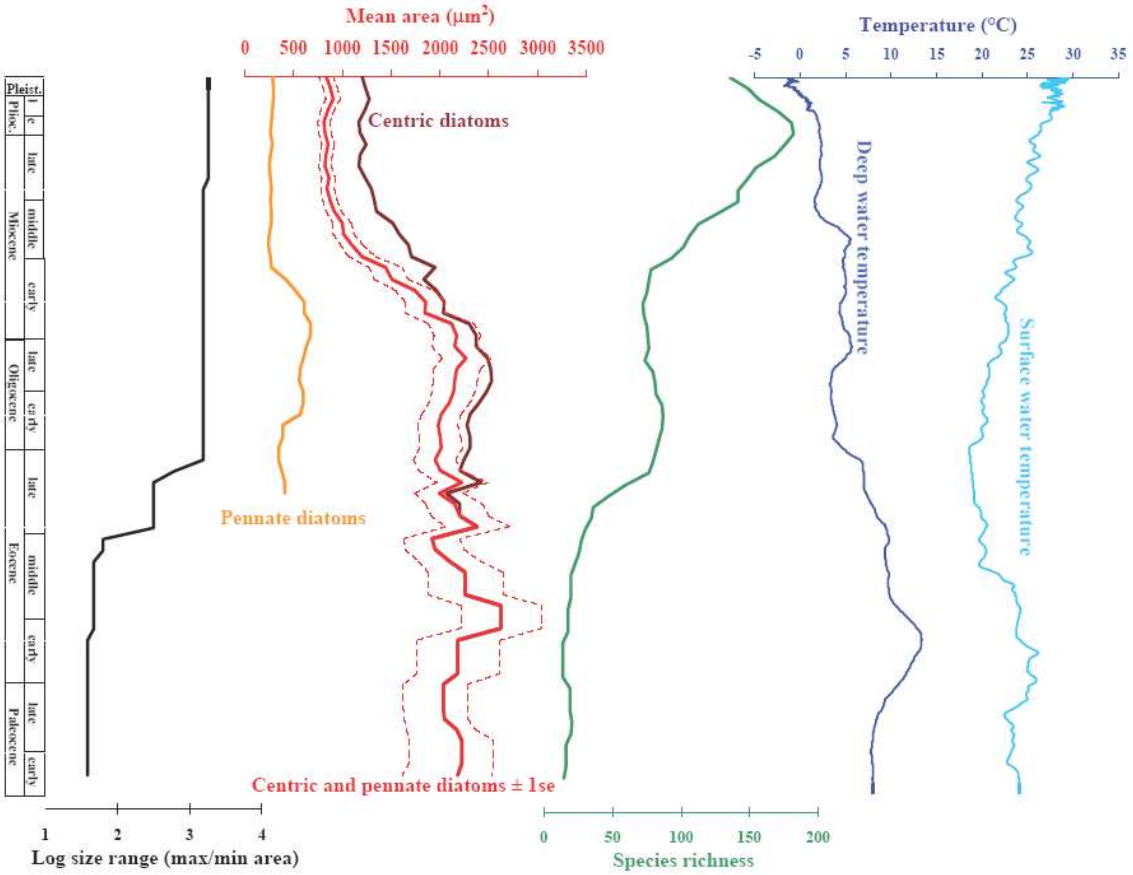

Figure 5-3. Estimates of the size structure of the diatom community using the Neptune database. A) Log multiplicative range of frustule area (maximum/minimum) of the diatom community, B) 5 million year 90% trimmed running mean of mean area (μm^2) of the diatom frustules with one standard error (dashed red lines), centric species only, pennate species only, C) diatom species richness (Spencer-Cervato 1999), and D) surface and deep oceanic temperature (°C) determined from tropical Pacific planktonic and benthic $\delta^{18}O$ of foraminifera (Wright 2001).

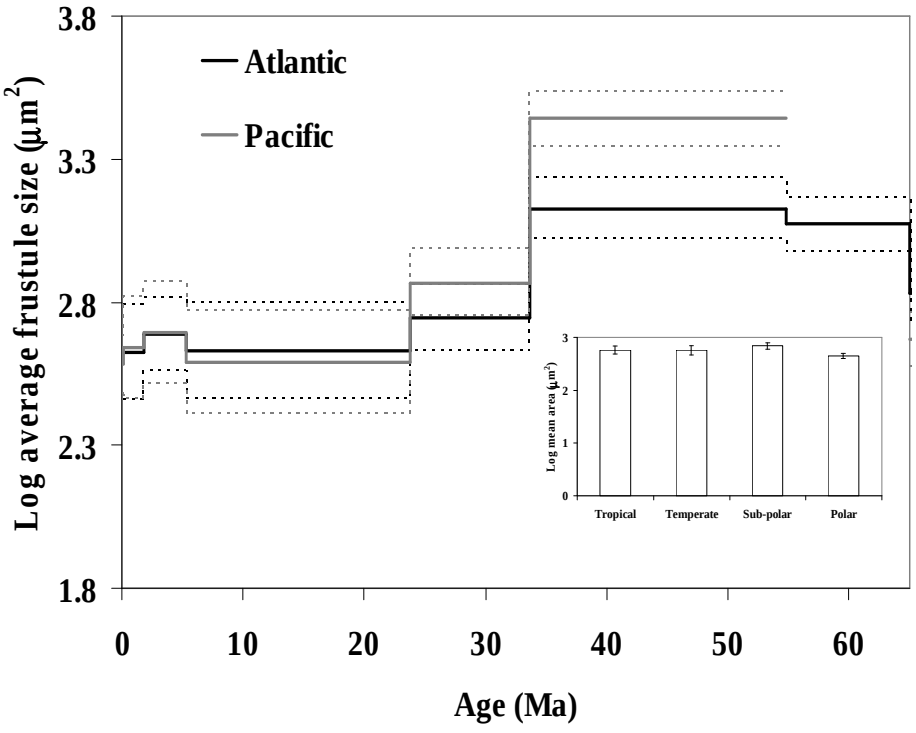

Figure 5-4. Log mean frustule size of the diatom community ($\mu m^2 \pm 2$ standard error dotted lines) as a function of ocean basin: Atlantic (black lines, n= 525), and Pacific (gray lines, n=396); and latitude: tropical (0-20°, n=320), temperate (21-45°, n=171), sub-polar (46-59°, n=390) and polar sites (60-90°, n=498).

as the relative proportion of smaller diatom species increased (Figure 5.2 & 5.3). Statistical tests considering the effect of temporally changing sample size confirm that the changes in mean size are statistically significant ($p<0.05$). There are differences in the average frustule size between communities in the Atlantic and Pacific and in different latitudinal bands, but the differences are not consistent over time and are small relative to the temporal trend (Figure 5.4). The secular change in the mean size of the frustule

within the centric (radially symmetric) and pennate (bilaterally symmetric) communities is qualitatively identical, but because the average size of pennates is generally smaller than the centrics, the increase in the relative diversity of pennate diatoms over the last 35 million years results in an additional decrease in the overall mean area of the diatom frustule over this time period. Tropical and sub-tropical foraminiferal communities also exhibit a change in body size over the last 20 million years (Schmidt et al. 2004), indicating that common environmental factors may be driving the macroevolutionary change in the size of planktonic organisms over the Cenozoic.

The fossil assemblage is a small and potentially biased sample of the species extant in the water column. If there is no temporal change in the size distribution in the water column, and small or large frustules are less likely to be preserved over time, then one would expect that a constriction in extreme frustule size towards the mean would occur over the Cenozoic. The contemporaneous decrease in the minimum and increase in the maximum size, and the statistically significant decrease in the mean size, indicate that size-dependent dissolution is unlikely to have been a primary factor in the observed temporal changes in the size structure of the diatom community over the Cenozoic. These patterns indicate that secular change in the maximum and minimum size are primarily a function of species diversification and neutral selection, while the change in mean size of the diatom frustule may be due to changes in active selection pressures. To assess the factors affecting the different macroevolutionary patterns in frustule size, we consider the different physiological, ecological, and evolutionary forces that control the mean versus the minimum and maximum size of diatom cells within phytoplankton communities.

Physiological boundary on the minimum size of the diatoms

Smaller phytoplankton cells have a higher surface area to volume ratio than larger cells, faster growth rates, and an inherently superior ability to harvest light and nutrients under equilibrium conditions (Kirk 1976; Munk and Riley 1952). The multiple physiological advantages of small size suggest there should be an inevitable evolutionary trend towards smaller phytoplankton taxa over time. A lower bound on the diameter of single-celled photosynthetic organisms of ~0.5 μm is set by minimum functional requirements for nucleic acid content and photosynthetic machinery (Raven 1994). The smallest eukaryotic phytoplankton cells, ~0.7 μm in diameter, come from one of the most ancient phytoplankton classes, the Prasinophyceae. In contrast the smallest diatom species known are ~2 - 4 μm in equivalent spherical diameter. The rate of decrease in the minimum area of the diatom frustule has slowed from 4% to slightly more that 2% per million years from the first to second half of the Cenozoic, suggesting that the diatoms may be approaching their minimum possible cell size. The frustule may be responsible for the relatively large minimum size of the diatoms. The frustule is constructed from multiple layers of aggregated and polymerized silica spheres that are ~30 to 40 nm in length that contribute to the estimate of the size of the diatom frustule and cell (Vrieling et al. 2000). Frustule size is affected by the reproductive cycle, during asexual reproduction each daughter cell develops within the parental cell wall, resulting in ~2-fold decrease in the size of individuals over several generations. Sexual reproduction is cued to a percent decrease in size, and results in a restoration of the original size (Mann et al. 2003), indicating no obvious causal relationship between reproductive strategies and evolutionary changes in the size of diatoms over time.

Physiological and ecological constraints on the maximum size of the diatoms

Very large changes in maximum body size are generally associated with the origination of fundamentally new taxonomic groups (Gould 1966). For example, the average cell diameter of fossil phytoplankton assemblages increased from 5 to 13 μm with the establishment of eukaryotic communities, ~1500 million years ago. Appearing relatively late in the Phanerozoic, diatoms contain species with among the largest cells of all the autotrophic marine phytoplankton groups; they have maximum linear dimensions of ~1 to 3 mm in the case of *Thalassiothrix longissima* and *Ethmodiscus rex*. Their upper size limit is physically constrained by diffusion; cells with diameters much larger than a millimeter can become seriously nutrient-limited due to a decreased diffusive flux as the surface area to volume ratios decrease and nutrient requirements increase (Munk and Riley 1952). Some of the larger extant diatoms have physiological or ecological strategies that compensate for the decrease in nutrient flux from diffusion, for example several *Ethmosdiscus* and *Rhizosolenia* spp. have the ability to migrate downward to take up nutrients and then return to the nutrient-depleted surface to photosynthesize (Ferrario 1995; Villareal and Lipshultz 1995), and other species have nitrogen-fixing symbionts that provide them with an intrinsic source of fixed nitrogen (Carpenter and Janson 2000; Janson et al. 1999). Larger diatoms are often elongated in one dimension, resulting in a greater surface area to volume ratio relative to more compact shapes (Niklas 1994), and have relatively larger nutrient storage vacuoles and lower carbon content on a volume basis (Raven 1987). These novel strategies may be at the root of the continued

evolutionary increase in the upper size of the diatom frustule, which has expanded ~4% every million years over the Cenozoic.

Environmental conditions actively select for macroevolutionary changes in the mean size of the diatom frustule

While changes in the minimum and maximum frustule size of the diatoms can be explained by increases in species diversity within physiological boundaries, the average size of the diatom frustule is highly correlated with environmental conditions. The largest changes in the mean size of the diatom frustule are associated with periods of paleoclimatic change (Table 5.1). The mean size of the diatom frustule is negatively correlated with deep-water temperatures and increases in the equator-to-pole and vertical oceanic temperature gradients (Figure 5.4). The global cooling trend since the early Eocene has led to the expansion of permanent ice on the Antarctic continent, lower bottom water temperatures, and an intensified and isolated Antarctic counter current (Zachos et al. 2001). Changes associated with these trends include a decrease in sea level, a reduction in flooded continental shelf area and increases in both the average equator-to-pole and surface-to-deep thermal gradients (Wright 2001). Over this same time period, the average size of the diatoms has decreased (Table 5.1).

Evolutionary changes in average diatom size in response to long-term environmental changes appear analogous to the ecological shifts in size structure in response to short-term temporal and spatial changes in environmental conditions. While smaller phytoplankton cells have an inherently superior ability to harvest light and nutrients

under equilibrium conditions (Kirk 1976; Munk and Riley 1952), many larger diatoms have nutrient storage vacuoles that provide them with proportionally larger nutrient

Table 5-1. Ordinary least squares regression analyses of the mean area of the diatom frustule (μm3) as a function of paleoclimactic indicators, all adjusted to a uniform timescale (see text for details). All slopes were statistically significant at $p<0.02$.

	Intercept	se	Slope	se	r^2
Sea level (m)	-41	50	1.0E-01	3.2E-02	0.46
% flooded coastal area	2	4	7.4E-03	2.6E-03	0.40
Surface-water temperature (°C)	30	1.5	-4.9E-03	1.0E-03	0.66
Deep-water temperature (°C)	-1.7	2.5	5.5E-03	1.6E-03	0.49
Temperature gradient (°C)	32	2.3	-1.0E-02	1.5E-03	0.79
$\delta^{13}C$ of organic carbon (‰)	-21	0.8	-3.1E-03	5.1E-04	0.67

storage capacity than smaller diatoms (Raven 1997; Stolte and Riegman 1995). As a result, large diatom cells may be able to out-compete smaller cells with faster intrinsic growth rates by achieving a slow but steady growth rate in a pulsed nutrient environment where a small cell can grow rapidly, but for only a small proportion of the time (Grover 1991; Stolte et al. 1994; Stolte and Riegman 1995; Tozzi et al. 2004). This suggests that a change in the availability of nutrients in the euphotic zone will favor diatoms of different sizes (Martin et al. 1994; Stolte et al. 1994). In the modern ocean, small phytoplankton cells dominate in areas characterized by stable, low nutrient conditions such as oceanic gyres. Where nutrient availability in the euphotic zone is high and more

temporally and spatially variable, such as coastal areas, larger cell sizes are favored (Chisholm 1992; Li 2002; Malone 1980).

Extrapolating this ecophysiological relationship to evolutionary scales implies that the size structure of fossil phytoplankton communities provides a qualitative record of the availability of nutrients in the euphotic zone through the Cenozoic. Although global phosphorus accumulation rates and C:P ratios imply a secular increase in nutrient input to the ocean (Follmi 1995; Martin 1996), increases in the thermal stratification of the water column will have moderated the availability of nutrients to phytoplankton in the euphotic zone. An increase in the thermal gradient between the equator and the poles acts to increase wind-driven heat transport (Rea 1994), but the concurrent increase in the average vertical temperature gradient acts to increase the stability of the water column and the energy required to mix nutrients from depth into the euphotic zone (Figure 5.5). The net effect of these changes in the thermal gradient is to alter the energy required to mix nutrient-poor surface waters with the nutrient-rich waters from below the thermocline (Genin et al. 1995), perhaps accounting for the large decrease in the average size of the diatom community in the Neogene (Figure 5.3). In addition, decreases in sea level and shallow flooded continental areas characterized by high nutrient upwelling zones may have selected against the larger diatoms that require intense mixing to avoid sinking out of the euphotic zone and against diatoms that form resting stages that require re-suspension into the euphotic zone after sinking to the sediment surface (McQuoid and Hobson 1996).

Conclusions and future directions.

Macroevolutionary change in diatom community size structure provides an additional framework to aid in the interpretation of paleoenvironmental indicators. For example, it has been hypothesized that the Cenozoic increase in the $\delta^{13}C$ of bulk marine organic matter, $\delta^{13}C_{org,}$ may have resulted from an increase in phytoplankton cell size through time, assuming primary and export production have remained relatively constant (Hayes et al. 1999). A negative correlation between the mean size of the diatom frustule and $\delta^{13}C_{org}$ (Figure 5.6) indicates that alternative hypotheses such as an increase in export production, or a change in the fractionation of carbon due to the increasing dominance of diatoms (Rau et al. 2001) with C_4 and β-carboxylation pathways (Reinfelder 2000), require consideration. In addition, the absence of a relationship between the mean size of the diatoms with traditional indicators of nutrient availability in the ocean (Martin 1996), phosphorus accumulation rates (Follmi 1995) and strontium isotopes (Howarth and McArthur 1997), and the high correlation with the vertical temperature gradient in the ocean, suggests nutrient availability in the upper mixed layer has been primarily forced by thermohaline circulation and not chemical weathering and nutrient input from the land into the coastal ocean. Currently the presence and absence of species is the most common biological signal used to identify large climatic events; examination of changes in the size distribution of organisms provides a complementary biological indicator of climatic change.

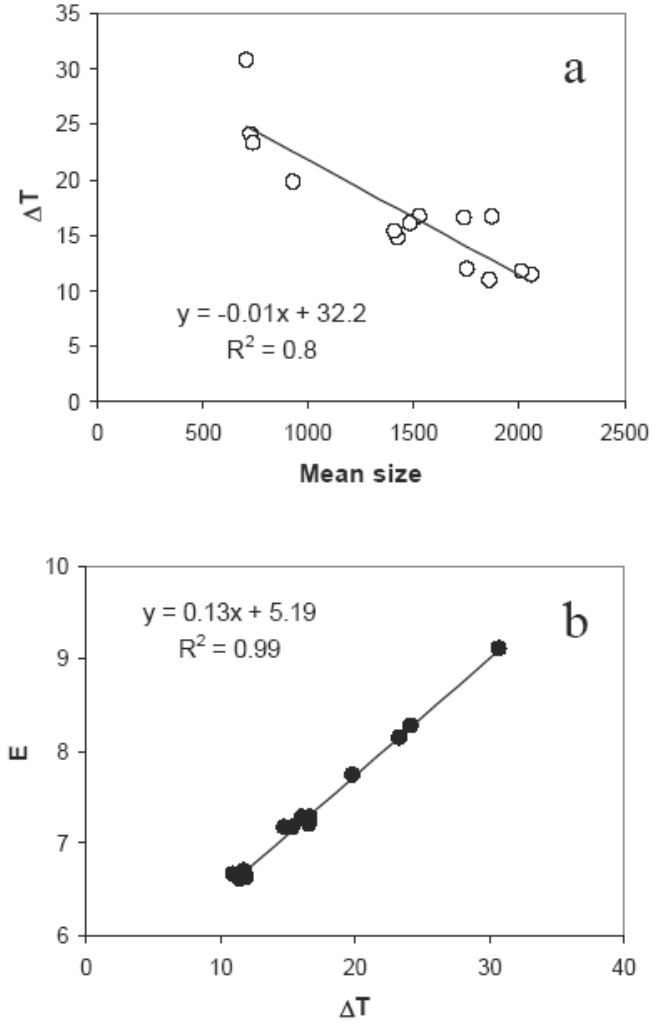

Figure 5-5. Mean area of the diatom frustule as a function of the tropical oceanic temperature gradient and water column stability (*E)*. A) 5 million year 90% trimmed running mean of mean area (μm^2) of the diatom frustule as a function of the vertical temperature gradient. We quantified the vertical temperature gradient from planktonic and benthic $\delta^{18}O$ of foraminiferal calcite from tropical Pacific sites. The vertical temperature gradient was estimated from d*T*/d*z*, where d*T* is the temperature difference between planktonic and benthic $\delta^{18}O$ and d*z* is the difference in depth between planktonic and benthic foraminiferal assemblages. B) Water column stability (*E*, m^{-1}) as a function

of vertical temperature gradient. Water column stability was calculated from the vertical density gradient, assuming pressure and salinity gradients have not changed appreciably over the Cenozoic: E (m^{-1}) = $1/\rho$ (ρ/z) - (g/c^2), where ρ is density as calculated from the linear equation of state, z is depth, g is gravity, and c is the velocity of sound in seawater.

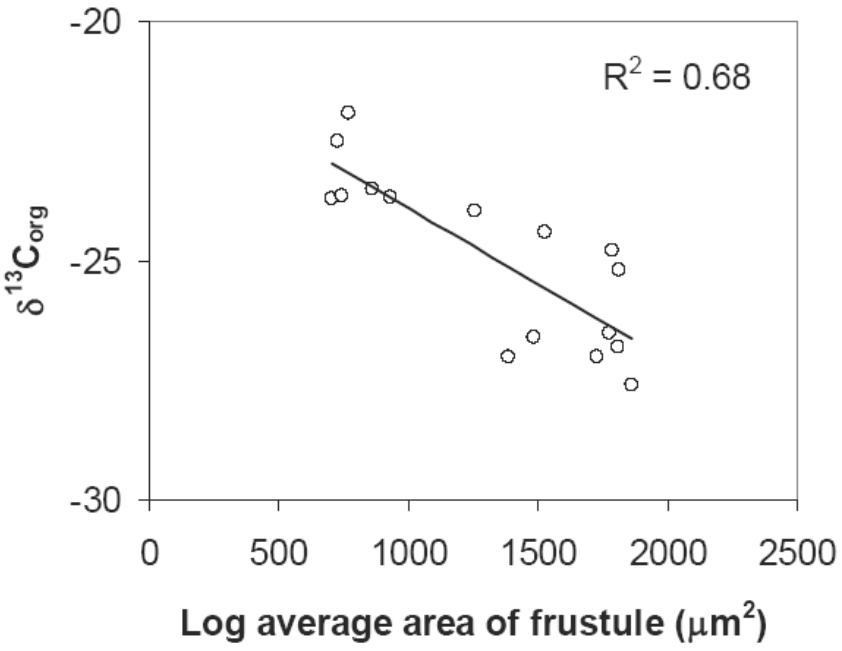

Figure 5-6. Cenozoic changes in the $\delta^{13}C$ of organic carbon (‰) as a function of the mean area of the diatom frustule (μm^2). The carbon data (Hayes et al. 1999) was interpolated to facilitate comparisons.

Appendix I.

Minimum, median, and maximum area (μm^2) of diatom species in Neptune database with the date (in myr) of their first (FAD) and last (LAD) occurrence in the fossil record and references for size estimates. Note in cases where there are more references than observations, linear dimensions were obtained.

Genus	species	Min	Median	Max	n	LAD	FAD	Ref.
Achtinoptychus	*senarius*	266	904	1032	4	0	40	(1-4)
Achtinoptychus	*bipunctatus*	590	592	595	2	0	2	(5)
Achtinoptychus	*splendens*	1417	1571	7933	3	14	33	(2, 4, 6)
Actinocyclus	*actinochilus*	81	442	803	2	0	2	(7)
Actinocyclus	*ochotensis*	111	311	1044	6	0	14	(8-10)
Actinocyclus	*curvatulus*	218	719	3317	17	0	33	(4, 11-14)
Actinocyclus	*ingens*	219	779	1759	14	0	22	(1, 3, 4, 7, 14-18)
Actinocyclus	*octonarius*	256	858	8679	8	0	32	(4, 6, 7)
Actinocyclus	*ellipticus*	317	777	1724	6	0	27	(1, 4, 16, 17, 19, 20)
Actinocyclus	*fryxellae*	572	1229	1885	2	7	11	(21)
Actinocyclus	*karstenii*	625	948	1436	14	2	12	(3, 7, 14)
Actinocyclus	*moronensis*	703	703	703	1	6	14	(15)
Actinocyclus	*lanceolatus*	875	875	875	1	0	6	(22)
Actinocyclus	*elongatus*	886	886	886	1	2	8	(23)
Actinocyclus	*fasciculatus*	1048	1575	2102	2	2	2	(24)
Actinocyclus	*oculatus*	1255	1325	1395	2	1	5	(4, 12)
Annellus	*californicus*	2102	2301	3106	6	12	16	(15, 25)
Asterolampra	*punctifera*	1108	5012	8507	7	27	35	(26, 27)
Asterolampra	*vulgaris*	1500	3683	9544	9	31	47	(24, 26, 28)
Asterolampra	*acutiloba*	1809	1809	1809	1	5	33	(15)
Asterolampra	*affinis*	2061	2061	2061	1	4	33	(27)
Asterolampra	*insignis*	3028	3795	7292	3	32	47	(26, 27)
Asterolampra	*schmidtii*	3293	4948	6372	6	28	38	(6, 26)
Asterolampra	*marylandica*	3524	3524	3524	1	0	37	(19)
Asterolampra	*grevillei*	4188	4188	4188	1	0	35	(29)
Asteromphalus	*petersonii*	385	685	843	3	0	5	(30)
Asteromphalus	*heptactis*	652	1932	3213	2	0	7	(11, 12)
Asteromphalus	*parvulus*	721	825	929	2	0	5	(11)
Asteromphalus	*arachne*	855	855	855	1	0	7	(4)
Asteromphalus	*darwinii*	961	961	961	1	2	9	(12)
Asteromphalus	*oligocenicus*	1175	4847	5746	4	17	34	(26, 27)
Asteromphalus	*hookeri*	1311	1311	1311	1	0	10	(11)
Asteromphalus	*robustus*	1385	3378	4776	3	0	9	(31)

Asteromphalus	*kennettii*	2155	2155	2155	1	4	10	(3)
Asteromphalus	*flabellatus*	2315	2315	2315	1	0	5	(31)
Asteromphalus	*imbricatus*	2566	6932	11298	2	0	13	(23, 32)
Asteromphalus	*symmetricus*	2900	2900	2900	1	20	28	(3)
Azpeitia	*endoi*	242	1265	3020	5	3	39	(7, 17)
Azpeitia	*tabularis*	314	481	1661	16	0	17	(3, 7, 14)
Azpeitia	*gombosi*	987	1370	1753	2	23	29	(7, 24)
Azpeitia	*oligocenica*	1194	1401	3035	3	11	41	(24, 27, 33)
Azpeitia	*vetustissima*	1340	2083	2826	2	0	30	(15, 34-36)
Azpeitia	*nodulifer*	1395	1395	1395	1	1	20	(4, 7, 29)
Bacteriastrum	*hyalinum*	79	79	79	1	0	3	(19)
Bacteriosira	*fragilis*	217	290	1111	7	0	3	(1, 10, 31)
Baxteria	*brunii*	254	841	920	4	28	35	(26)
Bogorovia	*praepaleacea*	159	159	159	1	9	13	(15)
Bogorovia	*veniamini*	372	372	372	1	21	27	(15)
Cestodiscus	*parmula*	459	459	459	1	26	33	(36)
Cestodiscus	*stokesiasus*	545	553	637	3	24	35	(36)
Cestodiscus	*demergitus*	679	685	1109	3	31	35	(37)
Cestodiscus	*trochus*	783	783	783	1	30	35	(36)
Cestodiscus	*pulchellus*	844	1320	5582	7	12	34	(15, 24, 36, 38)
Cestodiscus	*peplum*	1054	1429	1804	2	14	16	(15)
Cestodiscus	*reticulatus*	1558	2762	3966	2	25	34	(24, 39)
Cestodiscus	*robustus*	6644	6644	6644	1	28	34	(15)
Cestodiscus	*antarcticus*	21576	21576	21576	1	24	33	(39)
Cladogramma	*dubium*	355	355	355	1	9	29	(40)
Cocconeis	*costata*	295	307	319	2	0	9	(1, 11)
Cocconeis	*scutellum*	946	1072	1199	2	0	11	(1)
Cocconeis	*pseudomarginata*	1143	1143	1143	1	1	2	(41, 42)
Corethron	*criophilum*	810	810	810	1	3	11	(24)
Coscinodiscus	*flexuosus*	243	281	453	10	9	14	(31, 34, 35, 43)
Coscinodiscus	*praeyabei*	250	642	830	7	13	14	(31)
Coscinodiscus	*marginatus*	380	1337	9327	14	0	41	(11, 15)
Coscinodiscus	*nodulifer*	404	1265	6501	10	0	21	(1, 12, 15, 19, 32, 34, 35)
Coscinodiscus	*plicatus*	422	445	1661	3	0	14	(12, 15)
Coscinodiscus	*yabei*	452	505	3116	5	9	13	(12, 15, 31)
Coscinodiscus	*lewisianus*	529	1279	4070	6	12	33	(15, 17, 24)
Coscinodiscus	*temperei*	555	1104	1652	2	4	13	(15, 17)
Coscinodiscus	*stellaris*	568	2615	5475	10	0	35	(11)
Coscinodiscus	*vulnificus*	574	959	2133	6	2	3	(44)
Coscinodiscus	*crenulatus*	622	850	1077	2	0	40	(1, 11)
Coscinodiscus	*tuberculatus*	690	754	1017	4	9	14	(6, 15)
Coscinodiscus	*pustulatus*	702	1143	1982	6	2	7	(8, 45, 46)
Coscinodiscus	*deformans*	884	1074	1264	2	6	12	(34, 35)
Coscinodiscus	*rhombicus*	1024	1040	1669	3	17	34	(3, 15, 24)
Coscinodiscus	*africanus*	1117	2034	5529	6	0	7	(23, 30, 32)
Coscinodiscus	*radiatus*	1232	3574	3787	6	0	35	(4, 6, 15)
Coscinodiscus	*blysmos*	1256	1256	1256	1	13	17	(15)
Coscinodiscus	*gigas*	1329	1345	109363	3	1	13	(23, 30)

Coscinodiscus	*superbus*	2011	3399	6245	8	15	40	(26, 37)
Coscinodiscus	*excavatus*	2089	3646	13267	6	31	35	(15, 37)
Coscinodiscus	*elegans*	2381	2381	2381	1	0	10	(7)
Coscinodiscus	*kolbei*	2951	3538	4126	2	2	5	(47)
Coscinodiscus	*apiculatus*	4316	4316	4316	1	4	6	(37)
Coscinodiscus	*occulus-iridis*	6210	6321	6432	2	0	34	(6)
Coscinodiscus	*asteromphalus*	6669	6669	6669	1	0	34	(4, 11)
Coscinodiscus	*hajosiae*	14202	14202	14202	1	24	34	(36)
Coscinodiscus	*centralis*	110391	110391	110391	1	0	5	(48)
Cosmiodiscus	*insignis*	973	1026	1080	2	2	11	(1, 44)
Craspedodiscus	*umbonatus*	1393	1393	1393	1	40	44	(49)
Craspedodiscus	*coscinodiscus*	4069	10632	17195	2	11	27	(15)
Crucidenticula	*nicobarica*	31	55	191	12	12	18	(1, 16, 50, 51)
Crucidenticula	*kanayae*	76	159	256	19	15	18	(1, 16, 50, 51)
Crucidenticula	*punctata*	90	149	505	11	13	14	(1, 16)
Cussia	*lancettula*	85	101	259	3	2	13	(30)
Cyclotella	*striata*	318	338	599	5	0	6	(1, 32, 52)
Cymatogonia	*amblyoceras*	1204	1204	1204	1	15	22	(31)
Cymatosira	*compacta*	93	164	192	5	15	27	(34, 35)
Cymatosira	*debyi*	103	180	257	2	0	10	(1)
Cymatotheca	*weissflogii*	350	350	350	1	2	3	(53)
Dactyliosolen	*antarcticus*	120	120	120	1	0	24	(7)
Delphineis	*surirella*	40	105	221	3	0	10	(1, 4)
Delphineis	*ischaboensis*	44	122	182	8	2	3	(1)
Denticulopsis	*praedimorpha*	19	68	283	26	5	13	(1, 3, 15, 18)
Denticulopsis	*dimorpha*	34	121	314	57	1	13	(1, 16, 50, 51)
Denticulopsis	*seminae*	55	143	374	11	0	9	(19)
Denticulopsis	*hustedtii*	58	148	585	34	1	16	(1, 7, 15, 17, 18, 24)
Denticulopsis	*lauta*	60	123	601	27	2	16	(1, 16, 17)
Denticulopsis	*hyalina*	62	113	369	23	0	15	(1, 4, 16)
Denticulopsis	*maccollumii*	70	99	204	4	12	17	(7, 24, 50, 51)
Denticulopsis	*katayamae*	125	168	234	7	1	9	(1, 16)
Denticulopsis	*meridionalis*	148	193	231	4	10	12	(24)
Denticulopsis	*norwegica*	170	340	659	11	13	16	(16)
Denticulopsis	*miocenica*	183	263	347	4	13	14	(1, 16)
Denticulopsis	*punctata*	425	474	523	2	10	16	(15, 17)
Dimerogramma	*fossile*	92	132	156	3	20	22	(34, 35)
Diploneis	*bombus*	298	298	298	1	0	5	(1, 50, 51)
Diploneis	*smithii*	435	443	451	2	0	5	(1, 4)
Ethmodiscus	*rex*	164551	313994	636769	4	0	38	(54)
Eucampia	*antarctica*	541	572	603	2	0	19	(7)
Goniothecium	*decoratum*	624	1357	2091	2	15	28	(40)
Goniothecium	*odontella*	778	2995	3886	7	16	33	(6, 26)
Grunowiella	*gemmata*	632	632	632	1	56	63	(38)
Hemiaulus	*pungens*	87	166	263	5	27	33	(55)
Hemiaulus	*incisus*	143	665	1247	6	18	63	(6, 38)
Hemiaulus	*polycystinorum*	237	561	1100	23	16	41	(37, 38, 40)
Hemiaulus	*taurus*	393	393	393	1	21	34	(49)

Hemiaulus	*subacutus*	451	636	821	2	30	56	(37)
Hemiaulus	*polymorphus*	661	932	998	3	7	63	(6)
Hemiaulus	*altar*	790	790	790	1	31	37	(49)
Hemiaulus	*exiguus*	990	990	990	1	30	37	(37)
Hemiaulus	*caracteristicus*	1185	1185	1185	1	26	55	(6)
Hemiaulus	*peripterus*	4206	4684	5161	2	59	63	(39)
Hemiaulus	*rectus*	6055	6055	6055	1	18	32	(39)
Hemidiscus	*ovalis*	104	175	247	2	5	12	(1, 56, 57)
Hemidiscus	*karstenii*	439	558	678	2	0	10	(3, 7, 28, 37, 43, 51, 58, 59)
Hemidiscus	*cuneiformis*	496	993	1597	8	0	22	(1, 7, 10, 12, 15, 19, 23, 45, 51, 59-63)
Hemidiscus	*simplicissimus*	661	824	962	3	1	10	(10, 31)
Hemidiscus	*triangularus*	1020	1367	1808	4	5	8	(3)
Hyalodiscus	*obsoletus*	584	584	584	1	6	13	(1)
Ikebea	*tenuis*	43	136	297	8	6	14	(1, 18)
Katathiraia	*aspera*	76	104	129	4	9	14	(53)
Kisseleviella	*carina*	130	194	387	8	7	13	(1, 6)
Kozloviella	*minor*	820	1097	5220	3	27	32	(24, 26)
Lisitzinia	*ornata*	1234	1234	1234	1	21	28	(15, 24)
Lithodesmium	*minusculum*	39	387	413	3	5	10	(60)
Lithodesmium	*undulatum*	391	391	391	1	5	5	(11)
Lithodesmium	*reynoldsii*	611	611	611	1	7	11	(1)
Lithodesmium	*cornigerum*	1621	1621	1621	1	5	7	(64)
Macrora	*stella*	430	448	466	2	12	37	(27)
Mediaria	*splendida*	267	267	267	1	2	16	(3, 51)
Melosira	*albicans*	69	110	150	2	0	4	(1)
Navicula	*lyra*	242	2427	4300	9	0	28	(53, 64)
Navicula	*udentsevii*	292	292	292	1	32	33	(24, 27)
Navicula	*wisei*	714	728	742	2	3	4	(24)
Neodenticula	*kamtschatica*	7	67	211	44	0	14	(1, 16)
Neodenticula	*koizumii*	23	72	185	16	0	4	(4, 16)
Nitzschia	*cylindrus*	14	55	104	7	0	8	(11)
Nitzschia	*rolandii*	15	63	139	19	5	13	(1, 4, 16, 31, 46)
Nitzschia	*cylindrica*	21	71	188	3	3	9	(15)
Nitzschia	*bicapitata*	41	49	59	3	0	7	(11)
Nitzschia	*angulata*	42	177	548	23	0	4	(7, 11)
Nitzschia	*challengeri*	44	56	97	5	13	14	(31)
Nitzschia	*porteri*	45	58	70	4	4	14	(15, 31)
Nitzschia	*separanda*	48	167	542	16	0	2	(11)
Nitzschia	*kerguelensis*	62	198	593	12	0	4	(11)
Nitzschia	*grunowii*	63	134	362	11	0	9	(1, 11, 12)
Nitzschia	*curta*	64	82	203	5	0	4	(11)
Nitzschia	*miocenica*	64	187	252	6	5	10	(12, 15, 30)
Nitzschia	*maleinterpretaria*	75	119	163	2	12	25	(15, 24)
Nitzschia	*denticuloides*	78	105	264	5	9	15	(65)
Nitzschia	*interruptestriata*	90	148	251	4	0	8	(1, 4, 12)
Nitzschia	*fossilis*	93	223	335	7	0	10	(1, 4, 12, 15,

								31, 66)
Nitzschia	*granulata*	93	93	93	1	1	3	(31, 53)
Nitzschia	*pusilla*	95	114	133	2	15	19	(7, 34, 35)
Nitzschia	*ritscherii*	97	279	362	12	0	4	(11)
Nitzschia	*evenescens*	105	123	675	4	14	17	(24, 34, 35)
Nitzschia	*interfrigidaria*	122	158	248	3	2	4	(26, 34, 35, 67)
Nitzschia	*praeinterfrigidaria*	126	126	126	1	2	5	(21, 26)
Nitzschia	*grossepunctata*	127	194	261	2	12	16	(65)
Nitzschia	*jouseae*	134	230	366	9	2	6	(1, 4, 12, 15)
Nitzschia	*suikoensis*	144	276	351	4	6	7	(46)
Nitzschia	*januaria*	150	170	190	2	5	14	(7, 21)
Nitzschia	*efferans*	172	194	287	4	2	14	(34, 35)
Nitzschia	*sicula*	173	200	309	3	0	6	(11)
Nitzschia	*reinholdii*	191	330	891	14	0	12	(1, 4, 12, 15, 31)
Nitzschia	*braarudii*	208	208	208	2	0	2	(53, 68)
Nitzschia	*umaoiensis*	218	282	320	5	6	14	(1)
Nitzschia	*claviceps*	259	259	259	1	9	13	(34, 35)
Nitzschia	*pseudokerguelensis*	309	309	309	1	7	14	(65)
Nitzschia	*weaveri*	318	318	318	1	2	4	(7, 26)
Nitzschia	*donahuensis*	330	467	603	2	5	14	(18, 21, 34, 35)
Nitzschia	*seriata*	357	357	357	1	0	4	(11)
Nitzschia	*praereinholdii*	433	433	433	1	3	12	(15, 31)
Nitzschia	*kolaczeckii*	477	477	477	1	0	10	(4, 11)
Nitzschia	*panduriformis*	588	588	588	1	0	5	(2, 19, 37)
Nitzschia	*marina*	618	751	763	3	0	8	(4, 12)
Odontella	*tuomeyi*	182	1110	6723	7	16	29	(40, 64)
Odontella	*aurita*	309	398	486	2	0	29	(1)
Paralia	*sulcata*	105	228	315	7	0	63	(1, 7, 24)
Paralia	*architecturalis*	254	353	386	3	24	47	(15, 44, 49, 69)
Plagiogramma	*staurophorum*	95	345	594	2	1	9	(1)
Planktionella	*sol*	324	324	324	1	0	7	(1, 32)
Porosira	*glacialis*	745	997	1885	4	0	4	(8, 10)
Pseudoeunotia	*doliolus*	142	212	418	7	0	2	(1, 4, 11, 12, 23, 30-32, 62)
Pseudopodosira	*elegans*	211	351	746	3	1	11	(1, 8)
Pseudopodosira	*simplex*	402	402	402	1	22	63	(34, 35)
Pseudopyxilla	*russica*	74	87	89	3	22	61	(55, 69)
Pseudopyxilla	*americana*	116	116	116	1	9	29	(43, 69, 70)
Pseudotriceratium	*radiosoreticulatum*	750	750	750	1	28	35	(40)
Pseudotriceratium	*chenevieri*	759	1076	1570	5	9	44	(5, 40)
Pterotheca	*evermanni*	119	119	119	1	60	63	(37)
Pterotheca	*kittoniana*	166	205	244	2	56	63	(37)
Pterotheca	*clavata*	227	227	227	1	56	63	(71)
Pterotheca	*aculeifera*	553	553	553	1	24	61	(37)

Pyxilla	*reticulata*	1940	2381	10024	6	12	47	(19)
Rhabdonema	*arcuatum*	375	375	375	1	2	5	(41)
Rhabdonema	*japonicum*	596	596	596	2	2	10	(60)
Rhaphidodiscus	*marylandicus*	360	452	1305	5	12	22	(43, 72)
Rhaphoneis	*margaritalimbata*	58	59	60	2	15	15	(31, 34, 35, 73)
Rhaphoneis	*amphiceros*	213	306	400	2	0	36	(28, 67)
Rhaphoneis	*angustata*	227	227	227	1	0	16	(37)
Riedelia	*claviger*	389	389	389	1	33	37	(37)
Rocella	*praenitida*	102	463	782	5	21	33	(5, 24, 38)
Rocella	*vigilans*	429	1559	3724	12	12	31	(15, 24, 33, 39, 74)
Rocella	*gelida*	907	3957	9908	11	13	26	(15, 19, 67, 74)
Roperia	*tesselata*	210	615	2146	19	0	7	(1, 11, 12, 19, 30, 32)
Roperia	*praetesselata*	324	593	594	3	4	6	(30)
Rossiella	*tatsunokuchiensis*	125	158	200	5	3	7	(1, 4)
Rossiella	*praepaleacea*	225	225	225	1	6	14	(15)
Rossiella	*paleacea*	646	727	808	2	7	24	(15)
Rossiella	*symmetrica*	1535	2810	3821	3	20	29	(39)
Rouxia	*naviculoides*	97	116	122	4	1	14	(7, 9, 43, 44, 58)
Rouxia	*isopolica*	127	127	127	1	1	20	(58)
Rouxia	*peragalli*	147	202	287	8	2	12	(3, 8, 21, 43, 51)
Rouxia	*californica*	182	322	420	6	0	20	(1, 4, 9, 15, 44, 58)
Rouxia	*yabei*	260	298	336	2	6	12	(9)
Rouxia	*heteropolara*	300	300	300	1	2	6	(7, 44)
Rouxia	*obesa*	453	453	453	1	24	41	(26)
Rouxia	*granda*	1471	1471	1471	1	29	35	(26)
Sceptroneis	*grunowii*	92	94	96	2	28	33	(44, 69)
Sceptroneis	*pesplanus*	108	284	460	2	26	33	(26, 37)
Sceptroneis	*tenue*	425	425	425	1	29	34	(37)
Sceptroneis	*humuncia*	454	764	780	3	28	30	(27)
Sceptroneis	*lingulatus*	481	481	481	1	56	63	(37)
Simonseniella	*barboi*	115	473	604	3	0	28	(4)
Simonseniella	*praebarboi*	762	762	762	1	10	33	(7, 9, 19, 45)
Skeletonema	*barbadense*	199	199	199	1	31	37	(26, 49)
Sphynctolethus	*hemiauloides*	1021	1021	1021	1	59	63	(53, 75)
Stellarima	*microtrias*	1913	1913	1913	1	3	63	(7, 71)
Stellarima	*primalabiata*	3850	4692	6502	5	21	63	(71)
Stephanogonia	*hanzawae*	665	665	665	1	4	19	(40)
Stephanopyxis	*ornata*	430	430	430	1	34	35	(24)
Stephanopyxis	*dimorpha*	612	934	1256	2	0	3	(1, 31)
Stephanopyxis	*horridus*	1054	1306	1559	2	2	5	(8, 45)
Stephanopyxis	*grunowii*	2283	3149	3876	4	21	56	(6, 26, 37, 40)
Stephanopyxis	*spinosissima*	2427	3278	4130	2	24	34	(6, 34, 35)
Stephanopyxis	*marginata*	3946	4411	4724	4	22	61	(6, 40)
Stephanopyxis	*turris*	5247	5339	5431	2	0	63	(6, 8, 19, 30,

								37, 40, 45, 55, 76)
Synedra	*indica*	34	74	523	8	6	8	(52)
Synedra	*jouseana*	340	542	3790	4	4	33	(8, 24, 34, 40)
Synedra	*miocenica*	508	508	508	1	7	35	(34, 35)
Thalassionema	*nitzschioides*	53	53	53	1	0	32	(7, 23)
Thalassionema	*bacillaris*	168	168	168	1	0	7	(1)
Thalassionema	*schraderi*	304	411	634	4	7	10	(1)
Thalassionema	*robusta*	332	332	332	1	8	14	(31, 37)
Thalassionema	*hirosakiensis*	350	603	747	7	4	33	(31, 37, 45, 56, 77)
Thalassiosira	*oestrupii*	58	228	607	40	0	6	(1, 4, 7, 8, 11, 13, 15, 30-32, 40, 50, 62, 63, 78)
Thalassiosira	*nativa*	58	63	227	5	2	11	(10, 21, 30, 31, 78)
Thalassiosira	*nidulus*	88	285	689	5	0	10	(7, 8, 18, 31, 40, 78)
Thalassiosira	*decipiens*	94	181	338	4	0	9	(4, 8, 10, 11, 23, 31, 40)
Thalassiosira	*marujamica*	104	336	684	7	0	9	(1)
Thalassiosira	*delicatula*	112	138	392	5	3	7	(11)
Thalassiosira	*miocenica*	121	201	330	7	5	10	(1, 12, 15, 18, 21, 30, 46, 56, 62, 78)
Thalassiosira	*gracilis*	122	435	588	10	0	3	(7, 11, 43)
Thalassiosira	*lineata*	154	253	471	6	0	12	(1, 4, 8, 10, 11, 30, 32, 63)
Thalassiosira	*burckliana*	177	214	572	3	6	11	(56)
Thalassiosira	*praeconvexa*	177	177	177	1	5	10	(15, 30, 31, 46)
Thalassiosira	*yabei*	192	454	591	5	10	11	(1, 18)
Thalassiosira	*jacksonii*	196	205	214	2	1	9	(1, 21, 46, 78)
Thalassiosira	*gravida*	197	736	1658	8	0	9	(1, 4, 8, 11, 13, 31, 78)
Thalassiosira	*trifulta*	222	539	732	4	0	6	(1, 4, 12)
Thalassiosira	*opposita*	227	283	695	4	3	6	(46)
Thalassiosira	*leptopus*	254	962	15197	3	0	34	(4, 15, 19, 32, 62, 63)
Thalassiosira	*convexa*	254	678	1134	10	2	23	(1, 4, 15, 19, 30-32, 47, 50, 62, 63, 78)
Thalassiosira	*fraga*	254	351	1073	4	15	21	(1, 15, 24, 47)
Thalassiosira	*singularis*	260	458	590	3	6	9	(1)
Thalassiosira	*oliverana*	265	591	1102	5	0	10	(7, 50)
Thalassiosira	*antiqua*	272	630	1906	6	1	10	(1, 4, 8, 10, 31, 78)
Thalassiosira	*lentiginosa*	280	818	1248	6	0	4	(7)
Thalassiosira	*antarctica*	289	289	289	1	0	5	(7, 30, 43)
Thalassiosira	*temperei*	297	581	1388	8	6	10	(1, 16)
Thalassiosira	*lacustris*	365	365	365	2	0	9	(30)
Thalassiosira	*manifesta*	394	581	779	3	3	13	(1, 40)

Thalassiosira	*plicata*	404	852	1335	5	0	7	(4, 12, 30, 32, 46, 62, 63)
Thalassiosira	*hyalina*	408	408	408	1	0	4	(1, 8, 10, 40)
Thalassiosira	*symmetrica*	471	485	2426	4	0	7	(4, 11)
Thalassiosira	*eccentrica*	515	991	4983	10	0	33	(30, 31)
Thalassiosira	*nordenskioeldii*	544	544	544	1	0	5	(1, 8, 31, 44)
Thalassiosira	*spinosa*	633	633	633	1	12	22	(77)
Thalassiosira	*punctata*	635	1262	2524	3	2	10	(1, 8, 31, 78)
Thalassiosira	*kryophila*	757	757	757	1	0	5	(8)
Thalassiosira	*zabelinae*	758	758	758	1	2	9	(1, 8, 10, 31, 40, 78)
Thalassiosira	*gersondei*	825	1963	2375	3	7	11	(7)
Thalassiosira	*bukryi*	855	909	962	2	32	33	(15, 49)
Thalassiosira	*symbolophora*	855	1325	1795	2	0	11	(4, 30)
Thalassiosira	*spumellaroides*	907	964	1020	2	17	25	(15, 77)
Thalassiosira	*striata*	942	1983	3975	6	3	4	(7, 24, 59)
Thalassiosira	*pacifica*	1041	1180	3232	3	0	7	(31, 62, 63)
Thalassiosira	*tumida*	1911	1911	1911	1	0	5	(11)
Thalassiosira	*webbi*	4207	4862	5518	2	3	4	(24)
Thalassiosira	*usatschevii*	4586	5728	6870	2	3	9	(1)
Thalassiosira	*elliptipora*	4916	4916	4916	1	1	4	(59)
Thalassiothrix	*miocenica*	100	167	469	5	5	13	(31, 50)
Thalassiothrix	*frauenfeldii*	159	159	159	1	0	9	(7, 77)
Trachyneis	*aspera*	1051	1051	1051	1	0	4	(11)
Triceratium	*schulzii*	99	373	1067	17	29	63	(37, 69, 76)
Triceratium	*barbadense*	128	156	236	3	28	40	(37, 40)
Triceratium	*cinnamomeum*	362	555	778	4	0	19	(19, 23, 30, 31, 62)
Triceratium	*condecorum*	454	454	454	1	9	33	(31, 37)
Triceratium	*mirabile*	552	552	552	1	56	60	(32)
Triceratium	*acutangulum*	1500	1500	1500	1	3	7	(37)
Triceratium	*cellulosum*	2426	2782	3790	5	56	59	(55)
Triceratium	*unguiculatum*	3176	4927	7180	6	25	38	(26, 79)
Triceratium	*groningensis*	3421	7303	14992	6	21	31	(26, 37)
Trinacria	*deciusii*	134	1326	2517	2	56	63	(53)
Trinacria	*pileolus*	241	3064	6565	4	9	63	(6, 26, 37, 43, 79)
Trinacria	*excavata*	309	1381	1619	5	6	56	(6, 19, 30, 37, 40, 80)
Trinacria	*subcapitata*	466	466	466	1	32	34	(37)
Trinacria	*regina*	2479	8896	9772	6	10	47	(30, 80)
Trinacria	*simulacrum*	2647	2647	2647	1	45	56	(6, 19, 28, 37, 81)
Trochosira	*spinosa*	53	61	248	5	0	9	(27, 40, 71)
Trochosira	*concava*	260	338	416	2	7	10	(31)
Xanthiopyxis	*oblonga*	800	800	800	1	28	41	(6, 40, 77)
Xanthiopyxis	*acrolopha*	986	986	986	1	24	35	(6, 43)

References for the diatom frustule size database

1. Akiba, F. (1986) in *Initial reports of the Deep Sea Drilling Project; covering Leg 87A of the cruises of the drilling vessel Glomar Challenger, Yokohama, Japan, to Yokohama, Japan, June-July, 1982, and Leg 87B from Yokohama, Japan, to Hakodate, Japan, July-August, 1982*, eds. Kagami, H., Karig, D. E., Bray, C. J., Charvet, J., Coulbourn, W. T., Kinoshita, H., Lagoe, M. B., Lang, T. H., Lombari, G. A., Lundberg, N., Machihara, T., Mukhopadhyay, P., Smith, A. J., Stein, C. L., Taira, A., Akiba, F., Cadet, J.-P., Fujioka, K., Leggett, J. K., Matsumoto, R., Niitsuma, N. & Whalen, E. (Texas A & M University, Ocean Drilling Program, College Station, TX), Vol. 87, pp. 393-481.
2. Winter, D. M. (2001) in *Proceedings of the Ocean Drilling Program, scientific results, Northwest Atlantic sediment drifts; covering Leg 172 of the cruises of the drilling vessel JOIDES Resolution; Charleston, South Carolina, to Lisbon, Portugal; sites 1054-1064, 14 February-15 April 1997*, eds. Keigwin, L. D., Rio, D., Acton, G. D., Bianchi, G. G., Borowski, W. S., Cagatay, N., Chaisson, W. P., Clement, B. M., Cortijo, E., Dunbar, G. B., Flood, R. D., Franz, S.-O., Giosan, L., Gruetzner, J., Hagen, S., Haskell, B., Horowitz, M. J., Laine, E. P., Lund, S. P., Okada, M., Poli, M.-S., Raffi, I., Reuer, M. K., Ternois, Y. G., Williams, T., Winter, D. M., Yokokawa, M. E. & Arnold, E. (Texas A & M University, Ocean Drilling Program, College Station, TX), Vol. 172, pp. 49.
3. Censarek, B. & Gersonde, R. (2002) *Southern Ocean Eocene-Pleistocene stratigraphies; insights from ocean drilling* **45,** 309-356.
4. Olschesky, K. S. & Laws, R. A. (2002) *Proc. ODP, Sci. Results* **185,** 1-31.
5. Arney, J., McGonigal, K. L., Ladner, B. C. & Wise, S. W., Jr. (2003) in *Proc. ODP, Sci. Results, 183*, eds. Frey, F. A., Coffin, M. F., Wallace, P. J. & Quilty, P. G.
6. Hajos, M. & Stradner, H. (1975) *Initial Reports of the Deep Sea Drilling Project* **29,** 913-1009.
7. Iwai, M. & Winter, D. M. (2002) *Proceedings of the Ocean Drilling Program, scientific results, Antarctic glacial history and sea-level change; covering Leg 178 of the cruises of the drilling vessel JOIDES Resolution; Punta Arenas, Chile, to Cape Town, South Africa; sites 1095-1103; 5 February-9 April 1998* **178**, 57.
8. Koizumi, I. (1973) in *Initial Reports of the Deep Sea Drilling Project* (Texas A & M University, Ocean Drilling Program, College Station, TX), Vol. 19, pp. 805-855.
9. Schrader, H.-J. (1973) in *Initial reports of the Deep Sea Drilling Project, covering Leg 18 of the cruises of the drilling vessel Glomar Challenger, Honolulu, Hawaii to Kodiak, Alaska May-July 1971*, eds. Musich, L. F. & Weser, O. E. (Publisher: Texas A & M University, Ocean Drilling Program, College Station, TX, United States, Texas A & M University), Vol. 182.
10. Koizumi, I. (1975) in *Initial Reports of the Deep Sea Drilling Project* (Texas A & M University, Ocean Drilling Program, College Station, TX), Vol. 31, pp. 779-819.

11. Fenner, J., Schrader, H.-J. & Wienigk, H. (1976) *Initial Reports of the Deep Sea Drilling Project* **35,** 757-813.
12. Koizumi, I. & Tanimura, Y. (1986) in *Deep Sea Drilling Project Leg 86*, Vol. 86, pp. 269-300.
13. Koc, N. & Flower, B. P. (1998) *Proceedings of the Ocean Drilling Program; scientific results; East Greenland margin; covering Leg 152 of the cruises of the drilling vessel JOIDES Resolution, Reykjavik, Iceland, to St. John's, Newfoundland, sites 914-919, 24 September-22 November 1993* **152,** 209-219.
14. Zielinski, U. & Gersonde, R. (2002) *Marine Micropaleontology* **45,** 225-268.
15. Barron, J. A. (1985) in *Initial reports of the Deep Sea Drilling Project Leg 85, covering cruises of the Drilling Vessel Glomar Challenger, Los Angeles, California, to Honolulu, Hawaii, March-April 1982*, ed. Mayer, L. A., Theyer, Fritz, Barron, John A., Dunn, Dean A., Handyside, Tim; Hills, Scott, Jarvis, Ian, Nigrini, Catherine A., Pisias, Nicklas G.; Pujos, Annick, Saito, Tsunemasa, Stout, Paul Michael, Thomas, Ellen, Weinreich, Norbert, Wilkens, Roy H., Bailey, Marian G. (Initial Reports of the Deep Sea Drilling Project 85 Publisher: Texas A & M University, Ocean Drilling Program, College Station, TX), Vol. 85, pp. 413-456.
16. Akiba, F. & Yanagisawa, Y. (1986) in *Initial reports of the Deep Sea Drilling Project; covering Leg 87A of the cruises of the drilling vessel Glomar Challenger, Yokohama, Japan, to Yokohama, Japan, June-July, 1982, and Leg 87B from Yokohama, Japan, to Hakodate, Japan, July-August, 1982*, eds. Kagami, H., Karig, D. E., Bray, C. J., Charvet, J., Coulbourn, W. T., Kinoshita, H., Lagoe, M. B., Lang, T. H., Lombari, G. A., Lundberg, N., Machihara, T., Mukhopadhyay, P., Smith, A. J., Stein, C. L., Taira, A., Akiba, F., Cadet, J.-P., Fujioka, K., Leggett, J. K., Matsumoto, R., Niitsuma, N. & Whalen, E. (Texas A & M University, Ocean Drilling Program, College Station, TX), Vol. 87, pp. 483-554.
17. Burckle, L. H. (1996) in *Proceedings of the Ocean Drilling Program; scientific results, New Jersey continental slope and rise; covering Leg 150 of the cruises of the drilling vessel JOIDES Resolution, Lisbon, Portugal, to St. John's, Newfoundland, Sites 902-906, 25 May-24 July 1993*, eds. Mountain, G. S., Miller, K. G., Blum, P., Alm, P.-G., Aubry, M.-P., Burckle, L. H., Christensen, B. A., Compton, J. S., Damuth, J. E., Deconinck, J.-F., de Verteuil, L., Fulthorpe, C. S., Gartner, S., Guerin, G., Hesselbo, S. P., Hoppie, B. W., Katz, M. E., Kotake, N., Lorenzo, J. M., McCracken, S. R., McHugh, C. M. G., Quayle, W. C., Saito, Y., Snyder, S. W., ten Kate, W. G., Urbat, M., Van Fossen, M. C., Vecsei, A. & Dearmont, L. (Texas A & M University, Ocean Drilling Program, College Station, TX), Vol. 150, pp. 17-35.
18. Koc, N. & Scherer, R. P. (1996) *Proceedings of the Ocean Drilling Program; Scientific results, North Atlantic-Arctic gateways I; covering Leg 151 of the cruises of the drilling vessel JOIDES Resolution, St. John's Harbor, Newfoundland, to Reykjavik, Iceland, sites 907-913, 24 July-24 September 1993* **151,** 61-74.
19. Baldauf, J., G. (1984) in *Initial reports of the Deep Sea Drilling Project covering Leg 81 of the cruises of the drilling vessel Glomar Challenger; Southampton, United Kingdom, to Ponta Delgada, Azores Islands, July-September, 1981*, ed.

Roberts, D. G., Schnitker, D., Baldauf, J.G., Desprairies, A., Homrighausen, R., Huddlestun, P. F., Kaltenback, A. J., Krumsiek, Klaus A. O., Morton, A.C., Murray, J. W., Westberg-Smith, J., Zimmerman, H.B., Keene, J. B., Backman, J. (Texas A & M University, Ocean Drilling Program, College Station, TX, United States), Vol. 81, pp. 439-478.

20. Baldauf, J. G. (1985) in *Initial reports of the Deep Sea Drilling Project Leg 85, covering cruises of the Drilling Vessel Glomar Challenger, Los Angeles, California, to Honolulu, Hawaii, March-April 1982*, ed. Mayer, L. A., Theyer, Fritz, Barron, John A., Dunn, Dean A., Handyside, Tim; Hills, Scott, Jarvis, Ian, Nigrini, Catherine A., Pisias, Nicklas G.; Pujos, Annick, Saito, Tsunemasa, Stout, Paul Michael, Thomas, Ellen, Weinreich, Norbert, Wilkens, Roy H., Bailey, Marian G. (Initial Reports of the Deep Sea Drilling Project 85 Publisher: Texas A & M University, Ocean Drilling Program, College Station, TX), Vol. 85, pp. 457-475.
21. Baldauf, J. G. & Barron, J. A. (1991) in *Proceedings of the Ocean Drilling Program, Kerguelen Plateau-Prydz Basin; covering Leg 119 of the cruises of the drilling vessel JOIDES Resolution, Port Louis, Mauritius to Fremantle, Australia, sites 736-746, 14 December 1987-20 February 1988*, eds. Barron, J. A., Larsen, B., Baldauf, J. G., Alibert, C., Berkowitz, S., Caulet, J.-P., Chambers, S. R., Cooper, A. K., Cranston, R. E., Dorn, W. U., Ehrmann, W. U., Fox, R. D., Fryxell, G. A., Hambrey, M. J., Huber, B. T., Jenkins, C. J., Kang, S.-H., Keating, B. H., Mehl, K. W., Noh, I., Ollier, G., Pittenger, A., Sakai, H., Schroder, C. J., Solheim, A., Stockwell, D. A., Thierstein, H. R., Tocher, B., Turner, B. R., Wei, W., Mazzullo, E. K. & Stewart, N. J. (Texas A & M University, Ocean Drilling Program, College Station, TX), Vol. 119, pp. 547-598.
22. Bukry, D. (1973) *Initial Reports of the Deep Sea Drilling Project* **17,** 871-889.
23. Bukry, J. D. & Foster, J. H. (1973) *Initial Reports of the Deep Sea Drilling Project* **16,** 815-871.
24. Harwood, D. M. & Maruyama, T. (1992) in *Proceedings of the Ocean Drilling Program, Central Kerguelen Plateau; covering Leg 120 of the cruises of the drilling vessel JOIDES Resolution, Fremantle, Australia, to Fremantle, Australia, sites 747-751, 20 February to 30 April 1988; Part 2*, eds. Wise, S. W., Jr., Schlich, R., Palmer Julson, A. A., Aubry, M.-P., Berggren, W. A., Bitschene, P. R., Blackburn, N. A., Breza, J. R., Coffin, M. F., Harwood, D. M., Heider, F., Holmes, M. A., Howard, W. R., Inokuchi, H., Kelts, K., Lazarus, D. B., Mackensen, A., Maruyama, T., Munschy, M., Pratson, E. L., Quilty, P. G., Rack, F. R., Salters, V. J. M., Sevigny, J. H., Storey, M., Takemura, A., Watkins, D. K., Whitechurch, H., Zachos, J. & Barbu, E. M. (Texas A & M University, Ocean Drilling Program, College Station, TX), Vol. 120, pp. 683-733.
25. Bukry, D. (1984) in *Initial reports of the Deep Sea Drilling Project covering Leg 78A of the cruises of the drilling vessel Glomar Challenger, San Juan, Puerto Rico to San Juan, Puerto Rico, February-March 1981; and covering Leg 78B of the cruises of the drilling vessel Glomar Challenger, San Juan, Puerto Rico to Las Palmas, Grand Canary Island, March-April, 1981*, eds. Biju-Duval, B., Moore, J. C., Bergen, J. A. M., Blackinton, G., Claypool, G. E., Cowan, D. S., Davis, D. M., Guerra, R. T., Hemleben, C. H. J., Marlow, M. S., Pudsey, C. J.,

Renz, G. W., Tardy, M., Wilson, D. S., Wright, A. W., Natland, J. H., Hyndman, R. D., Salisbury, M. H., Ballard, A., Becker, K., Denis, J., Hickman, S. H., Jacobson, R. S., Langseth, M. G., Mathews, M. A., McGowan, D., Nechoroshkov, V. L., Ponomarev, V. N., Svitek, J. F., Wallerstedt, R. L. & Orlofsky, S. (Texas A & M University, Ocean Drilling Program, College Station, TX), Vol., 78A-78B, pp. 463-468.

26. Gombos, A. M., Jr. & Ciesielski, P. F. (1983) in *Initial reports of the Deep Sea Drilling Project covering Leg 71 of the cruises of the drilling vessel Glomar Challenger; Valparaiso, Chile, to Santos, Brazil, January-February, 1980*, eds. Ludwig, W. J., Krasheninnikov, V. A., Basov, I. A., Bayer, U., Bloemendal, J., Bornhold, B., Ciesielski, P. F., Goldstein, E. H., Robert, C., Salloway, J. C., Usher, J. L., von der Dick, H., Weaver, F. M., Wise, S. W., Jr., Blakeslee, J. H. & Lee, M. (Texas A & M University, Ocean Drilling Program, College Station, TX), Vol. 71, Part 2, pp. 583-634.
27. Scherer, R. P. & Koc, N. (1996) *Proceedings of the Ocean Drilling Program; Scientific results, North Atlantic-Arctic gateways I; covering Leg 151 of the cruises of the drilling vessel JOIDES Resolution, St. John's Harbor, Newfoundland, to Reykjavik, Iceland, sites 907-913, 24 July-24 September 1993* **151,** 75-99.
28. Gombos, A. M., Jr. (1976) *Antarctic Journal of the United States* **11,** 175-176.
29. Winter, D. M. (2001) *Proceedings of the Ocean Drilling Program, scientific results, Northwest Atlantic sediment drifts; covering Leg 172 of the cruises of the drilling vessel JOIDES Resolution; Charleston, South Carolina, to Lisbon, Portugal; sites 1054-1064, 14 February-15 April 1997* **172,** 49.
30. Schrader, H. J. (1974) in *Initial Reports of the Deep Sea Drilling Project* (Texas A & M University, Ocean Drilling Program, College Station, TX), Vol. 24, pp. 887-967.
31. Schrader, H.-J. (1973) *Initial reports of the Deep Sea Drilling Project, covering Leg 18 of the cruises of the drilling vessel Glomar Challenger, Honolulu, Hawaii to Kodiak, Alaska May-July 1971* **18,** 673-797.
32. Jouse, A. P., Kazarina, G. K. & Mukhina, V. V. (1982) in *Initial Reports of the Deep Sea Drilling Project covering Leg 67 of the cruises of the drilling vessel Glomar Challenger, Manzanillo, Mexico to Puntarenas, Costa Rica*, eds. Aubouin, J., von Huene, R., Azema, J., Coulbourn, W. T., Cowan, S. S., Curiale, J. A., Dengo, C. A., Faas, R. W., Harrison, W. E., Hesse, R., Ladd, J. W., Muzylov, N., Shiki, T., Thomson, P. R., Westberg, M. J. & Orlofsky, S. (Texas A & M University, Ocean Drilling Program, College Station, TX), Vol. 67, pp. 455-471.
33. Sanfilippo, A. & Fourtanier, E. (2003) in *Proc. ODP, Sci. Results,* Vol. 182, pp. 1-24.
34. Schrader, H.-J. & Fenner, J. (1976) *Initial Reports of the Deep Sea Drilling Project* **38,** 963-1099.
35. Schrader, H.-J. & Fenner, J. (1976) *Initial Reports of the Deep Sea Drilling Project* **38,** 921-962.

36. Fenner, J. M. (1984) *Initial reports of the Deep Sea Drilling Project covering Leg 75 of the cruises of the drilling vessel Glomar Challenger, Walvis Bay, South Africa to Recife, Brazil, July-September, 1980* **75,** 1245-1271.
37. Fenner, J. (1978) in *Initial reports of the Deep Sea Drilling Project; Supplement to volumes XXXVIII, XXXIX, XL, and XLI*, eds. White, S. M., Supko, P. R., Natland, J., Gardner, J. & Herring, J. (Texas A & M University, Ocean Drilling Program, College Station, TX), Vol. 38-41, pp. 491-624.
38. Scherer, R. P. & Koc, N. (1996) in *Proceedings of the Ocean Drilling Program; Scientific results, North Atlantic-Arctic gateways I; covering Leg 151 of the cruises of the drilling vessel JOIDES Resolution, St. John's Harbor, Newfoundland, to Reykjavik, Iceland, sites 907-913, 24 July-24 September 1993*, eds. Thiede, J., Myhre, A. M., Firth, J. V., Ahagon, N., Black, K. S., Bloemendal, J., Brass, G. W., Bristow, J. F., Chow, N., Cremer, M., Davis, L. L., Flower, B. P., Fronval, T., Hood, J., Hull, D., Koc, N., Larsen, B., Lyle, M. W., McManus, J., O'Connell, S., Osterman, L. E., Rack, F. R., Sato, T., Scherer, R. P., Spiegler, D., Stein, R., Tadross, M., Wells, S., Williamson, D., Witte, B., Wolf-Welling, T. C. W. & Riegel, R. N. (Texas A & M University, Ocean Drilling Program, College Station, TX), Vol. 151, pp. 75-99.
39. Fenner, J. (1984) *Micropaleontology* **30,** 319-342.
40. Dzinoridze, R. N., Jouse, A. P., Koroleva-Golikova, G. S., Kozlova, G. E., Nagaeva, G. S., Petrushevskaya, M. G. & Strelnikova, N. I. (1978) in *Initial reports of the Deep Sea Drilling Project; Supplement to volumes XXXVIII, XXXIX, XL, and XLI*, eds. White, S. M., Supko, P. R., Natland, J., Gardner, J. & Herring, J. (Texas A & M University, Ocean Drilling Program, College Station, TX), Vol. 38-41, pp. 289-427.
41. Boyer, C. S. (1927) *Proceedings of the Academy of Natural Sciences of Philadelphia* **78-79,** 584.
42. Hendey, N. I. (1964) *An introductory account of the smaller algae of British Coastal Waters, Part V, Bacillariophyceae (Diatoms). Ministry of Agriculture, Fisheries and Food.* (H.M. Stationary Office, London).
43. McCollum, D. W. (1975) in *Initial Reports of the Deep Sea Drilling Project* (Texas A & M University, Ocean Drilling Program, College Station, TX), Vol. 28, pp. 515-571.
44. Gombos, A. M., Jr. (1977) in *Initial Reports of the Deep Sea Drilling Project* (Texas A & M University, Ocean Drilling Program, College Station, TX), Vol. 36, pp. 575-687.
45. Barron, J. A. (1980) in *Legs 56 and 57 of the cruises of the drilling vessel Glomar Challenger; Yokohama, Japan to Yokohama, Japan; Leg 56, September-October 1977; Leg 57, October-December 1977; Part 2*, eds. Lee, M., Stout, L. N., Langseth, M., Okada, H., Adelseck, C. G., Jr., Bruns, T. R., Harper, H. E., Jr., Kurnosov, V., Mueller, G., Murdmaa, I., Pisciotto, K. A., Robinson, P., Sakai, T., Thompson, P. R., Whelan, J. K., Wories, H., von Huene, R., Nasu, N., Arthur, M. A., Barron, J. A., Bell, G. D., Cadet, J. P., Carson, B., Fujioka, K., Honza, E., Keller, G., Moore, G. W., Reynolds, R., Sato, S. & Shaffer, B. L. (Texas A & M University, Ocean Drilling Program, College Station, TX), Vol. 56-57, Part 2, pp. 641-686.

46. Koizumi, I. (1980) in *Initial reports of the Deep Sea Drilling Project covering Leg 55 of the cruises of the drilling vessel Glomar Challenger, Honolulu, Hawaii to Yokohama, Japan; July-September 1977*, eds. Shambach, J., Jackson, E., Koizumi, I., Avdeiko, G., Butt, A., David, D., Greene, H., Karpoff, A., Kirkpatrick, R., James, K., Masaru, H., McKenzie, J., Morgan, J. & Takayama, T. (Texas A & M University, Ocean Drilling Program, College Station, TX), Vol. 55, pp. 387-407.
47. Gersonde, R. & Harwood, D. M. (1990) in *Proceedings of the Ocean Drilling Program Scientific Results Vol. 113*, ed. Barber, P. F., Kennett, J.P., et al. (Ocean Drilling Program, College Station, Texas), Vol. 113, pp. 365-402.
48. Rattray, J. (1890) *Proc. Royal Soc. Edinburgh* **16,** 449-692.
49. Fenner, J. & Mikkelsen, N. (1990) in *Mascarene Plateau; covering Leg 115 of the cruises of the drilling vessel JOIDES Resolution, Port Louis, Mauritius, to Colombo, Sri Lanka, Sites 705-716, 13 May 1987-2 July 1987*, eds. Duncan, R. A., Backman, J., Peterson, L. C., Baker, P. A., Baxter, A. N., Boersma, A., Cullen, J. L., Droxler, A. W., Fisk, M. R., Greenough, J. D., Hargraves, R. B., Hempel, P., Hobart, M. A., Hurley, M. T., Johnson, D. A., Macdonald, A. H., Mikkelsen, N., Okada, H., Rio, D., Robinson, S. G., Schneider, D. A., Swart, P. K., Tatsumi, Y., Vandamme, D., Vilks, G., Vincent, E. & Barbu, E. M. (Texas A & M University, Ocean Drilling Program, College Station, TX), Vol. 115, pp. 433-463.
50. Censarek, B. & Gersonde, R. (2002) *Marine Micropaleontology* **45,** 309-356.
51. Censarek, B. & Gersonde, R. (2003) *Proceedings of the Ocean Drilling Program, scientific results; Southern Ocean paleoceanography; covering Leg 177 of the cruises of the drilling vessel JOIDES Resolution; Cape Town, South Africa, to Punta Arenas, Chile; sites 1088-1094; 9 December 1997-5 February 1998* **177,** 14.
52. Schrader, H. J. & Gersonde, R. (1976) *Il significato geodinamico della crisi di salinita' del Miocene terminale nel Mediterraneo; The geodynamic significance of the terminal Miocene salinity crisis in the Mediterranean region* **2,** 15-16.
53. (2003) *Ellis and Messina Catalogues: Diatoms* (Micropaleontology Press.
54. Lin, S. & Carpenter, E. J. (1995) *Journal of Phycology* **31,** 778-785.
55. Homann, M. (1991) *Die Diatomeen der Fur-Formation (Alttertiär) aus dem Limfjord-Gebiet, Nordjütland/Dänemark [Diatoms from the Early Tertiary Fur Formation, Limfjord region, Northern Jutland, Denmark.]* (E. Schweizerbart'sche Verlagsbuchhandlung, Science Publishers, Stuttgart).
56. Barron, J. A., Poore, R. Z. & Wolfart, R. (1981) in *Leg 63 of the cruises of the drilling vessel Glomar Challenger, Long Beach, California to Mazatlan, Mexico, October-November 1978*, eds. Orlofsky, S., Yeats, R. S., Haq, B. U., Barron, J. A., Bukry, D., Crouch, J., Denham, C., Douglas, A. G., Grechin, V. I., Leinen, M., Niem, A. R., Verma, S. P., Pisciotto, K. A., Poore, R. Z., Shibata, T. & Wolfart, R. (Texas A & M University, Ocean Drilling Program, College Station, TX), Vol. 63, pp. 927-941.
57. Barron, J. A. (1981) *Leg 63 of the cruises of the drilling vessel Glomar Challenger, Long Beach, California to Mazatlan, Mexico, October-November 1978* **63,** 507-538.

58. Schrader, H. J. (1976) in *Initial Reports of the Deep Sea Drilling Project* (Texas A & M University, Ocean Drilling Program, College Station, TX), Vol. 35, pp. 605-671.
59. Zielinski, U. & Gersonde, R. (2003) in *Proceedings of the Ocean Drilling Program, scientific results; Southern Ocean paleoceanography; covering Leg 177 of the cruises of the drilling vessel JOIDES Resolution; Cape Town, South Africa, to Punta Arenas, Chile; sites 1088-1094; 9 December 1997-5 February 1998*, eds. Gersonde, R., Hodell, D. A., Blum, P., Andersson, C., Austin, W. E. N., Billups, K., Channell, J. E. T., Charles, C. D., Diekmann, B., Filippelli, G. M., Flores, J.-A., Hewitt, A. T., Howard, W. R., Ikehara, M., Janecek, T. R., Kanfoush, S. L., Kemp, A. E. S., King, S. L., Kleiven, H. F., Kuhn, G., Marino, M., Ninnemann, U. S., O'Connell, S., Ortiz, J. D., Stoner, J. S., Sugiyama, K., Warnke, D. A. & Zielinski, U. (Texas A&M University, Ocean Drilling Program, College Station, TX), Vol. 177, pp. 10.
60. Schrader, H. J. (1974) *Initial Reports of the Deep Sea Drilling Project* **24,** 887-967.
61. Fenner, J., Schrader, H.-J. & Wienigk, H. (1976) in *Initial Reports of the Deep Sea Drilling Project* (Texas A & M University, Ocean Drilling Program, College Station, TX), Vol. 35, pp. 757-813.
62. Barron, J. A. (1980) in *Leg 54 of the cruises of the drilling vessel Glomar Challenger; Cristobal, Panama Canal Zone to Long Beach, California; May-June 1977*, eds. Powell, R., Rosendahl, B. R., Hekinian, R., Briqueu, L., Dmitriev, Y., Fodor, R. V., Goll, R. M., Hoffert, M., Humphris, S. E., Mattey, D. P., Natland, J. H., Petersen, N., Roggenthen, W., Schrader, E. L., Srivastava, R. K., Warren, N., Barron, J. A., Bukry, D. & Lynts, G. W. (Texas A & M University, Ocean Drilling Program, College Station, TX), Vol. 54, pp. 455-486.
63. Winter, D. M. & Iwai, M. (2002) *Proceedings of the Ocean Drilling Program, scientific results, Antarctic glacial history and sea-level change; covering Leg 178 of the cruises of the drilling vessel JOIDES Resolution; Punta Arenas, Chile, to Cape Town, South Africa; sites 1095-1103; 5 February-9 April 1998* **178,** 25.
64. Wornardt, W. W., Jr. (1967) *Miocene and Pliocene marine diatoms from California* (The Academy, San Francisco).
65. Censarek, B. & Gersonde, R. (2003) in *Proceedings of the Ocean Drilling Program, scientific results: Southern Ocean paleoceanography; covering Leg 177 of the cruises of the drilling vessel JOIDES Resolution; Cape Town, South Africa, to Punta Arenas, Chile; sites 1088-1094; 9 December 1997-5 February 1998*, eds. Gersonde, R., Hodell, D. A., Blum, P., Andersson, C., Austin, W. E. N., Billups, K., Channell, J. E. T., Charles, C. D., Diekmann, B., Filippelli, G. M., Flores, J.-A., Hewitt, A. T., Howard, W. R., Ikehara, M., Janecek, T. R., Kanfoush, S. L., Kemp, A. E. S., King, S. L., Kleiven, H. F., Kuhn, G., Marino, M., Ninnemann, U. S., O'Connell, S., Ortiz, J. D., Stoner, J. S., Sugiyama, K., Warnke, D. A. & Zielinski, U. (Texas A&M University, Ocean Drilling Program, College Station, TX), Vol. 177, pp. 14.
66. Koc, N., Labeyrie, L., Manthe, S., Flower, B. P., Hodell, D. A. & Aksu, A. (2001) *Marine Micropaleontology* **41,** 9-23.

67. Ciesielski, P. F. (1986) *Initial reports of the Deep Sea Drilling Project covering Leg 90 of the cruises of the drilling vessel Glomar Challenger, Noumea, New Caledonia, to Wellington, New Zealand, December 1982-January 1983* **90,** 863-885.
68. Hasle, G. R. (1964).
69. Hajos, M. (1976) *Initial Reports of the Deep Sea Drilling Project* **35,** 817-883.
70. Dell'Agenese, D. J. & Clark, D. L. (1994) *Journal of Paleontology* **68,** 31-47.
71. Fenner, J. (1994) *Aarhus Geoscience* **1,** 99-163.
72. Gladenkov, A. Y. (1996) *30th international geological congress; abstracts* **30, Vol. 2,** 33.
73. Hamphill-Haley, E. & Fourtanier, E. (1995) *Proceedings of the Ocean Drilling Program, Scientific Results* **146,** 233-249.
74. Gombos, A. M., Jr. (1983) in *Initial reports of the Deep Sea Drilling Project covering Leg 71 of the cruises of the drilling vessel Glomar Challenger; Valparaiso, Chile, to Santos, Brazil, January-February, 1980*, eds. Ludwig, W. J., Krasheninnikov, V. A., Basov, I. A., Bayer, U., Bloemendal, J., Bornhold, B., Ciesielski, P. F., Goldstein, E. H., Robert, C., Salloway, J. C., Usher, J. L., von der Dick, H., Weaver, F. M., Wise, S. W., Jr., Blakeslee, J. H. & Lee, M. (Texas A & M University, Ocean Drilling Program, College Station, TX), Vol. 71, Part 2, pp. 565-573.
75. Sims, P. A. (1986) *Diatom Research* **1,** 241-269.
76. Tapia, P. M. & Harwood, D. M. (2002) *Micropaleontology* **48,** 303-342.
77. Schrader, H.-J. (1976) *Initial Reports of the Deep Sea Drilling Project* **35,** 605-671.
78. Barron, J. A., Harper, H. E., Jr., Keller, G., Reynolds, R. A., Sakai, T., Shaffer, B. L. & Thompson, P. R. (1980) in *Legs 56 and 57 of the cruises of the drilling vessel Glomar Challenger; Yokohama, Japan to Yokohama, Japan; Leg 56, September-October 1977; Leg 57, October-December 1977*, eds. Lee, M., Stout, L. N., Langseth, M., Okada, H., Adelseck, C. G., Jr., Bruns, T. R., Harper, H. E., Jr., Kurnosov, V. B., Mueller, G., Murdmaa, I. O., Pisciotto, K. A., Robinson, P., Sakai, T., Thompson, P. R., Whelan, J. K., Wories, H., von Huene, R., Nasu, N., Arthur, M. A., Barron, J. A., Bell, G. D., Cadet, J. P., Carson, B., Fujioka, K., Honza, E., Keller, G., Moore, G. W., Reynolds, R., Sato, S. & Shaffer, B. L. (Texas A & M University, Ocean Drilling Program, College Station, TX), Vol. 56-57, Part 1, pp. 505-520.
79. Gombos, A. M., Jr. (1984) *Initial reports of the Deep Sea Drilling Project covering Leg 73 of the cruises of the drilling vessel Glomar Challenger, Santos, Brazil to Cape Town, South Africa, April to June, 1980* **73,** 495-511.
80. Gombos, A. M., Jr. (1984) in *Initial reports of the Deep Sea Drilling Project covering Leg 73 of the cruises of the drilling vessel Glomar Challenger, Santos, Brazil to Cape Town, South Africa, April to June, 1980*, eds. Hsue, K. J., LaBrecque, J. L., Carman, M. F., Jr., Gombos, A. M., Jr., Karpoff, A.-M., McKenzie, J. A., Percival, S. F., Jr., Petersen, N. P., Pisciotto, K. A., Poore, R. Z., Schreiber, E., Tauxe, L., Tucker, P., Weissert, H. J. & Bailey, M. G. (Texas A & M University, Ocean Drilling Program, College Station, TX), Vol. 73, pp. 495-511.

81. Gombos, A. M., Jr. (1987) *Initial reports of the Deep Sea Drilling Project covering Leg 93 of the cruises of the drilling vessel Glomar Challenger, Norfolk, Virginia, to Norfolk, Virginia, May-June, 1983* **93,** 793-799.

References

Agusti, S. 1991. Allometric Scaling of Light Absorption and Scattering by Phytoplankton Cells. Can. J. Fish Aquat. Sci. vol. 48:763-767.

Ahrens, M. A., and R. H. Peters. 1991. Patterns and limitations in limnoplankton size spectra. Canadian Journal of Fisheries and Aquatic Sciences 48:1967-1978.

Aksnes, D. L., and J. K. Egge. 1991. A theoretical model for nutrient uptake in phytoplankton. Marine Ecology Progress Series 70:65-72.

Allen, A. P., J. H. Brown, and J. F. Gillooly. 2002. Global biodiversity, biochemical kinetics, and the energetic-equivalence rule. Science 297:1545-1548.

Alroy, J. 1998. Cope's rule and the dynamics of body mass evolution in North American mammals. Science 280:731-734.

Armstrong, R. 1999. Stable model structures for representing biogeochemical diversity and size spectra in plankton communities. J. Plankton Res. 21:445-464.

Armstrong, R. A. 1994. Grazing limitation and nutrient limitation in marine ecosystems: Steady state solutions of an ecosystem model with multiple food chains. Limnology and Oceanography 39:597-608.

Azam, F., T. Fenchel, J. G. Field, J. S. Gray, L. A. Meyer-Reil, and F. Thingstad. 1983. The ecological role of water-column microbes in the sea. Marine Ecology Progress Series 10:257-263.

Azzalini, A., dal Cappello, T., Kotz, S. 2003. Log-skew-normal and log-skew-t distributions as models for family income data. Journal of income distribution:12-20.

Azzalini, A., Dalla Valle, A. 1996. The multivariate skew normal distribution. Biometrika 83:715-726.

Banavar, J. R., J. Damuth, A. Maritan, and A. Rinaldo. 2002. Supply-demand balance and metabolic scaling. Proceedings of the National Academy of Science of the United States. 99:10506-10509.

Banse, K. 1976. Rates of growth, respiration and photosynthesis of unicellular algae as related to cell size - a review. J. Phycol. 12:135-140.

Barron, J. 2003. Planktonic marine diatom record of the past 18 m.y.: appearances and extinctions in the Pacific and Southern Oceans. Diatom Research 18:203-224.

Behrenfeld, M., and P. Falkowski. 1997. A consumer's guide to phytoplankton primary productivity models. Limnology and Oceanography 42:1479-1491.

Belgrano, A., A.P. Allen, B.J. Enquist, J.F. Gillooly. 2002. Allometric scaling of maximum population density: a common rule for marine phytoplankton and terrestrial plants. Ecology Letters 5:611-613.

Berner, T., Z. Dubinsky, K. Wyman, and P. G. Falkowski. 1989. Photoadaptation and the 'package effect' in *Dunaliella tertiolecta* (Chlorophyceae). Journal of Phycology 25:70-78.

Berry, J., and O. Bjorkman. 1980. Photosynthetic response and adaptation to temperature in higher plants. Annual Review of Plant Physiology 31:491-543.

Beuchat, C. 1997. Allometric scaling laws in biology. Science 278:371.

Blackburn, T. M., Gaston, K.J. 1996. Abundance-body size relationships: the area you census tells you more. Oikos 75:303-309.

Bonner, J. T. 1988, The evolution of complexity by means of natural selection., Princeton University Press.

—. 2004. Perspective: the size-complexity rule. Evolution 58:1883–1890.

Boss, E., M. S. Twardowski, and S. Herring. 2001. Shape of the particulate beam attenuation spectrum and its inversion to obtain the shape of the particulate size distribution. Applied Optics 40:4885-4893.

Brand, L. E. 1981. Genetic variability in reproduction rates in marine phytoplankton populations. Evolution 35:1117-1127.

Brown, J. H. 1995, Macroecology. Chicago, University of Chicago Press.

Burckle, L., McLaughlin, R.B. 1977. Size changes in the marine diatom Coscinodiscus nodulifer A. Schmidt in the equatorial Pacific. Micropaleontology 23:216-222.

Burd, A. B., and G. A. Jackson. 2002. Modelling steady-state particle size spectra. Environ. Sci. Technol 36:323-327.

Campbell, J., D Antoine, R Armstrong, K Arrigo, W Balch, R Barber, M Behrenfeld et al. 2002. Comparison of algorithms for estimating ocean primary production from surface chlorophyll, temperature, and irradiance. Global Biogeochemical Cycles 16:9.

Carpenter, E. J., and S. Janson. 2000. Intracellular cyanobacterial symbionts in the marine diatom Climacodium frauenfeldianum (Bacillariophyceae). J Phycol 36:540-544.

Carroll, S. B. 2001. Chance and necessity: the evolution of morphological complexity and diversity. Nature 409:1102-1109.

Cavender-Bares, K. K., A. Rinaldo, and S. W. Chisholm. 2001. Microbial size spectra from natural and nutrient enriched ecosystems. Limnology and Oceanography 46:778-789.

Chan, A. T. 1978. Comparative physiological study of marine diatoms and dinoflagellates in relation to irradiance and cell size I. Growth under continuous light. Journal of Phycology 14:396--402.

Chisholm, S. W. 1992. Phytoplankton size, Pages 213-237 *in* P. G. Falkowski, and A. D. Woodhead, eds. Primary productivity and Biogeochemical cycles in the sea., Plenum Press.

Chisholm, S. W., R. J. Olson, E. R. Zettler, R. Goericke, J. B. Waterbury, and N. A. Welschmeyer. 1988. A novel free-living prochlorophyte abundant in the oceanic euphotic zone. Nature 334:340-343.

Cullen, J. J. 1982. The deep chlorophyll maximum: comparing vertical profiles of chlorophyll a. Canadian Journal of Fisheries and Aquatic Sciences 39:791-803.

Cullen, J. J., R. J. Geider, J. Ishizaka, D. A. Kiefer, J. Marra, E. Sakshaug, and J. A. Raven. 1993. Toward a general description of phytoplankton growth for biogeochemical models, Pages 153-176 *in* G. T. Evans, and M. J. R. Fasham, eds. Towards a Model of Ocean Biogeochemical Processes. NATO ASI Series. Berlin, Heidelberg, Springer-Verlag.

Cullen, J. J., and M. R. Lewis. 1988. The kinetics of algal photoadaptation in the context of vertical mixing. Journal of Plankton Research 10:1039-1063.

Cullen, J. T., M. P. Field, and R. M. Sherrell. 2001. Determination of trace elements in filtered suspended marine particulate material by sector field HR-ICP-MS. Journal of Analytical Atomic Spectrometry 16:1307-1312.

Damuth, J. 1981. Population density and body size in mammals. Nature 290:699-700.

—. 2001. Scaling of growth: plants and animals are not so different. PNAS 98:2113-2114.

Darveau, C. A., R. K. Suarez, R. D. Andrews, and P. W. Hochachka. 2002. Allometric cascade as a unifying principle of body mass effects on metabolism. Nature 417:166-170.

Dodds, S., D. H. Rothman, and J. S. Weitz. 2001. Re-examination of the `3/4-law' of Metabolism. Journal of Theoretical Biology 209:9-27.

Ducobu, H., J. Huisman, R. R. Jonker, and L. R. Mur. 1998. Competition between a prochlorophyte and a cyanobacterium under various phosphorus regimes: Comparison with the Droop model. Journal of Phycology 34:467-476.

Duysens, L. N. M. 1956. The flattening of the absorption spectrum of suspensions, as compared to that of solutions. Biochimica et Biophysica Acta 19:1-12.

Elser, J. J., R. W. Sterner, E. Gorokhova, W. F. Fagan, T. A. Markow, J. B. Cotner, J. F. Harrison et al. 2000. Biological stoichiometry from genes to ecosystems. Ecology Letters 3:540--550.

Eppley, R. W., and B. J. Peterson. 1979. Particulate organic matter flux and planktonic new production in the deep ocean. Nature 282:677-680.

Eppley, R. W., J. N. Rogers, and J. J. McCarthy. 1969. Half-saturation constants for uptake of nitrate and ammonium by marine phytoplankton. Limnology and Oceanography 14:912-920.

Eppley, R. W., and W. H. Thomas. 1969. Comparison of half-saturation constants for growth and nitrate uptake of marine phytoplankton. Journal of Phycology 5:375-379.

Evans, J. R., and H. Poorter. 2001. Photosynthetic acclimation of plants to growth irradiance: the relative importance of specific leaf area and nitrogen partitioning in maximizing carbon gain. Plant, Cell and Environment 24:755-767.

Falkowski, P. 1997. Evolution of the nitrogen cycle and its influence on the biological sequestration of CO_2 in the ocean. Nature 387:272-275.

Falkowski, P., and T. G. Owens. 1980. Light-shade adaptation. Plant Physiology 66:592-595.

Falkowski, P., and J. A. Raven. 1997. Aquatic Photosynthesis. Malden, Massachusetts, Blackwell.

Falkowski, P. G. 1994. The role of phytoplankton photosynthesis in global biogeochemical cycles. Photosynthesis Research 39:235-258.

—. 1998. Biogeochemical controls and feedbacks on ocean primary productivity. Science 281:200-206.

Falkowski, P. G., E. Boyle, J. Canadell, D. Canfield, J. J. Elser, N. Gruber, K. Hibbard et al. 2000. The global carbon cycle: A test of our knowledge of the Earth as a system. Science 290:291-294.

Falkowski, P. G., Z. Dubinsky, and K. Wyman. 1985. Growth-irradiance relationships in phytoplankton. Limnology and Oceanography 30:311-321.

Falkowski, P. G., Katz, M.E., Knoll, A.H., Quigg, A., Raven ,J.A., Schofield, O., F.J.R. Taylor. 2004. The evolution of modern eukaryotic phytoplankton. Science 305:354-360.

Falkowski, P. G., and J. LaRoche. 1991. Acclimation to spectral irradiance in algae. Journal of Phycology 27:8-14.

Fenchel, T. 1993. There are more small than large species? Oikos 68:375-378.

Fenster, E. J., U. Sorhannus, L. H. Burckle, and A. Hoffman. 1989. Patterns of morphological change in the Neogene diatom Nitzschia jouseae Burckle. Historical Biology 2:197-211.

Ferrario, M. E., Villafañe, V., Helbling, W., Holm-Hansen, O. 1995. The occurrence of the symbiont Richelia in Rhizosolenia and Hemiaulus in the north Pacific. Rev. Brasil. Biol. 55:439-443.

Finkel, Z. V. 2001. Light absorption and size scaling of light-limited metabolism in marine diatoms. Limnology and Oceanography 46:86-94.

Finkel, Z. V., and A. J. Irwin. 2000. Modeling size-dependent photosynthesis: Light absorption and the allometric rule. Journal of Theoretical Biology 204:361-369.

Finkel, Z. V., A. J. Irwin, and O. Schofield. 2004. Resource limitation alters the 3/4 size scaling of metabolic rates in phytoplankton. Marine Ecology Progress Series 273:269-279.

Flynn, K. J., H. Marshall, and R. J. Geider. 2001. A comparison of two N-irradiance interaction models of phytoplankton growth. Limnology and Oceanography 46:1794-1802.

Fogg, G. E. 1977. Excretion of organic matter by phytoplankton. Limnology and Oceanography 22:576--577.

Fogg, G. E., and B. Thake. 1987, Algal cultures and phytoplankton ecology. Madison, University of Wisconsin Press.

Follmi, K. B. 1995. 160 m.y. record of marine sedimentary phophorus burial: Coupling of climate and continental weathering under greenhouse and icehouse conditions. Geology 23:859-862.

Froneman, P. W., R. K. Laubscher, and C. D. Mcquaid. 2001. Size-fractionated Primary Production in the South Atlantic and Atlantic Sectors of the Southern Ocean. J. Plankton Res. 23:611-622.

Fujiki, T., and S. Taguchi. 2002. Variability in chlorophyll a specific absorption coefficient in marine phytoplankton as a function of cell size and irradiance. Journal of Plankton Research 24:859-874.

Furnas, M. J. 1991. Net in situ growth rates of phytoplankton in an oligotrophic, tropical shelf ecosystem. Limnology and Oceanography 36:13-29.

Garcia-Fernandez, J. M., N. T. de Marsac, and J. Diez. 2004. Streamlined Regulation and Gene Loss as Adaptive Mechanisms in Prochlorococcus for Optimized Nitrogen Utilization in Oligotrophic Environments. Microbiol. Mol. Biol. Rev. 68:630-638.

Gaston, K. J., Blackburn, T.M. 2000, Pattern and process in macroecology. London, Blackwell Science.

Gavis, J. 1976. Munk and Riley revisited: nutrient diffusion transport and rates of phytoplankton growth. Journal of Marine Research 34:161-179.

Geider, R. J., and J. LaRoche. 2002. Redfield revisited: variability of C:N:P in marine microalgae and its biochemical basis. Eur. J. Phycol. 37:1-17.

Geider, R. J., and B. A. Osborne. 1992, Algal photosynthesis. New York, Chapman and Hall.

Genin, A., B. Lazar, and S. Brenner. 1995. Vertical mixing and coral death in the Red Sea following the eruption of Mount Pinatubo. Nature 377:507-510.

Gersonde, R., and D. M. Harwood. 1990. Lower Cretaceous diatoms from ODP Leg 113 Site 693 (Weddell Sea). Part I: vegetative cells, Pages 365-402 *in* P. F. Barber, Kennett, J.P., et al., ed., Proceedings of the Ocean Drilling Program Scientific Results Vol. 113. College Station, Texas, Ocean Drilling Program.

Gillooly, J. F., J. H. Brown, G. B. West, V. M. Savage, and E. L. Charnov. 2001a. Effects of size and temperature on metabolic rate. Science 293:2248-2251.

Goericke, R., and N. A. Welschmeyer. 1992. Pigment turnover in the marine diatom *Thalassiosira weissflogii*. II. The $^{14}CO_2$-labeling kinetics of carotenoids. Journal of Phycology 28:507-517.

Goldman, J. C., McGillicuddy, D.J. Jr. 2003. Effect of large marine diatoms growing at low light on episodic new production. Limnology and Oceanography 48:1176-1182.

Gonzalez, J. M., E. B. Sherr, and B. F. Sherr. 1990. Size-Selective Grazing on Bacteria by Natural Assemblages of Estuarine Flagellates and Ciliates. Applied and Environmental Microbiology 56:583-589.

Gordon, J. E. 1991, Structures, or, Why things don't fall down. London, Penguin Books.

Gould, S. J. 1966. Allometry and size in ontogeny and phylogeny. Biol. Rev. 41:587-640.

—. 1997. Cope's rule as psychological artefact. Nature 385:199-200.

Griffiths, D. 1986. Size-abundance relations in communities. The American Naturalist 127:140-166.

—. 1992. Size, abundance, and energy use in communities. Journal of Animal Ecology 61:307-315.

Grover, J. P. 1989. Influence of cell shape and size on algal competitive ability. Journal of Phycology 25:402-405.

—. 1991. Resource competition in a variable environment: phytoplankton growing according to the variable-internal-stores model. American Naturalist 138:811-835.

Haldane, J. B. S. 1985. On being the right size and other essays, Pages 191 *in* J. M. Smith, ed. Oxford, Oxford University Press.

Hallam, A. 1975. Evolutionary size increase and longevity in Jurassic bivalves and ammonites. Nature 258:493-496.

Haq, B. U., J. Hardenbol, and P. R. Vail. 1987. Chronology of fluctuating sea levels during the Mesozoic. Historical Biol. 4:75-106.

Harwood, D. M., and R. Gersonde. 1990. Lower Cretaceous diatoms from ODP Leg 113 Site 693 (Weddell Sea). Part 2: resting spores, chrysophycean cysts, an endoskeletal dinoflagellate, and notes on the origins of the diatoms., Pages 403-425 *in* P. F. Barber, Kennett, J.P., et al., ed., Proceedings of the Ocean Drilling Program Scientific Results Vol. 113. College Station, Texas, Ocean Drilling Program.

Hayes, J. M., H. Strauss, and A. J. Kaufman. 1999. The abundance of C13 in marine organic matter and isotopic fractionation in the global biogeochemical cycle of carbon during the past 800 Ma. Chemical Geology 161:103-125.

Hein, M., M. Folager Pedersen, and K. Sand-Jensen. 1995. Size-dependent nitrogen uptake in micro- and macroalgae. Marine Ecology Progress Series 118:247-253.

Hemmingsen, A. M. 1960. Energy metabolism as related to body size and respiratory surfaces, and its evolution. Reports of the Steno Memorial Hospital 9:15-22.

Hewitt, E. J. 1983. A perspective of mineral nutrition: essential and functional minerals in plants, Pages 277-323 *in* D. A. Robb, and W. S. Pierpoint, eds. Metals and micronutrients, uptake and utilization by plants. London, Academic Press.

Ho, T.-Y., A. Quigg, Z. V. Finkel, A. J. Milligan, K. Wyman, P. G. Falkowski, and F. M. M. Morel. 2003. Elemental composition of some marine phytoplankton. Journal of Phycology 39:1145-1159.

Howarth, R. J., and J. M. McArthur. 1997. Statistics for strontium isotope stratigraphy: A robust LOWESS fit to the marine Sr-isotope curve for 0 to 206 Ma, with look-up table for derivation of numerical age. Journal of Geology 105:441-456.

Hudson, R. J., and F. M. M. Morel. 1993. Trace metal transport by marine microorganisms: implications of metal coordination kinetics. Deep-Sea Res. I 40:129-150.

Ihaka, R., and R. Gentleman. 1996. R: A Language for Data Analysis and Graphics. Journal of Computational and Graphical Statistics 5:299--314.

Jackson, G. A. 1990. A model of the formation of marine algal flocs by physical coagulation processes. Deep-Sea Research 1 37:1197-1211.

Janson, Wouters, Bergman, and Carpenter. 1999. Host specificity in the Richelia-diatom symbiosis revealed by hetR gene sequence analysis. Environ Microbiol 1:431-438.

Jones, R. I. 1978. Adaptations to fluctuating irradiance by natural phytoplankton communities. Limnology and Oceanography 23:920-926.

Kana, T. M., and P. M. Glibert. 1987. Effect of irradiances up to 2000 μE m^{-2} s^{-1} on marine *Synechococcus* WH7803--I. Growth , pigmentation, and cell composition. Deep Sea Research 34:479-495.

Katz, M. E., Z. V. Finkel, D. Gryzebek, A. H. Knoll, and P. G. Falkowski. 2004. Eucaryotic phytoplankton: evolutionary trajectories and global biogeochemical cycles. Annual Review of Ecology, Evolution and Systematics 35.

Kerr, S. R., Dickie, L.M. 2001, The biomass spectrum: A predator-prey theory of aquatic production.: Complexity in ecological systems series. New York, Columbia University Press.

Kiefer, D. A., and B. G. Mitchell. 1983. A simple, steady state description of phytoplankton growth based on absorption cross section and quantum efficiency. Limnology and Oceanography 28:770-776.

Kiorboe, T. 1993. Turbulence, phytoplankton cell size, and the structure of pelagic food webs. Advances in Marine Biology 29:1-72.

Kirk, J. T. O. 1975. A theoretical analysis of the contribution of algal cells to the attenuation of light within natural waters. I. General treatment of pigmented cells. New Phytol. 75:11-20.

—. 1976. A theoretical analysis of the contribution of algal cells to the attenuation of light within natural waters. III. Cylindrical and spheroidal cells. New Phytologist 77:341-358.

—. 1994, Light and Photosynthesis in Aquatic Ecosystems. Cambridge, Cambridge University Press.

Kitchell, J. A., Clark, D.L., Gombos, A.M., Jr. 1986. Biological selectivity of extinction: a link betwwen background and mass extinction. Palaios 1:504-511.

Klausmeier, C. A., E. Litchman, T. Daufresne, and S. A. Levin. 2004. Optimal nitrogen-to-phosphorus stoichiometry of phytoplankton. Nature 429:171-174.

Kleiber, M. 1947. Body size and metabolic rate. Physiological Reviews 27:511--541.

—. 1961, The fire of life: an introduction to animal energetics, R. E. Krieger.

Kooistra, W., and L. K. Medlin. 1996. Evolution of the diatoms (Bacillariophyta). Molecular phylogenetics and evolution 6:391-407.

La Brecque, M. 1992. To model the otherwise unmodelable. Mosaic 23:12-23.

Langdon, C. 1987. On the causes of interspecific differences in the growth-irradiance relationship for phytoplankton. Part 1. A comparative study of the growth-irradiance relationship of three marine phytoplankton species: Skeletonema costatum, Olisthodiscus luteus and Gonyaulax tamarensis. Journal of Plankton Research 9:459-482.

—. 1988. On the cause of interspecific differences in the growth-irradiance relationship for phytoplankton. II. A general review. J. Plank. Res. 10:1291-1312.

Laws, E. A., P. G. Falkowski, W. O. J. Smith, and J. J. McCarthy. 2000. Temperature effects on export production in the open ocean. Global Biogeochem. Cycles 14:1231-1246.

Lawton, J. H. 1990. Species richness and population dynamics of animal assemblages. Phil. R. Soc. Lond. B 330:283-291.

Lee, R. C. 1939. Size and basal metabolism in adult rabbits. Journal of Nutrition 18:489-500.

Legendre, L. 1981. Hydrodynamic control of marine phytoplankton production: the paradox of stability, Pages 191-207 *in* J. C. J. Nihoul, ed. Ecohydrodynamics. Amsterdam, Elsevier Scientific Publishing Company.

Legendre, L., Gosselin, M., Hirche, H.J., Kattner, G., Rosenberg, G. 1993. Environmental control and potential fate of size-fractionated phytoplankton in the Greenland Sea (75N). Marine Ecology Progress Series 98:297-313.

Ley, A. C., and D. C. Mauzerall. 1982. Absolute absorption cross-sections for photosystem II and the minimum quantum requirement for photosynthesis in Chlorella vulgaris. Biochimica et Biophysica Acta 680:95-106.

Li, W. K. W. 2002. Macroecological patterns of phytoplankton in the northwestern North Atlantic Ocean. Nature 419:154 - 157.

Li, W. K. W., and A. M. Wood. 1988. Vertical distribution of North Atlantic ultraphytoplankton: analysis by flow cytometry and epifluorescence microscopy. Deep-Sea Research 1 35:1615-1638.

MacIntyre, H. L., T. M. Kana, J. Anning, and R. Geider. 2002. Photoacclimation of photosynthesis irradiance response curves and photosynthetic pigments in microalgae and cyanobacteria. Journal of Phycology 38:17-38.

Malone, T. C. 1980. Size-fractionated primary productivity of marine phytoplankton, Pages 213-237 *in* P. G. Falkowski, ed. Primary productivity in the sea., Plenum Press.

Malone, T. C., Pike, S.E., Conley, D.J. 1993. Transient variations in phytoplankton productivity at the JGOFS Bermuda time series station. Deep Sea Res 40:903-924.

Mann, D. G., V. A. Chepurnov, and M. Idei. 2003. Mating system, sexual reproduction, and auxosporulation in the anomalous raphid diatom Eunotia (Bacillariophyta). J Phycol 39:1067-1084.

Maranon, E., Holligan, P.M., Barciela, R., Gonzalez, N., Mourino, B., Pazo, M.J., Varela, M. 2001. Patterns of phytoplankton size structure and productivity in contrasting open-ocean environments. Marine Ecology Progress Series 216:43-56.

Margalef, R. 1978. Life-forms of phytoplankton as survival alternatives in an unstable environment. Oceanologica Acta 1:493-510.

Martin, J. H., K. H. Coale, K. S. Johnson, S. E. Fitzwater, R. M. Gordon, S. J. Tanner, C. N. Hunter et al. 1994. Testing the Iron Hypothesis in Ecosystems of the Equatorial Pacific-Ocean. Nature 371:123-129.

Martin, R. E. 1996. Secular increase in nutrient levels through the Phanerozoic: Implications for productivity, biomass, and diversity of the marine biosphere. Palaios 11:209-219.

May, R. M. 1978. The dynamics and diversity of insect faunas, Pages 188-204 *in* L. A. Mound, Waloff, N., ed. Diversity of insect faunas. Oxford, Blackwell.

McGillicuddy, D. J., A. R. Robinson, D. A. Siegel, H. W. Jannasch, R. Johnson, T. D. Dickey, J. McNeil et al. 1998. Influence of mesoscale eddies on new production in the Sargasso Sea. Nature (in press).

McQuoid, M. R., and L. A. Hobson. 1996. Review: Diatom resting stages. Journal of Phycology 32:889-902.

McShea, D. W. 1994a. Mechanisms of large-scale evolutionary trends. Evolution 48:1747-1763.

Medlin, L. K., and I. Kaczmarska. 2004. Evolution of the diatoms: morphological and cytological support for the major clades and a taxonomic revision. Phycologia 43:1-29.

Medlin, L. K., Kooistra, W.H.C.F., Potter, D., Saunders, G.W., Anderson, R.A. 1997. Phylogenetic relationships of the "golden algae" (haptophytes, heterokonts, chrysophytes) and their plastids. Plants Systematics and Evolution 11:187-210.

Menden-Deuer, S., and E. J. Lessard. 2000. Carbon to volume relationships for dinoflagellates, diatoms, and other protist plankton. Limnology & Oceanography 45:569-579.

Michaels, A. F., and M. W. Silver. 1988. Primary production, sinking fluxes and the microbial food web. Deep-Sea Research 1 35:473-490.

Moffett, J. W. 1995. Temporal and spatial variability of copper complexation by strong chelators in the Sargasso Sea. Deep-Sea Research I 42:1273-1295.

Moloney, C. L., and J. G. Field. 1991. The size-based dynamics of plankton food webs. I. A simulation model of carbon and nitrogen flows. Journal of Plankton Research 13:1003-1038.

Moloney, C. L., J. G. Field, and M. I. Lucas. 1991. The size-based dynamics of plankton food webs: II. Simulations of three contrasting southern Benguela food webs. Journal of Plankton Research 13:1039-1092.

Montagnes, D. J. S., J. A. Berges, P. J. Harrison, and F. J. R. Taylor. 1994. Estimating carbon, nitrogen, protein, and chlorophyll a from volume in marine phytoplankton. Limnology and Oceanography 39:1044-1060.

Montagnes, D. J. S., and D. J. Franklin. 2001. Effect of temperature on diatom volume, growth rate, and carbon and nitrogen content: Reconsidering some paradigms. Limnology and Oceanography 46:2008-2018.

Moon-Van Der Staay, S. Y., R. De Wachter, and D. Vaulot. 2001. Oceanic 18S rDNA sequences from picoplankton reveal unsuspected eukaryotic diversity. Nature 409:607 - 610.

Morel, A., and A. Bricaud. 1981. Theoretical results concerning light absorption in a discrete medium, and application to specific absorption of phytoplankton. Deep-Sea Research 1 28A:1375-1393.

Morris, I., and H. E. Glover. 1974. Questions on the mechanism of temperature adaptation in marine phytoplankton. Marine Biology 24:147-154.

Muggli, D. L., and P. J. Harrison. 1996. Effects of nitrogen source on the physiology and metal nutrition of Emiliania huxleyi grown under different iron and light conditions. Marine Ecology Progress Series 130:255-267.

Munk, W. H., and G. A. Riley. 1952. Absorption of nutrients by aquatic plants. Journal of Marine Research 11:215-240.

Nee, S., Harvey, P.H., May, R.M. 1991. Lifting the veil on abundance patterns. Proc. R. Soc. Lond. B. 243:161-163.

Niklas, K. J. 1994. Size-dependent variations in plant growth rates and the "3/4-power rule". Americal Journal of Botany 81:134-144.

Niklas, K. J., and B. J. Enquist. 2001. Invariant scaling relationships for interspecific plant biomass production rates and body size. Proceedings of the National Academy of Science of the United States. 98:2922-2927.

Partensky, F., W. R. Hess, and D. Vaulot. 1999. Prochlorococcus, a Marine Photosynthetic Prokaryote of Global Significance. Microbiol. Mol. Biol. Rev. 63:106-127.

Pasciak, W. J., and J. Gavis. 1974. Transport limitation of nutrient uptake in phytoplankton. Limnology and Oceanography 19:881-888.

Peters, R. H. 1983a, The ecological implications of body size, Cambridge University Press.

—. 1983b. Size structure of the plankton community along the trophic gradient of Lake Memphremagog. Canadian Journal of Fisheries and Aquatic Sciences 40:1770-1778.

Post, A. F., Z. Dubinsky, K. Wyman, and P. G. Falkowski. 1984. Kinetics of light-intensity adaptation in a marine planktonic diatom. Marine Biology 83:231-238.

Prezelin, B., G. Samuelsson, and H. A. Matlick. 1986. Nutrient-dependent kinetics of photosynthesis parameters and photoinhibition of photosystem II during high light photoadaptation in Gonyaulax polyedra. Marine Biology 93:1-12.

Price, N. M., G. I. Harrison, J. G. Hering, R. J. Hudson, P. M. V. Nirel, B. Palenik, and F. M. M. Morel. 1988/89. Preparation and chemistry of the artificial algal culture medium Aquil. Biological Oceanography 6:443-461.

Quigg, A., Z. V. Finkel, A. J. Irwin, Y. Rosenthal, T.-Y. Ho, J. R. Reinfelder, O. Schofield et al. 2003. The evolutionary inhertitance of elemental stoichiometry in marine phytoplankton. Nature 425:291-294.

Rau, G. H., F. P. Chavez, and G. E. Friederich. 2001. Plankton C-13/C-12 variations in Monterey Bay, California: evidence of non-diffusive inorganic carbon uptake by phytoplankton in an upwelling environment. Deep-Sea Research Part I-Oceanographic research papers 48:79-94.

Raven, J. A. 1984. A cost-benefit analysis of photon absorption by photosynthetic unicells. New Phytologist 98:593--625.

—. 1987. The role of vacuoles. New Phytologist 106:357-422.

—. 1988. The iron and molybdenum use efficiencies of plant growth with different energy, carbon and nitrogen sources. New Phytol. 109:279-287.

—. 1990. Predictions of Mn and Fe use efficiencies of phototrophic growth as a funciton of light availability for growth and of C assimilation pathway. New Phytol. 116:1-18.

—. 1994. Why are there no picoplanktonic O_2 evolvers with volumes less than 10^{-19} m^3 ? Journal of Plankton Research 16:565-580.

—. 1997. The vacuole: a cost-benefit analysis, Pages 59-82 *in* R. A. Leigh, and D. Sanders, eds. The Plant Vacuole. Advances in botanical research incorporating advances in plant pathology. San Diego, Academic press.

Raven, J. A., and J. E. Kubler. 2002. New light on the scaling of metabolic rate with the size of algae. Journal of Phycology 38:11-16.

Rea, D. K. 1994. The paleoclimatic record provided by eolian deposition in the deep sea: the geologic history of wind. Reviews of Geophysics 32:159-195.

Reinfelder, J. R., Kraepeil, A.M.L., Morel, F.M.M. 2000. Unicellular C4 photosynthesis in a marine diatom. Nature 407:996-999.

Richardson, K., J. Beardall, and J. A. Raven. 1983. Adaptation of unicellular algae to irradiance: an analysis of strategies. New Phytologist 93:157-191.

Rinaldo, A., A. Maritan, K. K. Cavender-Bares, and S. W. Chisholm. 2002. Cross-scale ecological dynamics and microbial size spectra in marine ecosystems. Proceedings of the Royal Society of London. Series B. 269:2051-2059.

Riper, D. M., T. G. Owens, and P. Falkowski. 1979. Chlorophyll turnover in *Skeletonema costatum*, a marine plankton diatom. Plant Physiology 64:49-54.

Rodriguez, J., and M. Mullin. 1986. Relation between biomass and body weight of plankton in a steady state oceanic ecosystem. Limnology and Oceanography 31:361-370.

Ronov, A. B. 1994. Phanerozoic transgressions and regressions on the continents: A quantitative approach based on areas flooded by the sea and areas of marine and continental deposition. Americal Journal of Science 294:777-801.

Rosenweig, M. L. 1995, Species diversity in space and time. Cambridge., CUP.

Round, F. E., R. M. Crawford, and D. G. Mann. 1990, The Diatoms: biology and morphology of the genera. Cambridge, Cambridge University Press.

Ryther, J. H. 1969. Photosynthesis and fish production in the sea. Science 166:72-76.

Sanudo-Wilhelmy, S. A., Tivar-Sanchez, A., Fu, F-X., Capone, D.G., Carpenter, E.J., Hutchins, D.A. 2004. The impact of surface-adsorbed phosphorus on phytoplankton Redfield stoichiometry. Nature 432:897-901.

Sarmiento, J., T. Hughes, R. Stouffer, and S. Manabe. 1998. Simulated response of the ocean carbon cycle to anthropogenic climate warming. Nature 393:245-249.

Sarmiento, J. L., and S. C. Wofsy. 1999. A US Global Cycle Science Plan, Pages 69, Carbon and climate working group.

Schlesinger, D. A., L. A. Molot, and B. G. Shuter. 1981. Specific growth rates of freshwater algae in relation to cell size and light intensity. Canadian Journal of Fisheries and Aquatic Sciences 38:1052--1058.

Schmidt, D. N., H. R. Thierstein, J. Bollmann, and R. Schiebel. 2004. Abiotic forcing of plankton evolution in the Cenozoic. Science 207:207-210.

Schopf, W. J., and D. Z. Oehler. 1976. How old are the Eucaryotes? Science 193:47-49.

Sciandra, A., J. Gostan, Y. Collos, C. Descolas-Gros, C. Leboulanger, V. Martin-Jezequel, M. Denis et al. 1997. Growth-Compensating Phenomena in Continuous Cultures of Dunaliella tertiolecta Limited Simultaneously by Light and Nitrate. Limnology and Oceanography 42:1325-1339.

Sciandra, A., L. Lazzara, H. Claustre, and M. Babin. 2000. Responses of growth rate, pigment composition and optical properties of Cryptomonas sp. to light and nitrogen stresses. Mar. Ecol. Prog. Ser. 201:107-120.

Shalapyonok, A., R. J. Olson, and L. S. Shalapyonok. 1998. Ultradian Growth in Prochlorococcus spp. Appl. Environ. Microbiol. 64:1066-1069.

Sharp, J. H. 1977. Excretion of organic matter by marine phytoplankton: Do healthy cells do it? Limnology and Oceanography 22:381--399.

Sheldon, R. W., and S. R. Kerr. 1972. The population density of monsters in Loch Ness. Limnology and Oceanography 17:796-798.

Sheldon, R. W., and T. R. Parsons. 1967. A continuous size spectrum for particulate matter in the sea. Journal of the Fisheries Research Board of Canada 24:909-915.

Sheldon, R. W., A. Prakash, and W. H. Sutcliffe, Jr. 1972. The size distribution of particles in the ocean. Limnology and Oceanography 17:327-340.

Shuter, B. G. 1978. Size dependence of phophorus and nitrogen subsistence quotas in unicellular microrganisms. Limnology and Oceanography 23:1248-1255.

Sigman, D., and E. Boyle. 2000. Glacial/interglacial variations in atmospheric carbon dioxide. Nature 407:859-869.

Smetacek, V. 1999. Diatoms and the ocean carbon cycle. Protist 150:25-32.

Sommer, U. 1989. Maximal growth rates of Antarctic phytoplankton: Only weak dependence on cell size. Limnology and Oceanography 34:1109-1112.

Sorhannus, U., E. J. Fenster, L. H. Burckle, and A. Hoffman. 1988. Cladogenetic and anagenetic changes in the morphology of Rhizosolenia praebergonii Mukhina. Historical Biology 1:185-205.

Sorhannus, U., E. J. Fenster, A. Hoffman, and L. Burckle. 1991. Iterative evolution in the diatom genus *Rhizosolenia* Ehrenberg. Lethaia 24:39-44.

Spencer-Cervato, C. 1999. The Cenozoic Deep Sea Microfossil Record: Explorations of the DSDP/ODP Sample Set Using the Neptune Database. Palaeontologia Electronica 2:1-268.

Sprules, W. G., and M. Munawar. 1986. Plankton size spectra in relation to ecosystem productivity, size and perturbation. Canadian Journal of Fisheries and Aquatic Sciences 43:1789-1794.

Stanley, S. M. 1973. An explanation for Cope's Rule. Evolution 27:1-25.

Sterner, R. W., and J. J. Elser. 2002, Ecological stoichiometry: The biology of the elements from molecules to the biosphere. Princeton, Princeton University Press.

Stolte, W., T. McCollin, A. A. M. Noordeloos, and R. Riegman. 1994. Effect of nitrogen source on the size distribution within marine phytoplankton populations. Journal of Marine Experimental Biology and Ecology 184:83-97.

Stolte, W., and R. Riegman. 1995. Effect of phytoplankton cell size on transient-state nitrate and ammonium uptake kinetics. Microbiology 141:1221-1229.

Strathmann, R. R. 1967. Estimating the organic carbon content of phytoplankton from cell volume or plasma volume. Limnology Oceangraphy 12:411--418.

Strzepek, R. F., and N. M. Price. 2000. Influence of irradiance and temperature on the iron content of the marine diatom Thalassiosira weissflogii (Bacillariophyceae). Marine Ecology-Progress Series 206:107-117.

Sunda, W., and S. A. Huntsman. 2004. Relationships among photoperiod, carbon fixation, growth, chlorophyll a, and cellular iron and zinc in a coastal diatom. Limnology and Oceanography 49:1742-1753.

Sunda, W. G. 1994. Trace metal/phytoplankton interactions in the sea, Pages 213-247 *in* G. Bidoglio, and W. Stumm, eds. Chemistry of Aquatic Systems: Local and Global Perspectives. Brussels and Luxembourg, ECSC, EEC, EAEC.

Sunda, W. G., and S. A. Huntsman. 1997. Interrelated influence of iron, light and cell size on marine phytoplankton growth. Nature 390:389-392.

—. 1998a. Interactive effects of external manganese, the toxic metals copper and zinc, and light in controlling cellular manganese and growth in a coastal diatom. Limnology and Oceanography 43:1467-1475.

—. 1998b. Processes regulating cellular metal accumulation and physiological effects: Phytoplankton as model systems. Sci. Total Environ. 219:165-181.

Sweeney, E. N., D. J. McGillicuddy, and K. O. Buesseler. 2003. Biogeochemical impacts due to mesoscale eddy activity in the Sargasso Sea as measured at the Bermuda Atlantic Time Series (BATS) site. Deep-Sea Research II 50:3017-3039.

Taguchi, S. 1976. Relationship between photosynthesis and cell size of marine diatoms. Journal of Phycology 12:185-189.

Tamigneaux, E., Legendre, L., Klein, B., Mingelbier, M. 1999. Seasonal dynamics and potential fate of size-fractionated phytoplankton in a temperate neashore enviroments (Western Gulf of St Lawrence, Canada). Estuarine, Coastal and Shelf Sci. 48:253-269.

Tang, E. P. Y. 1995. The allometry of algal growth rates. Journal of Plankton Research 17:1325--1335.

Tappan, H. 1980, The paleobiology of plant protists. USA, W.H. Freeman and Company.

Thompson, P. A., P. J. Harrison, and J. S. Parslow. 1991. Influence of irradiance on cell volume and carbon quota for ten species of marine phytoplankton. Journal of Phycology 27:351-360.

Tilman, D. 1977. Resource Competition between Plankton Algae: An Experimental and Theoretical Approach. Ecology 58:338-348.

Tittel, J., B. Zippel, W. Geller, and J. Seeger. 1998. Relationships beteen planton community structure and plankton size distribution in lakes of northern Germany. Limnology and Oceanography 43:1119-1132.

Tozzi, S., O. Schofield, and P. Falkowski. 2004. Historical climate change and ocean turbulence as selective agents of phytoplankton functional groups. Marine Ecology Progress Series 274:123-132.

Trammer, J. 2002. Power formula for Cope's rule. Evolutionary Ecology Research 4:147-153.

Tremblay, J. E., Legendre, L. 1994. A model for the size-fractionated biomass and production of marine phytoplankton. Limnology and Oceanography 39:2004-2014.

van Bleijswijk, J., R. S. Kempers, and M. Veldhuis. 1994. Cell and growth characteristics of types A and B of Emiliania huxleyi (Prymnesiophycese) as determined by flow cytometry and chemical analyses. Journal of Phycology 30:230-241.

Van Valen, L. 1973. Body size and numbers of plants and animals. Evolution 27:27-35.

Vasconcelos, M. T. S. D., M. F. C. Leal, and C. M. G. van den Berg. 2002. Influence of the nature of the exudates released by different marine algae on the growth, trace metal uptake and exudation of Emiliana huxleyi in natural seawater. Mar. Chem. 77:187-210.

Verity, P. G. 1981. Effects of temperature, irradiance, and daylength on the marine diatom Leptocylindrus danicus Cleve. II. Excretion. Journal of Experimental Marine Biology and Ecology 55:159-169.

Villareal, T. A., and F. Lipshultz. 1995. Internal nitrate concentrations in single cells of large phytoplankton from the Sargasso Sea. J. Phycol. 31:689-696.

Vrieling, E. G., T. P. M. Beelen, R. A. van Santen, and W. W. C. Gieskes. 2000. Nanoscale uniformity of pore architecture in diatomaceous silica: a combined small and wide angle x-ray scattering study. J Phycol 36:146-159.

Watson, A. J., and P. S. Liss. 1998. Marine biological controls on climate via the carbon and sulphur geochemical cycles. Phil. Trans R. Soc. Lond B. 353:41-51.

Welschmeyer, N. A., and C. J. Lorenzen. 1981. Chlorophyll-specific photosynthesis and quantum efficiency at subsaturating light intensities. Journal of Phycology 17:283-293.

West, G. B., J. H. Brown, and B. J. Enquist. 1997. A general model for the origin of allometric scaling laws in biology. Science 276:122-126.

—. 1999. The fourth dimension of life: Fractal geometry and allometric scaling of organisms. Science 284:1677-1679.

Westall, J. C., J. L. Zachary, and F. M. M. Morel. 1986. MINEQL: A computer program for the calculation of the chemical equilibrium composition of aqueous systems, Pages 91. Corvallis, Oregon, Oregon State University.

Whitfield, J. 2001. All creatures great and small. Nature 413:342-344.

Wimpenny, R. S. 1936. The size of diatoms. I. The diameter variation of Rhizosolenia styliformis Brightw. and R. alata Brightw. in particular and of pelagic marine diatoms in general. Mar. Biol. Assoc. Jour. 21:29-60.

Wright, J. D. 2001. Cenozoic Climate - Oxygen Isotope Evidence, Pages 415-426 *in* J Steele, S Thorpe, and K. Turekian, eds. In: Encyclopedia of Ocean Sciences. London, Academic Press.

Zachos, J., M. Pagani, L. Sloan, E. Thomas, and K. Billups. 2001. Trends, Rhythms, and Aberrations in Global Climate 65 Ma to Present. Science 292:686-693.

Zlotnik, I., and Z. Dubinsky. 1989. The effect of light and temperature on DOC excretion by phytoplankton. Limnology and Oceanography 34:831-839.

Zubkov, M. V., M. A. Sleigh, G. A. Tarran, P. H. Burkill, and R. J. G. Leakey. 1998. Picoplanktonic community structure on an Atlantic transect from 50 degrees N to 50 degrees S. Deep-Sea Research 45:1339-1355.

Curriculum Vita of Zoe Vanessa Finkel

Education:

2000-2005 Rutgers University , Oceanography, Ph.D.
1995-1998 Dalhousie University, Biology, M. Sc.
1990-1995 University of Manitoba, Environmental Science, B. Sc.

Refereed Publications:

Z. V. Finkel, M. Katz, J. Wright, O. Schofield & P. Falkowski. 2005. Climatically-driven evolutionary change in the size of diatoms over the Cenozoic. Proceedings of the National Academy of Sciences USA. In revision.

P. Frost, M. Evans-White, Z. V. Finkel, T. Jensen, V. Matzek. 2005. Are you what you eat? Physiological constraints on organismal stoichiometry in an elementally imbalanced world. *Oikos*. **109**:18-28.

M.E. Katz, Z.V. Finkel, D. Gryzebek, A.H. Knoll, P.G. Falkowski. 2004. Eucaryotic phytoplankton: evolutionary trajectories and global biogeochemical cycles. *Annual Review of Ecology, Evolution and Systematics*. 35: 523-556.

Z. V. Finkel, A. J. Irwin and O. Schofield. 2004. Resource limitation alters the ¾ size scaling of metabolic rates in phytoplankton. *Marine Ecology Progress Series*, Special theme section: *Emergent properties of complex marine systems: a macroecological perspective*. **273**: 269-279.

O. Schofield, Arnone, R., Bissett, P., Davis, C., Finkel, Z., Oliver, M., M. Moline. 2004. Watercolors in the coastal zone: what can we see? *Oceanography*. 17(2): 30-37.

A.S. Quigg, Z. V. Finkel, A. J. Irwin, Y. Rosenthal, T-Y Ho, J. R. Reinfelder, O. Schofield, F. M. M. Morel and P. G. Falkowski. 2003. The evolutionary inheritance of elemental stoichiometry in marine phytoplankton. *Nature*, **425**: 291-294.

T-Y Ho, A. Quigg, Z. V. Finkel, A. J. Milligan, K. Wyman, P. G. Falkowski, and F. M. M. Morel. 2003. The Elemental Composition of Some Marine Phytoplankton. *Journal of Phycology*, **39**(6): 1145-1159.

Z. V. Finkel and A.J. Irwin. 2001. Light absorption and the filter amplification correction: species-specific and size-specific effects. *Journal of Experimental Marine Biology and Ecology*, **259**: 51-61.

Z. V. Finkel. 2001. Light absorption and the size scaling of light-limited growth and photosynthesis in marine diatoms. *Limnology & Oceanography*, **46**(1): 86-94.

Z. V. Finkel and A.J. Irwin. 2000. Modelling size-dependent photosynthesis: light absorption and the allometric rule. *Journal of theoretical Biology*, **204**: 361-369.

Papers submitted or in preparation

Z. V. Finkel, A. Irwin, O. Schofield & P. Falkowski. Scaling up from size dependent physiology to the size structure of phytoplankton communities over a resource gradient. In review**.**

Z. V. Finkel, A. Quigg, O. Schofield & P. Falkowski. Irradiance induced changes in the elemental composition of marine phytoplankton. In prep.